Master Thesis, Department of Geosciences

Reservoir quality of the Lower Jurassic Cook Formation in the Knarr area, northern North Sea

A petrographic, sedimentological and petrophysical approach

Jenny Torsæter

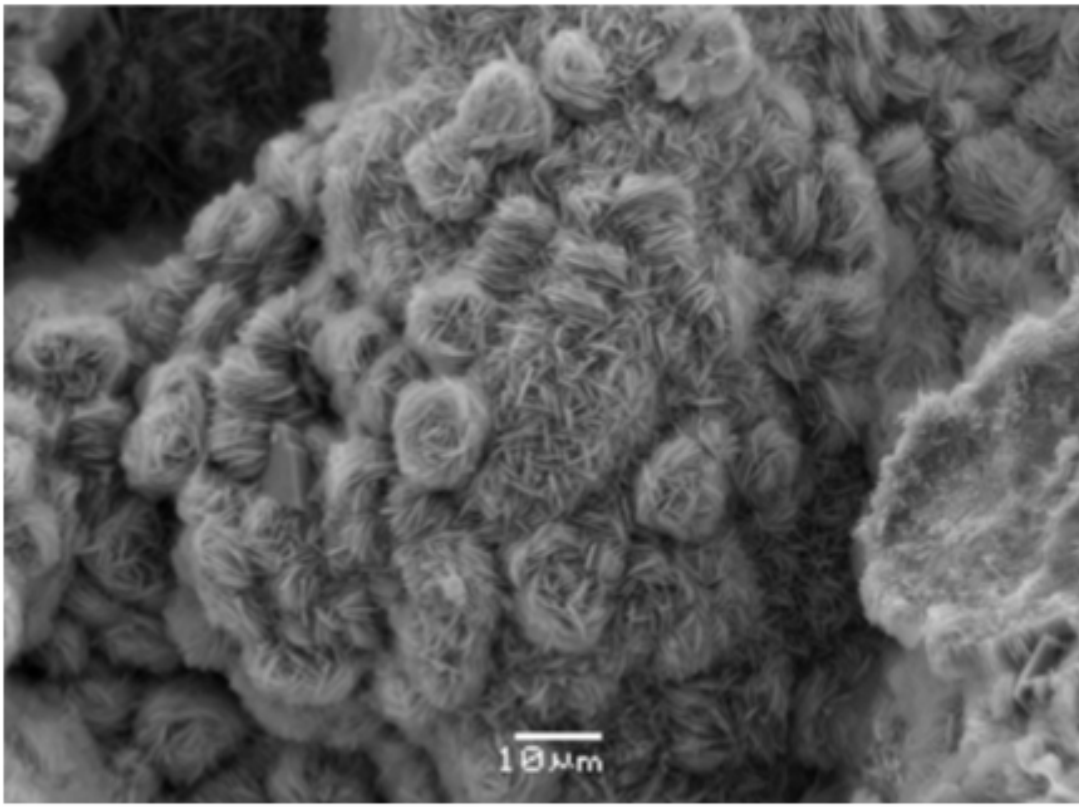

UNIVERSITY OF OSLO

FACULTY OF MATHEMATICS AND NATURAL SCIENCES

Reservoir quality of the Lower Jurassic Cook Formation in the Knarr area, northern North Sea

A petrographic, sedimentological and petrophysical approach

Jenny Torsæter

Master Thesis in Geosciences

Discipline: Petroleum geology and petroleum geophysics

Department of Geosciences

Faculty of Mathematics and Natural Science

UNIVERSITY OF OSLO

02.06.2014

Supervisors: Jens Jahren (UiO) and Audun Vestheim Kjemperud (Idemitsu)
This work is published digitally through DUO – Digitale Utgivelser ved UiO
http://www.duo.uio.no
It is also catalogued in BIBSYS (http://www.bibsys.no/english)

ACKNOWLEDGEMENT

I acknowledge my supervisors Associate Professor Jens Jahren and Dr. Audun Vestheim Kjemperud for valuable and constructive suggestions during this research work. My grateful thanks are also extended to Berit Løken Berg, for her assistance in the SEM-lab.

My friends at the geology department, especially everyone from room 217, deserve grateful thanks for enthusiastic encouragement and invaluable discussions.

I would like to thank my mom and dad for great support by sending me letters and several “Flax lodd”. Unfortunately, I did not become a millionaire. Last, but not least, I would like to thank Espen Andersen for being very encouraging and an excellent chef during these five months of hard work.

June 2014

Jenny Torsæter

ABSTRACT

The present study examines the Lower Jurassic Cook Formation in the Knarr area, northern North Sea, in order to characterise the effect of chlorite coating and potential porosity destroying mechanisms.

Cored reservoir intervals from three wells have been examined by petrographic, sedimentological and petrophysical methods in order to determine the distribution and diagenetic history of the observed chlorite coating and to determine the reservoir quality. Petrographic methods include SEM and optical microscopy, whereas core description makes up the sedimentological analysis. Lithology, porosity and density were the key properties studied for the petrophysical analysis.

The Cook Formation has been subdivided into five sandstone units, separated by layers of mudstone. These sandstone units are suggested to be stacked tidal bars deposited close to a tidally influenced deltaic setting. Mudstone intervals are associated with mud banks and interpreted to be deposited during relative sea level rise.

The reservoir quality in the Cook Formation is overall very good, due to the extensive chlorite coating preserving the porosities. Origin and distribution of the chlorite present in the Cook Formation is believed to develop from a mixed clay precursor that has partly developed to berthierine. The effect of chlorite coating in intermediate to deeply buried reservoirs is difficult to predict. However, understanding the origin and distribution of chlorite coating will make predictions easier in future exploration.

TABLE OF CONTENTS

1 Introduction

1.1 Introduction

This master thesis is part of a collaboration project with Idemitsu and BG Norge AS on the reservoir quality in the Lower Jurassic sandstone reservoirs in the Knarr area in the North Sea. The Knarr Field is formerly known as the Jordbær prospect, and is located in production licence 373 S of block 34/3 in the northern North Sea. In this study, 4 wells, 23 thin sections, 12 plugs for SEM analysis and numerous pictures and logs of cored intervals have been provided. The research project consists of two master studies; one thesis concerning the reservoir quality and one regarding a more detailed study of the depositional environment and diagenesis of the Knarr area. Christopher Kjølstad performs the latter thesis (Kjølstad, 2014).

1.2 Purpose and methods

Sandstones with high porosity and permeability at intermediate to deep burial depth (2000 - 4000m below sea floor (m bsf)) are of economic importance since a significant amount of hydrocarbons have been discovered in such reservoirs worldwide. Thus, the main purpose of this thesis is to provide valuable information about reservoir quality in intermediate to deeply buried reservoirs as a function of quartz cementation and porosity preserving mechanisms as grain coating. Petrophysical and petrographic methods were applied to investigate the lateral and vertical variations in the sandstone. Subsequently, the main objectives of this study are:

- Document the main depositional characteristics and facies of the selected samples, and determine if there are any variations between the sandstone units in the wells provided.
- Characterise the nature of authigenic chlorite, both grain coating and pore filling and see if the variations in the sandstone units can be linked to facies.
- Characterise the nature of diagenetic quartz cements present and investigate if there are any variations between the sandstone units. Additionally, see if there is a link between the presence of chlorite and quartz cement.
- Distinguish the nature of the pore systems, and determine how the porosity varies between facies.
- Compare and interpret the obtained results to perform a characterisation of the reservoir quality on the selected samples, and their associated sandstone units.

1.3 Study area

In June 2011 the Norwegian government approved the Knarr project, and the first production is expected in 2014 (Offshore-Technology, 2014). The field is located in production license 373 S of block 34/3 in the Norwegian North Sea (Figure 1.1). BG is the operator of the field with 45% working interest, whereas partners include Idemitsu Petroleum Norge (25%), Wintershall Norge (20%) and RWE Dea (10%) (NPD, 2013). The production duration of the field is estimated from 6 to 20 years based on oil prices and operating costs (Offshore-Technology, 2014). The Knarr area is situated in the Tampen area and the reservoir is within the Cook Formation which is buried to a depth of 3800 – 4000 m with a water depth of about 400m (NPD, 2013). The thickness variations within the Cook Formation in the Knarr area are small.

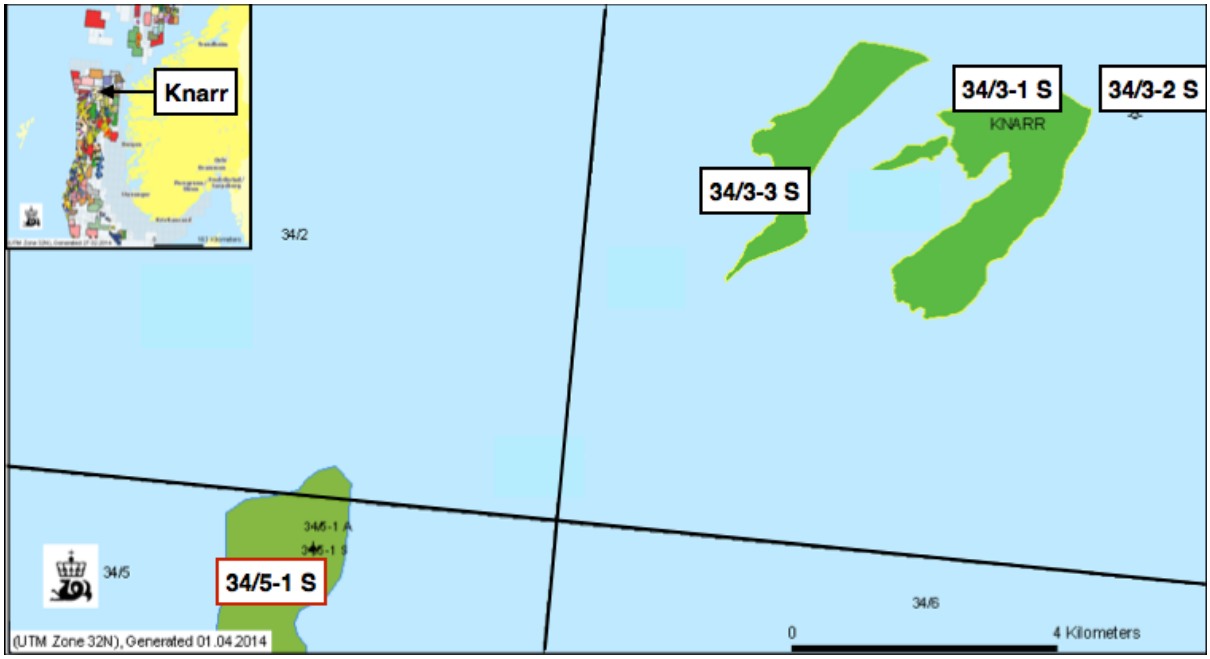

Figure 1.1 Map of the study area with the three studied wells (black squares) and a fourth well (red square) used for well correlation (NPD Factmaps, 2014).

2 Geological background – The northern North Sea

2.1 Introduction

The northern North Sea is dominated by the Viking Graben, which continues into the Sogn Graben towards north. The grabens are flanked by the East Shetland Basin and the Tampen Spur to the west, where also the Knarr area is located, and the Horda Platform to the east (Figure 2.1). This chapter gives an overview of the geological framework, both local and regional, in the North Sea, with an emphasis on the Knarr area. Structural and stratigraphic features will be described. However, more complete descriptions of the North Sea and its petroleum geology is found in Glennie (1998) *Petroleum geology of the North Sea* and Evans (2003) *The Millennium atlas: petroleum geology of the central and northern North Sea.*

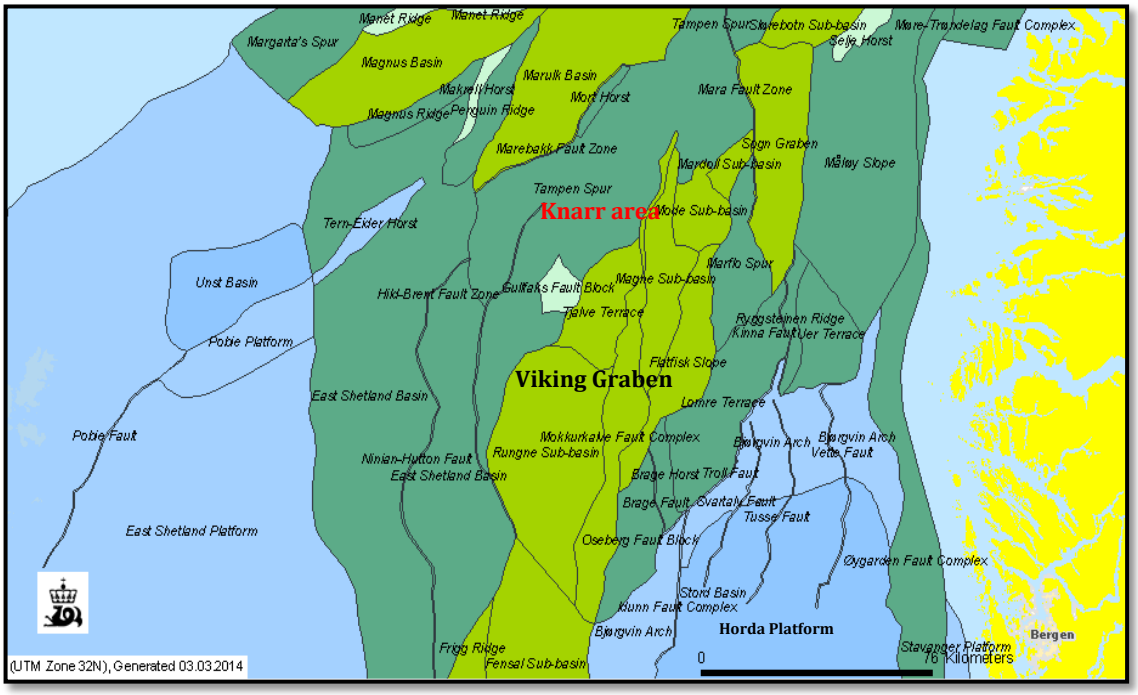

Figure 2.1 Map of the structural elements in the northern North Sea. The Knarr area is located on the Tampen Spur (NPD Factmap, 2014).

2.2 Structural setting of the northern North Sea

The northern North Sea is a 150-200km wide north-south oriented zone of extended crust (Fjeldskaar et al., 2004). The crustal architecture in the area is generally accepted to be the result of two lithospheric extension events and their associated thermal subsidence episodes (Faleide and Berge, 2000). Consequently, the area is characterised by large rotated fault blocks and sedimentary basins in asymmetric half-grabens, features that are associated with extension and thinning of the crust (Fjeldskaar et al., 2004). Evidence exists for a third tectonic event in the Tertiary (Rüpke et al., 2008), however, major tectonic activity is commonly thought to have ceased after the late Jurassic rifting.

The Permian-Triassic event is the first major rifting event that has affected the architecture of the northern North Sea. The rift axis is thought to be located where the Horda Platform is situated today (Christiansson et al., 2000) (Figure 2.1). Several of the master faults formed during this episode were later reactivated during the second major rifting phase. The initiation of this second rifting event is dated to late Middle Jurassic, and took place where presently the Viking Graben is located (Christiansson et al., 2000) (Figure 2.1). Rifting climax occurred during the Upper Jurassic, with fault activity concentrated on only a few faults along the Viking Graben margins. This resulted in a more pronounced graben relief and the development of graben topography, including platforms and platform marginal heights (Gabrielsen et al., 1990). The late Jurassic rifting was followed by post-rift subsidence due to cooling (Marcussen et al., 2010).

2.2.1 Structural setting of the Cook Formation

The Lower Jurassic Cook Formation (Figure 2.3) formed in the northern part of the Viking Graben rift basin (Figure 2.1). The formation was deposited during a phase of overall tectonic inactivity, however, subsidence after the first rifting episode in the Permian-Triassic were on-going (Folkestad et al., 2012). Seismic from the newly discovered Knarr area clearly illustrates how the Upper Jurassic rifting has affected the present day burial depths within the Cook Formation (Figure 2.2).

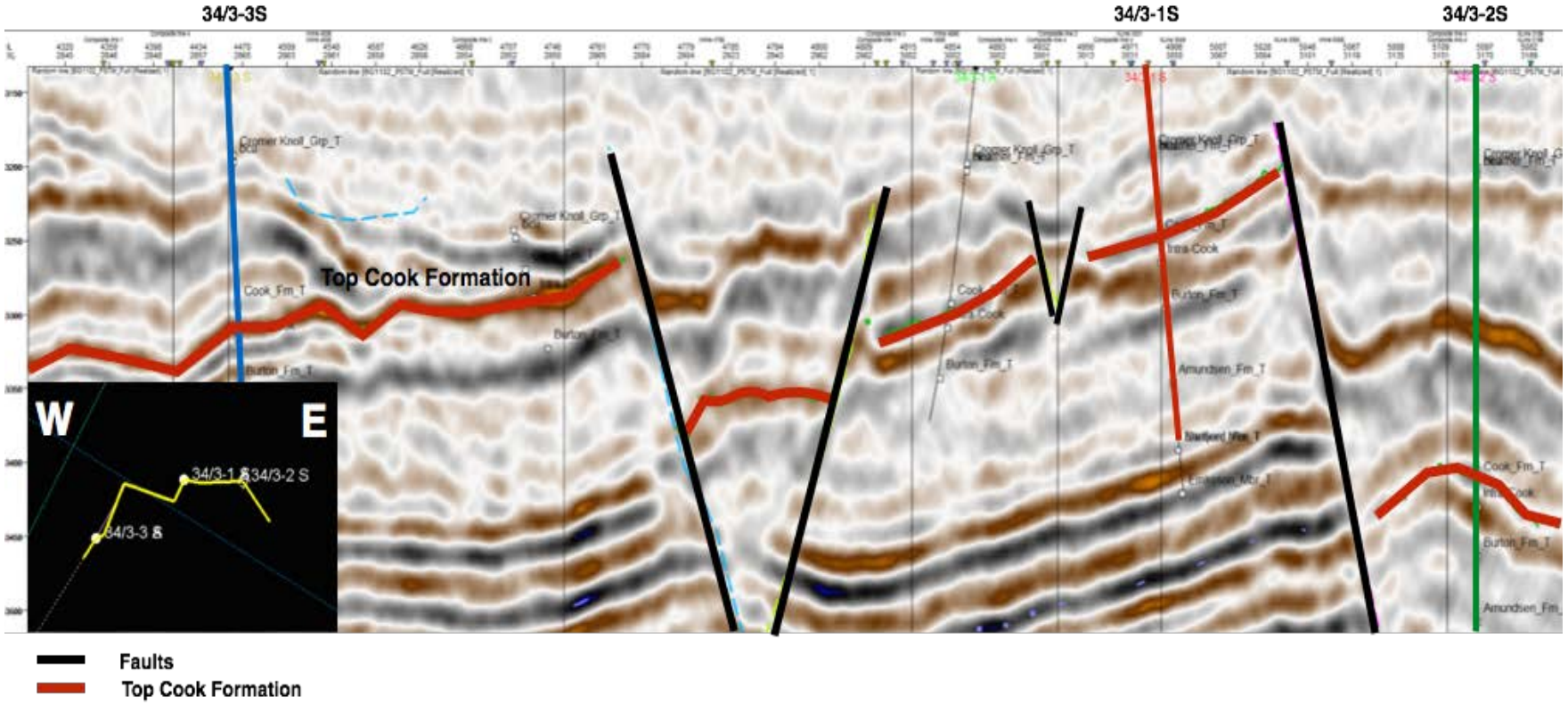

Figure 2.2 Seismic sections between well 34/3-1S, 34/3-2S and 34/3-3S. Note the big faults causing depth variations between the three wells within the Cook Formation.

2.3 Stratigraphic setting

The Jurassic sequence stratigraphic subdivision has been summarised by Vollset and Doré (1984). Lower Jurassic rocks in the Norwegian North Sea include the Statfjord Group and the Dunlin Group, with the overlying Middle Jurassic Brent Group (Figure 2.3). The Dunlin Group has been divided into five formations on the Norwegian sectors: Amundsen Formation, Johansen Formation, Burton Formation, Cook Formation and Drake Formation (Vollset and Doré, 1984) (Figure 2.3). The sandstone distribution of the Lower Jurassic sandstones are primary controlled by variations in sediment supply, tectonic subsidence and accommodation space, and are therefore represented by repeated progradation and retrogradation (Charnock et al., 2001). Description of the Dunlin Group and its over – and underlying units are listed in Table 2.1.

2.3.1 Lithostratigraphy of the Cook Formation

The five sandstone units observed in the Knarr area will be referred to as the abbreviated names C1, C2, C3, C4 and C5 throughout this study. Unit C1, C2, C3 and C4 have associated layers of shale at the bottom of the sandstone unit; however, these shaly layers are not included in the abbreviated names. Figure 2.4 illustrates all sandstone units of the Cook Formation within four wells in the Knarr area.

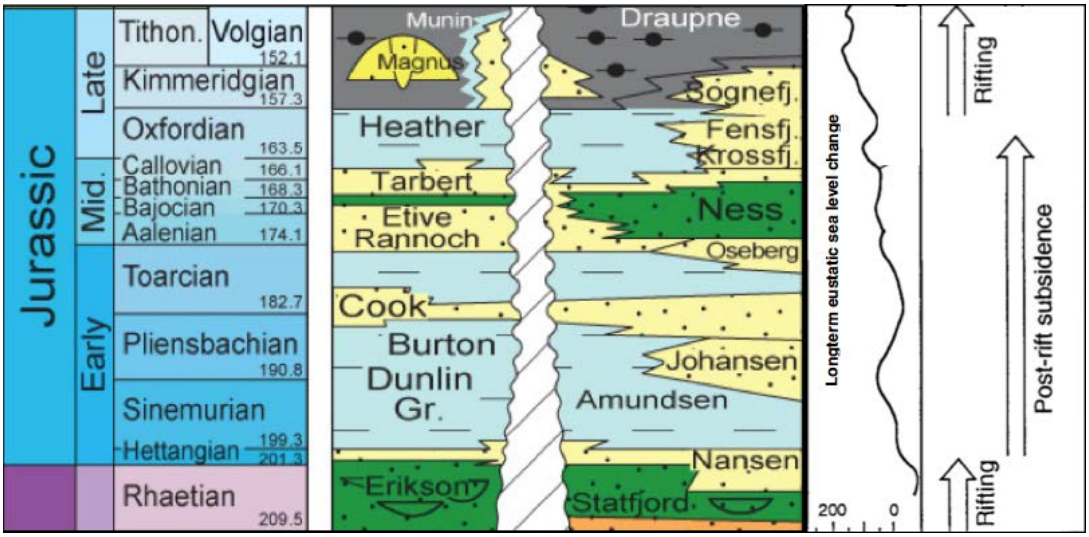

Figure 2.3 Stratigraphy from Upper Permian up to Jurassic (Norlex, 2014) in the Tampen Spur area with eustatic sea level curve (Haq et al., 1987) and rift episodes.

Table 2.1 Description and interpretations of the depositional environment of formations within the Dunlin Group, as well as the Statfjord Group and the Brent Group.

Gr.	Fm.	Depositional environment	References
Brent Gr. (part)	**Rannoch Fm.**	Represents the middle shoreface of a progradational delta. Dominated by fine sand with horizontal to wavy laminations. The transition from Brent Gr. to Dunlin Gr. separates marine strata from deltaic deposits.	(Scott, 1992) (Charnock et al., 2001)
Dunlin Group	**Drake Fm.**	Contains shaly intervals with an upward coarsening trend caused by increase in siltstone and sandstone. The formation is interpreted as offshore/shelf deposits. On the Horda Platform the formation interfingers with the Cook Formation.	(Marjanac and Steel, 1997)
	Cook Fm.	See Table 2.2.	
	Burton Fm.	The shaly formation is interpreted to be outer shelf/offshore deposits.	(Marjanac and Steel, 1997)
	Johansen Fm.	Consists of fine-grained sandstones and siltstones. Interpreted as a lowstand prograding delta system with a thin upper transgressive layer. At the base it is interfingereing with shales and heterolithic facies of the Amundsen Formation. The formation is only deposited on the Horda Platform.	(Marjanac and Steel, 1997) (Marjanac, 1995)
	Amundsen Fm.	Sea level rise initiated the deposition of the shaly Amundsen Fm. Consequently; the heterolithic facies with varying sandstone content are interpreted to be depostited in the outer shelf.	(Marjanac and Steel, 1997)
Statfjord Group (part)	**Nansen Fm.**	Subaerial depositional conditions are suggested for parts of the fine-grained units by the presence of calcrete, coals and root-traces. The upper part of the sequence is interpreted to have been deposited in a marine environment. In the Gullfaks and Statfjord area the formation is interpreted as marine.	(Lervik, 2006) (Scull and Deegan, 1977)
	Eirikson Fm.	Interpreted as a graben-axial fluvial system oriented north-south in the northern North Sea. Includes medium-coarse grained channel sandbodies. The boundary between the Statfjord Gr. and the Dunlin Gr. represents the transition from the marginal marine environment to the deep marine conditions in the Amundsen Fm.	(Dalrymple, 2001) (Charnock et al., 2001)

2.3.1 Sequence stratigraphic framework of the Lower Jurassic

A number of important climatic, tectonic and relative sea level changes occurred during the Triassic – Jurassic interval (Steel, 1993). During the Early Jurassic a transgression transformed the non-marine Triassic basins to a thoroughly marine basin (Ziegler and Mij, 1982). A Late Triassic – Early Jurassic climate change in the North Sea is documented by the change from ephemeral fluvial sedimentary facies to the alluvial sandstones, shales and coals associated with more humid and well established river systems (Røe and Steel, 1985).

Middle Triassic to Late Jurassic is regarded a post-rift interval, and therefore changes in relative sea level is a controlling factor on deposition. Lower Jurassic sediments are found within a megasequence which is divided into four transgressive – regressive cycles in the North Viking Graben (Parkinson and Hines, 1995). The characteristics of this megasequence is the clastic wedges dominated by a thick regressive part and a thin overlying transgressive part (Steel, 1993). A rapid fall in sea level during the late Pliensbachian to early Toarcian corresponds to the deposition of the Cook Formation (Gibbons et al., 2003). Consequently, the Cook Formation deposited as extensive sand sheet across, developing highly progradational units. Basinward extent of the formation resulted in abrupt change from basinal shales to extensive sand sheets (Steel, 1993). Dreyer and Wiig (1995) assumed that the sediments of the Cook Formation were supplied mostly from the eastern flanks and shoulders of the rift Viking Graben. At present, in the Knarr area, the sandstones and mudstones of the Cook Formation are buried at a depth of about 3400-3700m bsf. Due to the tectonic inactivity during deposition of the formation the thickness variations in the Knarr area are rather small and only ranges up to about 20 meters (Figure 2.4).

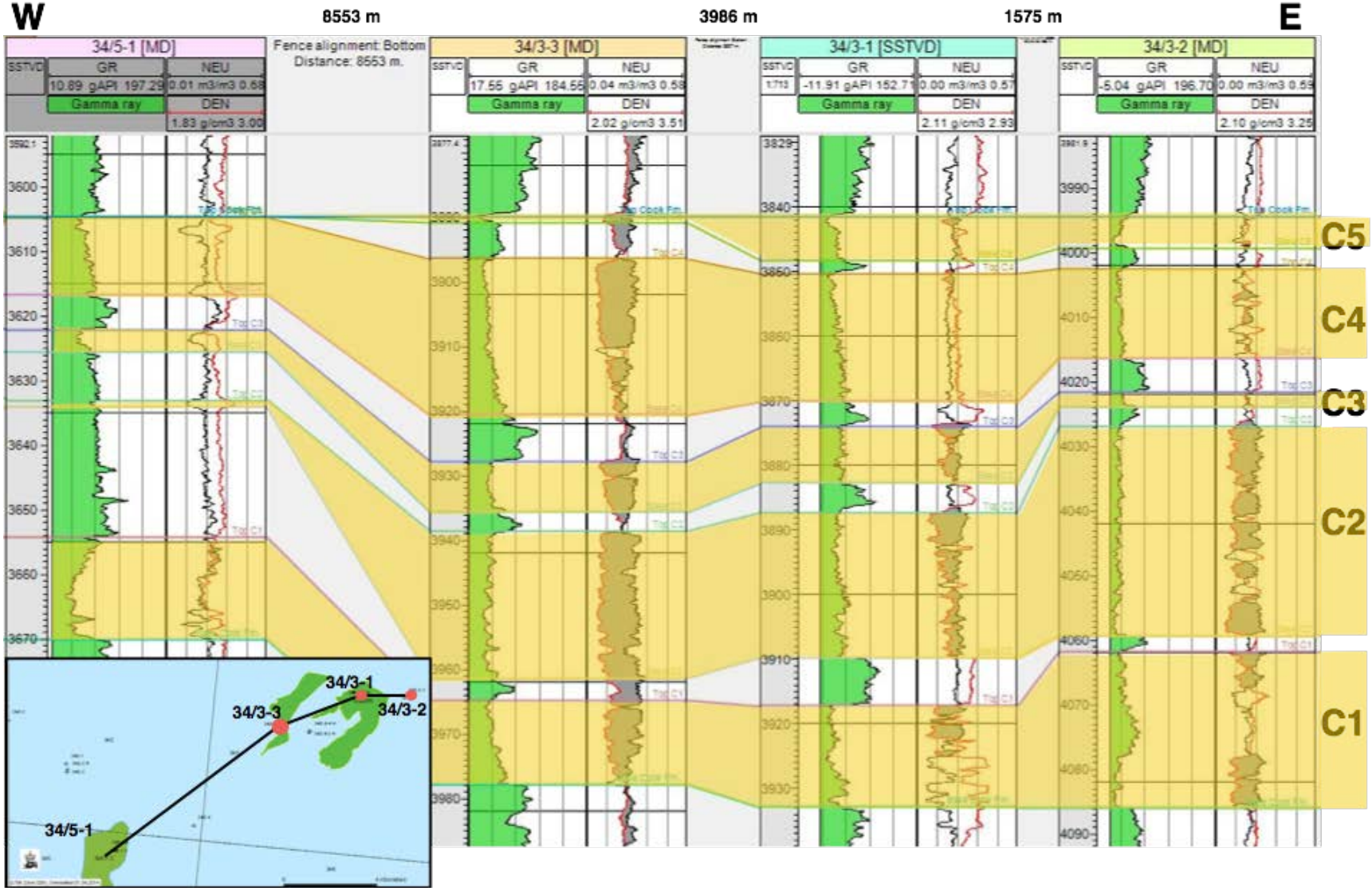

Figure 2.4 Well correlation between the four wells provided from the Knarr area. Note the small differences in thickness in well 34/3-2S, 34/3-1S and 34/3-3S

2.4 Depositional system of the Cook Fm.

Due to the extensive distribution of the Cook Formation different proposals of the depositional environment depending on location are reported in literature. Table 2.2 summarises the proposed depositional environments for the Cook Formation in several fields in the northern North Sea. Numerous sequence stratigraphic studies, among others Charnock et al. (2001), Marjanac and Steel (1997) and Dreyer and Wiig (1995), agrees that the laterally extensive Cook Formation has been deposited in a marine environment, including both shallow and deep settings depending on location in the basin.

Folkestad et al. (2012) divided the Cook Formation into upper and lower depositional environments (Figure 2.5B). In the Gullfaks Field a significant change in depositional environment can be observed from the lower to upper part. The sandstone units within the Cook Formation are most likely deposited in a variety of subenvironments. These subenvironments will be studied in more detail throughout this study and in Kjølstad (2014).

Table 2.2 Earlier works description and interpretation of the depositional environment of the Cook Formation. Figure 2.5A illustrates the location of the fields described.

Location	Depositional environment	References
Oseberg Field	Subdivided into three units; Cook A, B and C. Cook A was deposited as a prograding subtidal sand body. Cook C was deposited as an offshore ridge, whereas Cook B separates Cook A and C.	(Livbjerg and Mjøs, 1989)
Gullfaks Field	Lower part of the Cook Fm. represents an offshore to lower shoreface environment on the distal parts of a wave-influenced shelf. The upper unit was interpreted as a marginal to shallow marine deltaic setting characterized by tidal influence.	(Dreyer and Wiig, 1995) (Folkestad et al., 2012) (Livbjerg and Mjøs, 1989, Marjanac and Steel, 1997)
Snorre Field	Offshore mudstones.	(Underhill, 1998) (Nystuen and Fält, 1995)
Statfjord Field	Marine shoal sands.	(Dalrymple, 2001)
Horda platform	The Cook Formation is characterised by estuarine and marine shoreface sandstones deposited during periods of lowstand incision, progradation and transgression.	(Charnock et al., 2001)

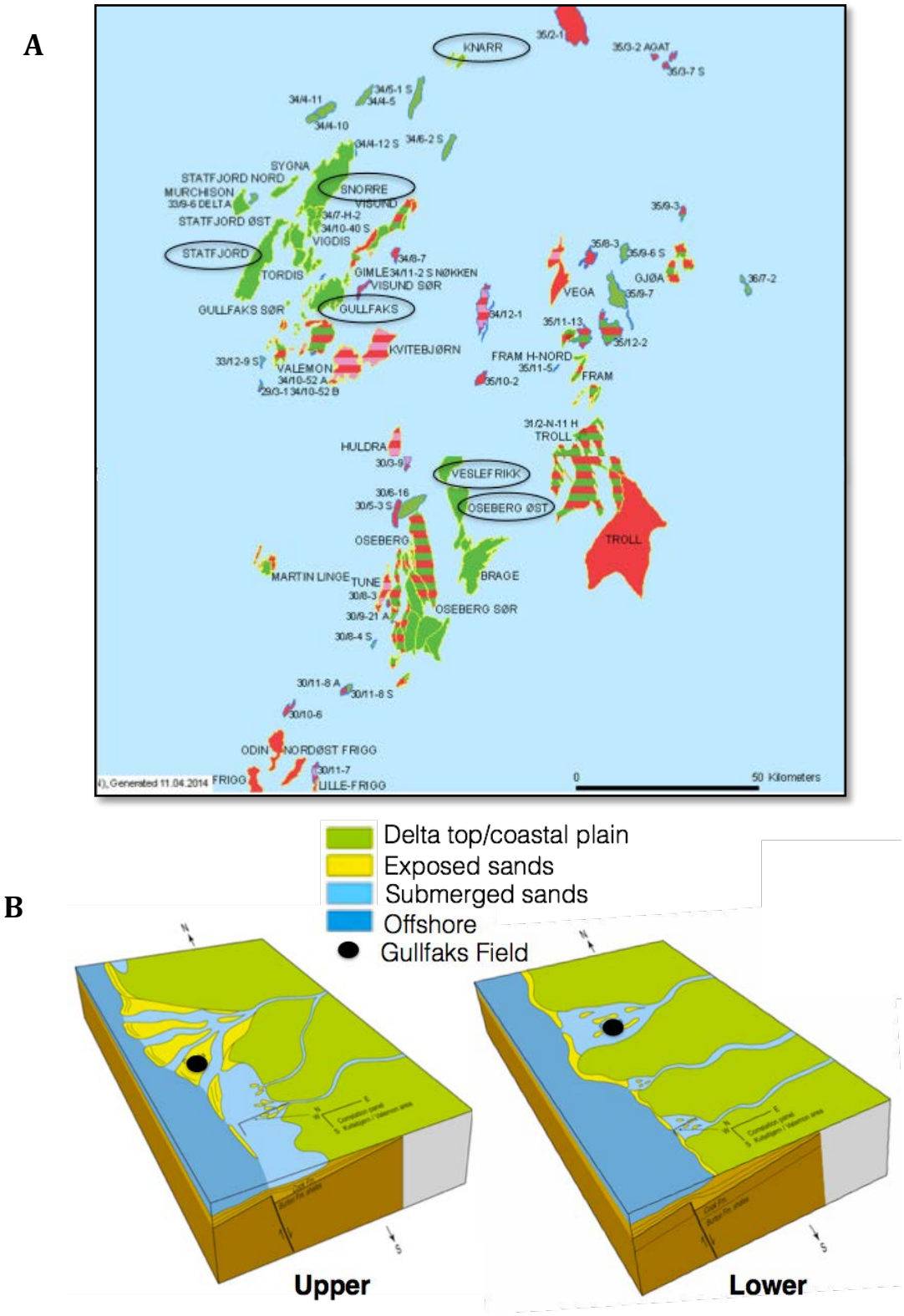

Figur 2.5 A) Map of some of the fields was the Cook Formation is present. B) The upper and lower depositional environment of the Cook Formation suggested by Folkestad et al. (2012). Note the significant changes in depositional environment from lower and upper setting in the Gullfaks Field. Similar changes are most likely to be found within the Cook Formation in the Knarr area.

3 Theoretical background

3.1 Introduction

Sandstones buried to a depth of about 3500 meters have been exposed to a large range of mechanical and chemical diagenetic processes. Quartz cement is commonly the most detrimental factor for the reservoir quality in these sandstones, since the cement causes reduction in porosity by filling the available pore spaces (Ehrenberg, 1990). Porosity preserving mechanism may prevent the growth of cement, and thereby preserve the reservoir quality at great depths. Both porosity preserving mechanisms and cement are determined by the initial composition of the sandstone, which is linked to facies and the depositional environment. Consequently, the initial mineral composition, grain size and texture are important factors regarding chemical and mechanical diagenesis of sandstone and prediction of reservoir quality at great depths.

This chapter comprises general information about the main diagenetic processes acting on sandstones prior to, during and after burial. A special emphasis was put on the quartz cementation and the porosity preserving mechanism chlorite coating in intermediate to deeply buried reservoirs.

3.2 Diagenetic processes in sandstones

Texture, mineralogy and diagenetic processes control the primary composition of sandstone. Furthermore, the properties of the sandstone depend on the initial composition, temperature and stress, parameters that are important to understand in order to predict porosity and permeability of the reservoir sandstone. Diagenesis comprises all the processes that change the composition of sediments after deposition and prior to metamorphism. Diagenetic processes referred to in this thesis are:

- Early diagenesis
- Mechanical compaction
- Chemical compaction

However, the main focus will be on chemical diagenesis, precipitation of cement and porosity preserving mechanisms. Chemical processes influencing the reservoir properties in the Cook Formation reported in this thesis are:

- Feldspar dissolution and precipitation of kaolinite
- Carbonate cementation
- Albitization of K-feldspar
- Quartz cementation
- Precipitation of authigenic illite

Diagenetic processes in the sandstone will be described in a chronological order; beginning with the early diagenesis at shallow depth and on to the late diagenesis appearing in deeply buried sandstones.

3.3 Early diagenesis

The early diagenesis find place at shallow depth (<1-10m) including processes near the surface are included. Early digenesis in marine or meteoric environments may strongly influence the diagenetic reactions at deep burial (Bjørlykke, 1998).

Biogenic activity

Bioturbation change the textural composition of the sediments after deposition. This may reduce the permeability and porosity of the sand by mixing clay into the clean sand. Biogenic material from calcareous and siliceous organisms will be an important source of carbonate and silica cement at deeper burial depth (Morad, 1998). Consequently, the distribution of carbonate cement is related to facies and sequence stratigraphy. Regarding sequence stratigraphy, the carbonate cement may be controlled by transgressive and regressive events, as well as paleoclimate (El-Ghali et al., 2013). Furthermore, burrowing worms produce faecal material that may develop into smectite-rich clays, which in turn may develop into chlorite. This signifies how important the early diagenesis is for the diagenesis occurring at deep burial.

Meteoric water

Early diagenetic processes like meteoric water flushing and carbonate cementation are also linked to facies, and strongly influence the burial diagenesis and the reduction in porosity at depth (Bjørlykke and Jahren, 2010, Morad, 2009). Meteoric water will dissolve carbonates and unstable minerals like mica and feldspar in sandstones. Leaching and precipitation of minerals are functions of the flux of the groundwater flowing through the rock volume per

unit of time (Bjørlykke, 1998). To precipitate only a few percentages of kaolinite a total meteoric flow of 10^3 – 10^4 m^3/m^2 through the sandstone is required (Bjørlykke, 1994). The flow will then dissolve significant quantities of feldspars and mica and precipitate kaolinite. The reactions from feldspar to kaolinite and muscovite to kaolinite are presented in Formula 3.1 and 3.2 (from Bjørlykke, 1998).

Formula 3.1

$$2K(Na)AlSi_3O_8 + 2H^+ + 9H_2O \quad = Al_2Si_20_5(OH)_4 + 4H_4SiO_4 + 2K^+(2Na^+)$$

Feldspar = Kaolinite + dissolved silica + dissolved cations

Formula 3.2

$$2KAl_3Si_3O_{10}(OH)_2 + 2H^+ + 3H_2O = 3Al_2Si_20_5(OH)_4 + 2K^+$$

Muscovite = Kaolinite

A low ratio of K^+/H^+ is needed to form kaolinite. The exact temperatures for kaolinite to form are hard to calculate because of the uncertainty of the isotropic composition of the pore water. However, it is unlikely that it forms diagenetically at high temperatures (Bjørlykke, 1994). Dickite often replaces some of the kaolinite when temperatures exceed $100C^o$. The kaolinite is not usually pervasive through the sandstone, but is found locally. However, Bjørlykke and Aagaard (1992) has shown that the distribution of kaolinite in sandstones in the North Sea can be related to facies and climate. By comparing Permian and Triassic sandstones deposited in a dry climate with Jurassic sandstones deposited in a humid climate, a trend can be seen. Sandstones deposited in a dry climate contain less kaolinite than sandstones deposited in a humid climate.

Carbonate cementation

Carbonate cements in sandstones are dominated by calcite, dolomite, ankerite and siderite (Morad, 1998). Marine organisms composed of aragonite dissolve at shallow burial and precipitates as carbonate cement in pore spaces. There are commonly no other major sources of carbonate cement (Morad, 1998). Upper Jurassic and younger sandstones often contain abundant calcite cements due to a large amount of pelagic calcareous organisms that evolved during the Late Jurassic. Lower Jurassic sandstones also contains some calcite cement, but not to such a high degree as in the Upper Jurassic sandstones.

Carbonate cements are among the dominant components of diagenesis. Hence, they are of significant importance in determining the reservoir quality of sandstone sequences (Morad, 1998). Destruction of reservoir properties occurs when sandstones are massively cemented by carbonates, and act as barriers for water and hydrocarbons flow from source rock to reservoir. Furthermore, compaction of laterally continuous carbonate cemented sandstone may cause development of overpressure in the underlying, weakly cemented zones (Morad, 1998).

3.4 Mechanical compaction

Compaction of sediments is the process that reduces the sediment volume during progressive burial. It is an important process in sedimentary basins because it causes changes in physical properties of the sediments during burial. As a result, changes in physical properties such as porosity, density and velocity are functions of mechanical and chemical processes (Mondol et al., 2007). Clastic sediments compact mechanically at temperatures below 70-80 C^o, corresponding to depth from 0-3km (Ramm, 1992). At greater depth the compactions is chemical, and mostly a function of temperature (Bjørlykke, 1999).

Mechanical compaction is a function of effective stress, whereas the effective stress controls the compaction by the weight of the overburden. The process starts immediately after deposition. Physical processes that is involved during compaction is reorientation and fracturing of brittle grains and plastic deformation of ductile components (Berner, 1980). For well-sorted arenites consisting of component grains the mechanical compaction diminishes after only a small reduction in porosity. This is due to the increasing stability and resistance to reorientation of angular grains in such sandstones (Palmer and Barton, 1987). Sandstones with a higher degree of clay matrix, mica or rock fragments will undergo a more severe loss of porosity. For that reason, the susceptibility of mechanical compaction is related to the amount of ductile grains in the sandstone (Rittenhouse, 1971).

3.5 Chemical compaction

3.5.1 Intermediate buried sandstones

Intermediate buried sandstones are sandstones buried to a depth of about 2000-3500 m bsl, corresponding to temperatures of about 50-120C^o. At this depth quartz cement effectively prevent further mechanical compaction, and chemical diagenesis control the processes.

Albitisation of detrital plagioclase is one of the most important changes that occur in feldspathic sandstones at this depth (Boles, 1982). The albitisation process starts at about 65C^o and ends at about 105C^o (Saigal et al., 1988). During albitisation of plagioclase Ca_2^+ will be released and may precipitate as calcite, but the amount is limited.

3.5.2 Deeply buried sandstones

Commonly at this depth, >3500-4000m (>120C^o), the cementation is rampant and fills the pore spaces. Furthermore the kaolinite has been dissolved and replaced by illite. The illitisation process is an important diagenetic process in deeply buried sandstone, together with quartz overgrowth (Bjørlykke et al., 1995).

Sandstones with abundant smectite have poor reservoir quality. Illitisation of smectite-rich sandstones can improve the reservoir quality, because illite has a lower specific surface area than smectite. However, due to the fibrous state of illite a reduction in permeability will take place resulting in a poor reservoir quality. It grows at the expense of kaolinite and from alternation of smectite.

Illite is commonly found as a replacement of an earlier Al-rich mineral phase, like kaolinite (Bjørlykke, 1998). Formation of illite from smectite occurs in sandstones at about 70-100C^o. K-feldspar is the most common source of potassium, and therefore required for formation of illite as shown in Formula 3.3 (from Bjørlykke et al., 1995). However, illite may also form from a different reaction, where also albite is formed as shown in Formula 3.4 (from Bjørlykke et al., 1995).

Formula 3.3

$$KAlSi_3O_8 + Al_2Si_2O_5(OH)_4 = KAl_3Si_3O_{10}(OH)_2 + 2SiO_2 + H_2O$$

K-feldspar + Kaolinite = Illite + Quartz

Formula 3.4

$$2KAlSi_3O_8 + 3Al_2Si_2O_5(OH)_4 + 2Na^+ = 2KAl_3Si_3O_{10}(OH)_2 + 2NaAlSi_3O_8 + 2H^+ + 3H_2O$$

Kaolinite + K-feldspar = Illite + Albite

The reaction between K-feldspar and kaolinite occurs at about $130C^o$. The two minerals are not thermodynamically metastable below 130C°. A significant increase in illite content at 3700-4000 m depth is seen in the North Sea (Bjørlykke and Aagaard, 1992) and at Haltenbanken (Ehrenberg, 1990). These depths correspond to temperatures of 120 – 140C°. If sandstone is derived from albite-rich gneiss the K-feldspar content is likely to be too low and hence much of the kaolinite would not be illitised. Consequently, illite would not be formed in sandstones with little kaolinite or smectite content.

3.6 Quartz cementation

Quartz cementation is the main processes causing overall reduction in porosity during deep burial in quartz rich sandstones on the Norwegian continental shelf (Ehrenberg, 1990). The preservation of porosity therefore relies on factors inhibiting quartz cementation and mechanical compaction. Modelling of quartz cementation has proved to be very useful regarding porosity as a function of the temperature history of the reservoir sandstones. Temperature, time and quartz surface area available control the progress of quartz cementation within sandstone. Consequently, grain size, detrital grain mineralogy and abundance of grain coatings are crucial input parameters for quartz cementation. Provenance and the depositional environment control these input parameters (Walderhaug et al., 2000).

Distribution and origin of quartz cement

Significant quartz cementation corresponds to temperatures of about 70-80C^o (Bjørlykke et al., 1989). Walderhaug et al. (2000) suggest that quartz cementation involves three steps: quartz grain dissolution at the contacts between the quartz grains and clay or mica, short range diffusional transport of the dissolved silica, and precipitation as syntaxial quartz overgrowths on the surfaces of detrital quartz grains. The amount of quartz cementation may vary with differences in grain size, quartz clast content and the degree of grain coatings (Walderhaug et al., 2000).

Prediction of quartz cement and its distribution must be based on the burial history, temperature and pressure, and also on the local sandstone petrography which can determine rates of dissolution and precipitation of quartz (Bjørlykke and Egeberg, 1993). The distribution of quartz cement can be related to mineralogy, grain size and stylolites. Fine-grained sands tend to have an increasing amount of quartz cementation compared to coarser sands, due to the increased surface area available for quartz precipitation (Walderhaug, 1996). Furthermore, the mineralogy of the sands plays a role in order to precipitate quartz cement. Pure quartz sands get more rapidly quartz cemented than arkosic sands, due to a higher degree of available surface area in pure quartz sandstone (Walderhaug, 1996).

3.6.1 Stylolites

Walderhaug et al. (2000) defines stylolites as all clay rich or micaecous laminae where quartz is dissolved within the laminae because of the catalytic effect of clay and mica on quartz dissolution. This definition includes that all features of clay and mica is considered a stylolite, from single mica grains to laminae with tens of meters of lateral extent. The silica dissolved at stylolites with some lateral extent is transported by diffusion to the grain surfaces where the quartz overgrowth forms (Bjørlykke and Jahren, 2012) (Figure 3.2). Consequently there is a correlation between the distance to the nearest stylolite and the volume of quartz cement. Quartz cement will then decrease away from stylolites. Walderhaug and Bjørkums (2003) study suggest that sandstones with exceptionally few clay-rich or micaeous laminae and without clay or mica individual grain contacts have significantly less quartz cement than other sandstones exposed to similar temperature histories. With this definition of stylolites and evidences for quartz grain dissolution at stylolites in deeply buried sandstones on the Norwegian shelf, stylolite may be the dominant source of quartz cement (Walderhaug et al., 2000) in sandstones. Low abundance of stylolite precursors may be of only local importance for preserving reservoir quality on the Norwegian Continental Shelf (Walderhaug and Bjørkum, 2003).

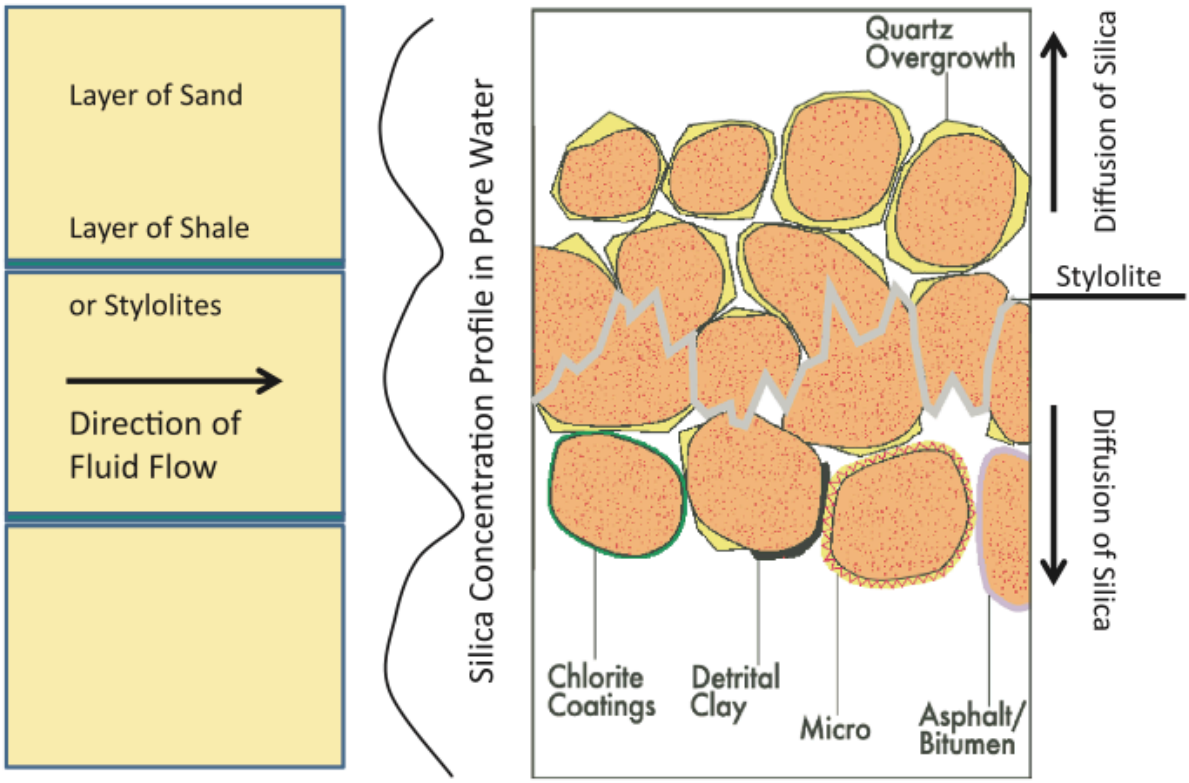

Figure 3.2 Illustration of a stylolite. The silica is transported away from the stylolite by diffusion, a transportation method that makes it difficult to transport the silica over long distances. Note also how different grain coatings prevent the growth of authigenic quartz (Bjørlykke and Jahren, 2012).

3.7 Porosity-preserving mechanisms

The diagenetic history of sandstones, from shallow to deep burial, will affect the reservoir quality. Mechanical compaction and quartz cementation is shown to be the most porosity reducing factors. For the porosity to be preserved at deep burial porosity-preserving mechanisms is needed. There are three main factors reported in literature that preserves porosity to great depths; grain coatings, early hydrocarbon emplacement or fluid overpressure (Bjørlykke and Jahren, 2010, Bloch et al., 2002). However, early hydrocarbon emplacement and fluid overpressure will not be discussed in detail here because they have a minor effect on this particular reservoir.

3.7.1 Grain coating

Grain coating minerals, such as authigenic chlorite and microquartz, have been observed as porosity preserving mechanisms in several sandstones within the North Sea region (e.g. Ehrenberg, 1993). In this study, the main emphasis will be on the authigenic chlorite.

Grain coating chlorite

Grain coating chlorite is the most widely described grain-coating mineral in the literature, and chlorite coating are reported from a large number of settings worldwide, for example in the Vicksburg Formation in South Texas (Grigsby, 2001), the Sawan gas field in Pakistan (Berger et al., 2009), and the Jurassic Tilje, Tofte, Garn, Statfjord and Intra-Dunlin Formations in the North Sea (Ehrenberg, 1993).

Grain coating chlorite only exists at temperatures above 80-100 C^o(Aagaard et al., 2000). Commonly, the chlorite is divided into two categories, Fe-rich and Mg-rich. The Fe-rich chlorites are most common in marine settings, whereas the Mg-rich chlorite is most likely found in arid to semi-arid continental deposits (Maast, 2013). The porosity variations in clean sandstones is often correlated with an abundance of grain-coating chlorite and lack of quartz cementation (Ehrenberg, 1993).

Precipitation of chlorite requires a Fe and Mg source. Possible sources are clastic biotite, basic rock fragments and volcanic rock fragments or early diagenetic Fe minerals formed in deltaic or estuarine environments by the supply of Fe from rivers (Bjørlykke, 1998). Near the river mouth, increase in salinity causes the Fe to be flocculated and deposited, mainly in an amorphous and therefore highly reactive state. This forms a layer of clay-rich, gel-like material from which ooids could be formed at points of maximum current energy (Ehrenberg 1993). According to Ehrenberg (1993) an important factor controlling the occurrence of chlorite-rich sand zones is the abundant supply of reactive, amorphous Fe-hydroxides delivered by local river discharge. The geometry of the distribution of chlorite is mainly dependent on the sedimentary facies architecture and the pattern of paleo-river discharge into the architecture (Ehrenberg, 1993).

3.7.2 IGV – Intergranular volume

Intergranular volume (IGV) is the degree of porosity loss by mechanical compaction at the onset of chemical compaction, and is a function of grain size. IGV is the porosity prior to quartz cementation and is about 25-30% for well-sorted quartz rich sandstone. Generally, in the North Sea the IGV varies from 28-38% (Maast, 2013). The IGV is the sum of pore spaces, cements and detrital matrix:

$$IGV\ (\%) = V_{intergranular\ porosity} + V_{intergranular\ cement} + V_{detrital\ matrix}$$

4 Methods and Data

4.1 Introduction

In order to get reasonable results and detect uncertainties throughout this study, several levels of investigation have been carried out. The methods used have different resolution and subsequently measurement errors may occur. Methods include:

- **Petrographic analysis**
  - Thin section analysis
  - Scanning Electron Microscopy (SEM)
- **Petrophysical evaluation**
  - Well correlation
  - Well log interpretation and porosity estimation
  - Cross plotting
- **Core description**
  - Facies analysis and facies associations

Referencing in this study

Depths in this study are, if no other is stated, in measured depth (MD). Polycrystalline- and monocrystalline quartz have all been counted as quartz during the point counting process. Additionally, all feldspars are counted as K-feldspar. Secondary porosity, and its impact on reservoir quality, is not addressed in this thesis. The mudprone facies in between the sandstone intervals has not been investigated in this study, as it is outside the scope of this thesis. A more complete analysis of the mudprone intervals is described in (Kjølstad, 2014).

4.2 Petrographic analysis

This study presents 23 thin sections from 3 wells in the Knarr area. 12 thin sections from well 34/3-1 S, 7 from 34/3-2 S and 4 from 34/3-3 S have been analysed in great detail to understand the reservoir quality within the different sandstone units. Furthermore, textural analysis has been carried out in order to determine if the different sandstones have been deposited in different environments.

4.2.1 Thin section analysis

The petrographic microscope makes it possible to examine a two-dimensional cross section through the sandstone, estimate the bulk mineral composition, and make important observations regarding composition and texture.

23 sandstone samples were examined in thin section using a standard petrological microscope. Thin sections were point counted at a rate of 300 points per sample, and the results recorded in a spreadsheet. Carbonates and feldspars had chemical staining and were therefore more easily identified. Textural features were added from a visual scan of the entire slide, and grain size measurements were conducted using the software ImageJ. Grain size was measured on 50 grains from each thin section, and these measurements were inserted to the grain size analysis program GRADISTAT v 4.0 created by Blott (2000).

4.2.2 SEM

With the Scanning Electron Microscopy (SEM) one has the ability to look down into the pores, identify the smallest minerals, and examine the distribution of these minerals within the pores. The Scanning Electron Microscope type JEOL JSM-6460LV with LINK INCA Energy 300 (EDS) from Oxford Instruments was applied with a standard wolfram filament of 15kV. The scanning electron microscope allows examination of rough surfaces at a magnification range from x20 to x200 000. However, the purposes of examining the general characteristics and porosity of clastic rocks, magnifications from x300 to x100 000 were most suitable. The samples were glued onto aluminium stubs and coated with gold to obtain an electrically conducting surface. Furthermore, an elemental analysis was performed with the SEM, whereas the peaks in the spectrums were identified in order to determine the different minerals. The SEM Petrology Atlas by Welton (2003) where frequently used for the identification of spectrums.

Investigation of the authigenic chlorite and quartz cementation will contribute to see lateral differences within the sandstone intervals of the Cook Formation. SEM analysis was performed on 12 thin sections and 12 stubs. General studies of the mineralogy from all three wells were also attained.

Detailed analysis of chlorite

In order to understand the origin of the chlorite coating in the sandstone sequences, the chlorite grains were studied in the SEM. Samples from sandstone unit C2 from all three wells where crushed in an ethanol-filled agate mortar. A drop of this dilute alcohol suspension were placed on a graphite plate. As the alcohol evaporated the sample were studied in the SEM and the composition of the chlorite could be identified. The general formula for chlorite is $(Mg,Fe,Al)_6(Al,Si)_4O_{10}(OH)_8$. The composition of the chlorite was calculated for Si, Mg, Fe and Al using Equation 4.1.

Eq. 4.1

$$(\frac{Mg}{X}\frac{Fe}{X}\frac{Al}{X}\frac{Si}{X})x = 28$$ *where X is either Si, Mg, Fe or Al.*

4.2.3 XRD

X-ray powder diffraction (XRD), is an instrumental technique that is used to identify minerals. XRD results were provided from well reports by BG Norge, and the technique it self has not been carried out in this study. However, the provided XRD results will complement the mineralogical methods, such as optical light microscopy and scanning electron microscopy.

4.2.4 Uncertainties regarding petrographic analysis

Several uncertainties must be considered for the petrographic analysis. First, by including more samples in the study a more detailed research could be implemented. Misinterpretation of minerals during thin section analysis and point counting may happen. 300 counts for the point counting only gives an estimate, more counts could be needed for more accurate research. Furthermore, too many and too large pores may occur during thin section preparation. 50 grains from each thin section where included in the grain size analysis, this might give partly inaccurate measurements of the grain sizes. Misreading of grain sizes due to quartz overgrowth and cementation may also occur.

For the SEM analysis, preparation of stubs may give unnatural features that could be interpreted as natural features. Additionally, confusion of the spectrums may give an impression of minerals that might not be present. However, the interpretation of spectrums were, in addition, based on the experience of the SEM operator (Berit Løken Berg) and the

use of the SEM Petrology Atlas (Welton, 2003). For the chlorite analysis more chlorite grains could be investigated in order to get a more accurate average composition of the chlorite.

4.3 Petrophysical evaluation

4.3.1 Well correlation and interpretation of well logs

For the well correlation the three wells provided in this study were correlated with a fourth well (34/5-1 S), in order to achieve a better overview of the sandstone units and their lateral and vertical distribution. The correlation was carried out using the software Petrel, whereas information from NPD has been an important contributor. Porosity logs and lithology logs were calculated, and further compared with logs made from cores. Well logs provided in this study are caliper, sonic, gramma ray, neutron, resistivity and density.

4.3.2 Porosity measurements

The porosity was calculated from the provided well logs using different equations (Eq. 4.5 and Algorithm 4.2 and 4.3), whereas the parameters are listed in Table 4.1.

The bulk density of pure sandstone is found

$$\rho_b = \phi * \rho_f + (1 - \phi)\rho_{qz} \qquad \textbf{(Eq. 4.2)}$$

Sandstone with shale:

$$\rho_b = \phi * \rho_f + V_{sh}\rho_{sh} + (1 - \phi - V_{sh})\rho_{qz} \qquad \textbf{(Eq. 4.3)}$$

Porosity equation:

$$\phi = \frac{(V_{sh}(\rho_{sh} - \rho_{qz}) + \rho_{qz} - \rho_b}{(\rho_{qz} - \rho_f)} \qquad \textbf{(Eq.4.4)}$$

If the density of the shale is the same as the density of the pure sandstone, the equation is:

$$\phi = \frac{(\rho_{qz} - \rho_b)}{(\rho_{qz} - \rho_f)} \qquad \textbf{(Eq. 4.5)}$$

The magnitude of the gamma ray is related to the shale content of the formation of interest. A shale-sand boundary was set at 60API, whereas gamma ray readings above 60 correspond to shale and below corresponds to sand. Consequently, the volume of shale is of importance for porosity calculations. V_{sk} is a fraction of the bulk volume of the rock and volume of the shale. For this study, the volume of shale were calculated using the non linear empirical Equation 4.6 for older rocks by Larionov (1969) (Eq. 4.6).

$V_{sh} = 0{,}33(2^{(2-IGR)} - 1)$ **(Eq. 4.6)**

Where IGR is the Gamma Ray Index shown in Equation 4.7.

$IGR = \frac{GR_{log} - GR_{clean}}{GR_{shale} - GR_{clean}}$ **(Eq. 4.7)**

For Equation 4.7 the gamma ray values for shale, GR_{shale}, where set to be the mean gamma ray readings for shale (Table 4.1). The gamma ray values for clean sand, GR_{clean}, were set to be equal to the minimum gamma ray reading (Table 4.1).

Porosity was corrected for using the calculated $V_{sh,}$ resulting in the final porosity equation (Eq. 4.8).

$\phi = \frac{(V_{sh}(\rho_{sh} - \rho_{qz}) + \rho_{qz} - DEN}{(\rho_{qz} - \rho_f)}$ *where DEN is the density from the density log.* **(Eq. 4.8)**

Table 4.1 Table of parameters used in the porosity calculations.

Well	Min. GRclean	Average GRshale	Density of shale	$\rho_{sh} - \rho_{qz}$	Density of matrix	Fuid density	Density of drilling mud
34/3-1	26,72	79,6	2,55	-0,1	2,65	1,01	1,03-1,87
34/3-2	20,06	68,4	2,58	-0,07	2,65	1,01	1,37-1,92
35/3-3	33,38	75,44	2,48	-0,17	2,65	1,01	1,03-1,80

Some of the described well logs can be used in analysing porosity, facies, environments and sequences, which was the aim for this thesis. Using Algorithm 4.1, where the meaning of the values is described in Table 4.2, performed a coarse construction of lithology.

Litho_facies= If(GR>20 And GR<60,0 ,1) **Algorithm 4.1**

Table 4.2 Lithologies used in Algorithm 4.1 with their corresponding numbers and gamma ray values.

Number	Gamma ray value	Lithology
0	>20 and <60	Sand
1	>60	Shale

The construction of porosities from the density log was executed using Algorithm 4.2. In Algorithm 4.2 the values used are found in Table 4.1, where DEN is the log value. Porosities calculated from the bulk density were obtained using input values from Table 4.1. Volume of shale is not included in this algorithm.

Density_Por=(2.65-DEN)/(2.65-1.01) **Algorithm 4.2**

4.3.3 Cross-plotting

A cross-plot shows relations between different plotted quantities. It usually produces a scatter plot that is used in lithology, mineralogy, saturation and hydrocarbon determination. By cross-plotting two values the result can be used to define the relationship between the two variables, or to define the upper and lower limits of the variables Rider and Kennedy (2011) suggest that three types of log cross-plots exists:

- Cross-plots of compatible logs, such as porosity. This is usually performed in order to define lithology.
- Cross-plots of incompatible logs, such as gamma ray and resistivity. The two logs do not measure the same parameter. This method is commonly used to quantify lithology and fluid content.

In this study, Excel, Interactive Petrophysics (IP), Hampson Russel (HR) and Petrel were used interactively to make the wanted cross-plots, well correlation and porosity measurements.

4.3.4 Uncertainties regarding petrophysical evaluation

Porosity calculation from the well logs described requires knowledge of the parameters related to the rock in investigation. Determining such parameter may be difficult if there are uncertainties regarding the lithology. For this study, it is assumed that the sandstone is clean with a matrix density of 2,65 (clean quartz). The fluid density is based on the density of water and the density of the drilling mud (Table 4.1), and is assumed to be 1,01g/cm^3. However, the sandstone of the Cook Formation in the Knarr area comprises calcite cement, drilling fluids and hydrocarbons that may all affect the chosen parameters. In this study, uncertainties are addressed by a variety of cross-plots that can act as a quality check for parameters used.

4.3.5 Core description

Core photos provided by BG Norge were used for the making of sedimentological core logs (Appendix A), whereas grain size of the cores were based on interpretation by Kjølstad (2014). Description of facies and facies associations were made mainly based on observations from core photos. Furthermore, the core logs were compared with wire line logs for quality check and further interpretation. Uncertainties regarding core description are of course the non-presence of the cores and the lack of an outcrop displaying large-scale features, resulting in misinterpretation of sedimentological structures within the cores.

5 Sedimentological results

5.1 Introduction

Core description and sedimentological logs (Appendix A) will provide a tangible description of the facies and facies associations within the Cook Formation, resulting in improved understanding of the depositional environment. Table 5.1 lists the thicknesses of the five sandstone units and the cored intervals studied. The three wells studied are located within a total bottom hole distance of 5560 m, whereas the distance between well 34/3-2 S and well 34/3-1S is 1580 m and the distance between well 34/3-1 S and well 34/3-3 S is 3990 m (Figure 2.4).

Facies has been described by the characteristics of its lithology, texture and sedimentary structures, as well as electrical logs. These characteristics aid in determining the processes that where active during the time of deposition. By recognising the associations of the proposed facies it is possible to establish a combination of processes that were dominant in the Cook Formation in the Knarr area. In uncored wells facies will be determined using only electrical logs. Based on core description and facies analysis, a link between facies associations and depositional environments can be drawn, and will be further discussed in Chapter 8.

Table 5.1 Top and bottom burial depth (m bsf) of the five interpreted sandstone bodies within the Cook Formation in well 34/3-1S, 34/3-2S and 34/3-3S. Cored intervals are also presented.

	34/3-1S		34/3-2S		34/3-3S	
Sandstone unit	**Depth (m bsf)**	**Thickness (m)**	**Depth (m bsf)**	**Thickness (m)**	**Depth (m bsf)**	**Thickness (m)**
Top Cook Fm.	3456,37	6,9	3603,4	4,8	3507,86	1,0
Base C5	3463,24		3608,22		3508,83	
Top C4	3465,32	19,7	3611,5	13,8	3514,37	24,2
Base C4	3485		3625,28		3538,53	
Top C3	3489	8,6	3630,53	2,3	3545,76	7,9
Base C3	3497,63		3632,82		3553,61	
Top C2	3502,27	22,4	3635,78	32,5	3556,53	22,8
Base C2	3524,67		3668,26		3579,3	
Top C1	3532,19	15,7	3670,72	24,3	3582,69	13,3
Base Cook Fm.	3547,84		3694,99		3595,85	
Cored interval (MD, m)	**3868 – 3932,5 (C2-C5)**		**4053 – 4079,85 (C2)**		**3910,85 – 3981(C1-C5)**	

5.2 Facies

Facies analysis was based on the provided core photos and electrical logs. Gamma ray patterns (Figure 5.1), neutron and density logs contribute to the facies analysis, and were the main tool for analysing uncored intervals in this study (Table 5.1). The observed facies are summarised in Table 5.2.

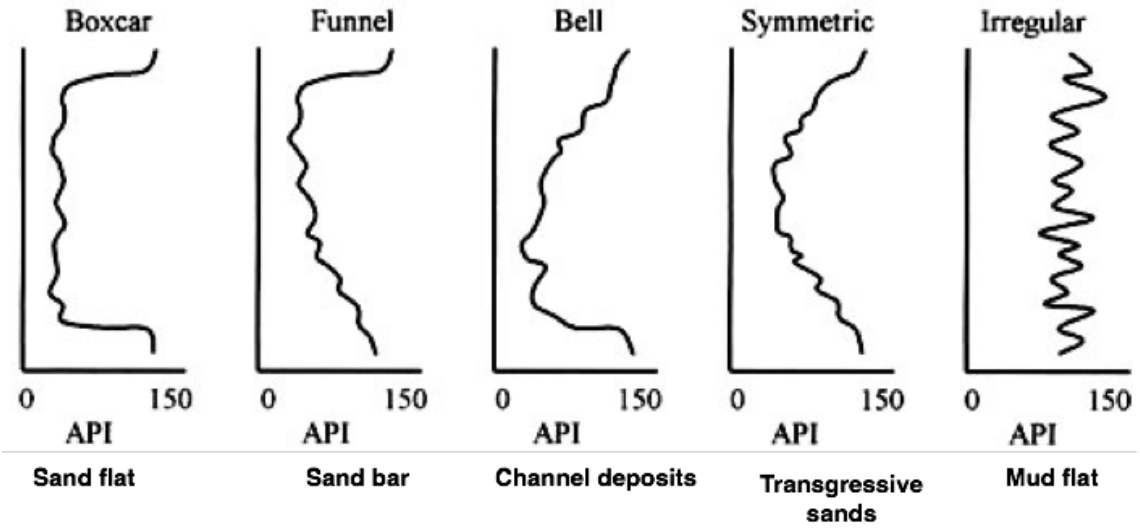

Figure 5.1 Simple gamma ray log patterns used for suggesting facies associations in Table 7.3 (based on Cant, 1992).

The textural changes and grain size changes between sedimentary layers make it possible to distinguish the different layers. Furthermore, an increase in clay content is correlated to a decrease in grain size and increase in gamma ray reading (Figure 5.1). The most common layers encountered within the studied cores are cross-stratified sandstone, laminated sandstone, interlayered sandstone and mudstone. Among these, cross-stratified sandstone of different types was observed most frequently. Cross-stratification within dunes was observed by its relatively large scale cross-bedding with steeply dipping lamina. Small symmetrical undulations were recognised as current ripple lamination. Lenticular bedding was observed as isolated ripples of sandstone surrounded by mudstone. Intervals with almost equal proportions of fine sandstone and mudstone the beds were characterised as wavy (Figure 5.2). Mud drapes were observed in wave and current ripple laminated sandstones as thin layers of mudstone (Figure 5.2). Furthermore, bioturbation was observed frequently, and occurred as a change in texture and mixing of sediments (Figure 5.2).

Table 5.2 describes briefly the observed facies of the studied cores. Lithology is divided into sandstone, heterolithics and mudstone, whereas sedimentary structures and bioturbation subdivides the lithology into five facies.

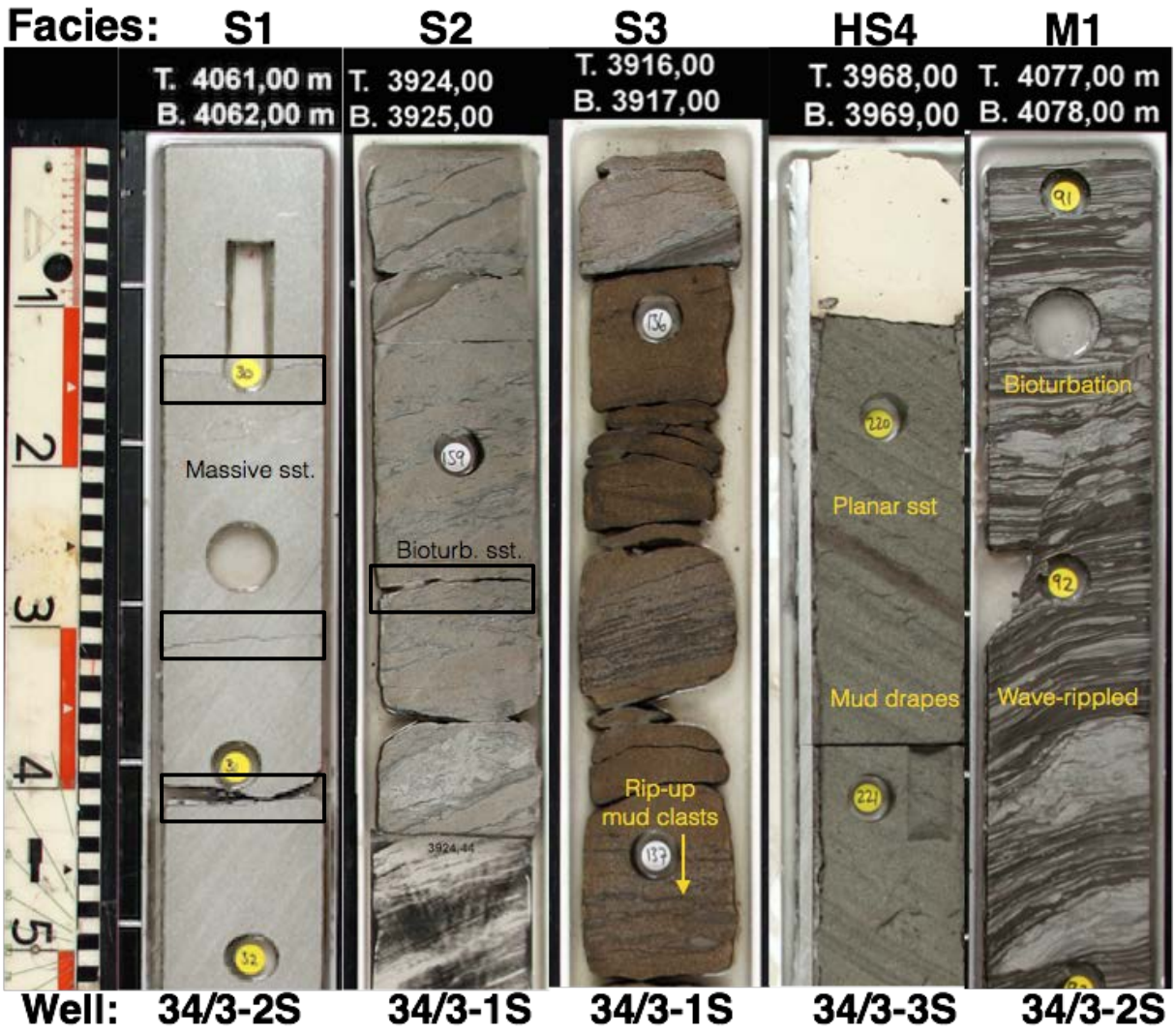

Figure 5.2 Core photos representing the observed facies from Table 7.2. Possible stylolites are illustrated in balck squares.

Table 5.2 Observed facies from the cored sections in all three wells, Figure 5.2 illustrates representative core photos of all observed facies.

Facies	Lithology	Grain size	Bioturbation	Description	Sedimentary structures	Common appearance	Reservoir potential
S1	Sandstone	m/c	Minor	Massive, structureless sandstone. Well sorted. Low gamma ray readings with a boxcar/irregular shape.		Within sandstone units	Very good
S2		f	Moderate	Sandstone with mud beds. Moderate to well sorted.	Current ripples, mud drapes, swaley cross-stratification and dunes. Interlayered sand/mud bedding.	Within sandstone units	Moderate - good
S3		m/c	Minor	Upward coarsening, sandstone. Funnel shaped gamma ray curve.	Dunes, cross-stratification, mud clasts and mud drapes,	Within sandstone units	Good
HS4	Heterolithic sst.	f	Minor	Sandstone with alternating thin layers of mud.	Flaser bedding, current ripples and mud drapes.	Base of coarsening upward units	Poor - moderate
M1	Mudstone	Clay/silt	Intense	Silty mudstone with high gamma ray readings.	Wavy ripple cross-lamination. Lenticular bedding.	Above flooding surface	Poor - none

5.3 Facies association

Facies outlined in this study form an apparently conformable succession of dominantly fine to coarse-grained sandstones sharply separated by mudstone intervals (Table 5.2). The dominance of cross-stratification, mud drapes, mud clasts and ripples is important aspects regarding interpretation of facies association (Table 5.3), and indicates that these sediments are most likely deposited in a tide-dominated environment. Cook Formation deposits can be divided into four facies associations; tidal channels, sand sheets, tidal bars and transgressive mud. Description and interpretations of these facies associations are presented.

Tidal channel deposits

Cross-stratification and cross-lamination are sedimentary structures commonly observed in channel settings (Miall, 1985) (Facies S2/S3, Figure 5.5). Point bars are channel deposits that consist of stratified and laminated sandstone (Facies S3) with mud in the upper part (Facies M1, Figure 5.5B). Channel deposits is often characterised by upwards-fining sandstone (Figure 5.1 and 5.3). Upward-fining trends show evidence for decrease in flow velocities from channel thalwegs onto adjacent channel point bars (Nichols, 2009). Channel deposits are characterised by fine-grained mud and silt, and the animal life present on these flats result in extensive biotubation (Facies M1).

Tidal sand flat deposits

Flaser bedding (Facies HS4), small-scale cross stratification and current ripples (Facies S2 and S3, Figure 5.5D) are the most common sedimentary structures seen within tidal sand flat associations. The gamma ray pattern is generally boxcar-like (Figure 5.1). Sand flats forms in the subtidal zone where the energy level is relatively high (Figure 5.3).

Tidal sand bar deposits

Tidal inclined beds containing heterolithic cross-stratified sandstones (Facies HS4), relatively homogeneous cross-stratified sandstones (Facies S1 and S3) and moderate bioturbated sandstones (Facies S2, Figure 5.5A) are commonly observed throughout the cored intervals (Figure 5.4). Furthermore, moderate gamma ray readings decreasing upwards, resulting in a funnel-shaped gamma ray pattern (Figure 5.1) is observed for this facies association (Figure 5.3). Consequently, these inclined beds are interpreted as tidal bars within a subtidal environment (Figure 5.3).

Mud bank deposits

Lenticular lamination (Facies M1) and finely interlayered sand and mud (Facies HS4) seem to be the dominant sedimentary structures within the mud bank association (Table 5.3). Very high gamma ray readings indicate sediment starvation and concentration of organic-rich clay at some sites (Figure 5.4). Futhermore, extensive bioturbation by a rich trace fossil assemblage suggests relatively open marine conditions (Figure 5.5B).

Table 5.3 Facies associations based on lithofacies analysis and electrical logs. In Figure 5.4 the different facies associations are located based in their gamma ray patterns and density – neutron values. Figure 6.3 illustrates a conceptual model of the suggested facies associations.

Facies	Facies associations	Interpretation	Description	Common gamma log patterns
HS4 S2	**FA 1**	Tidal channel	Deposited in the inter-subtidal zone.	Boxcar
S2 S3 HS4	**FA 2**	Tidal sand flat	Deposited in high energy, subtidal environment.	Bell
S1 S2 S3	**FA 3**	Tidal sand bar	Deposited in a subtidal environment.	Funnel
M1	**FA 4**	Mud bank	Deposited over the sandstone surface during relative sea level rise.	Irregular

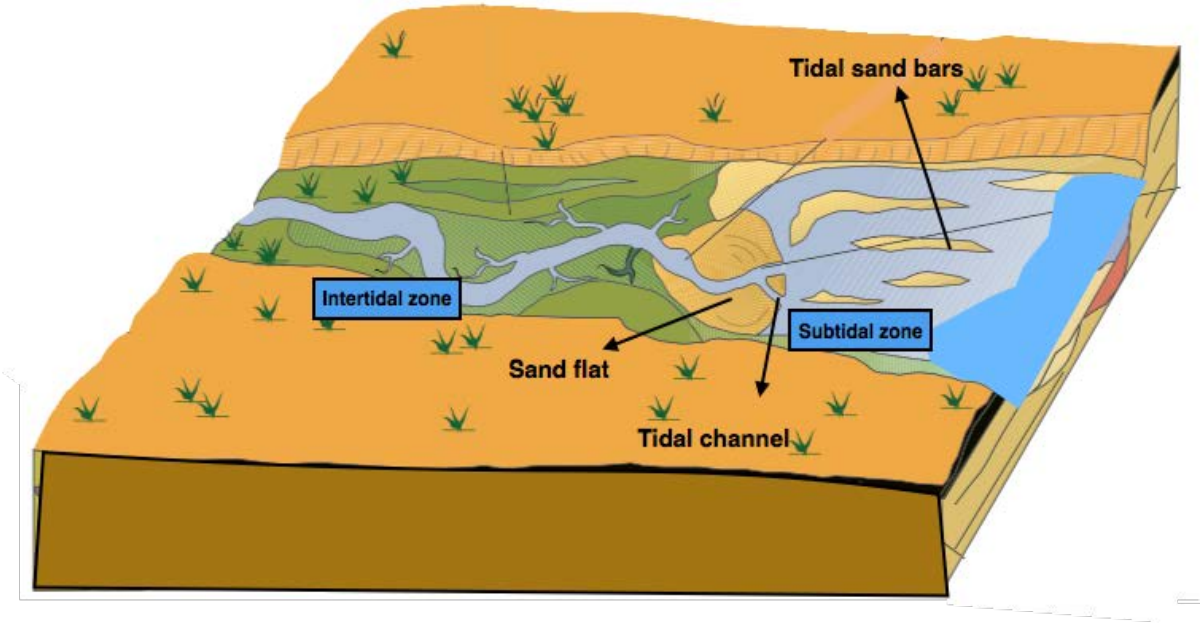

Figure 5.3 Conceptual model of the depositional environment with the location of the suggested facies associations (modified after Morad et al., 2010).

5.4 Large-scale trends within the Cook Fm.

Sedimentary cores encountered in well 34/3-1S, 34/3-2S and 34/3-3S consist of siliciclastic sediments, and are mainly medium- to coarse-grained. The facies associations change between the three wells (Figure 5.4), both vertical and lateral. Stacked upward-coarsening sandstone units are the dominant architecture of the Cook Formation (Figure 5.3). Consequently, the five sandstone bodies (C1-C5) are marked by a significant increase in gamma ray readings at the top and bottom (Figure 5.4), indicating a sharp boundary from sandstone to mudstone. The sandstone units are associated with different sedimentary environments; however, tidal sand bars (FA 3) are encountered most frequently (Figure 5.3). All sandstone units in the studied wells are separated by mudstone intervals, associated with mud bank deposits (FA 4) (Figure 6.4). Both the mudstone intervals (Facies M1) and the bioturbated sandstones (Facies S2) are situated above flooding surfaces (Figure 5.4) indicating a relatively open marine environment. Bioturbation is common throughout the entire formation, but typically decreases upward, illustrated by a coarsening upward trend in the gamma ray readings (Figure 5.4).

Thickness variations between the three wells are not noteworthy, however, the westernmost well, 34/5-1 S, in the Knarr area shows significant changes in thickness where almost all five sandstone units are vanished (Figure 2.4). The lateral extent of the sandstone units towards east, north and south is unknown. Sedimentological log for the C2 unit in well 34/3-1 S is

illustrated in Figure 5.5, the remaining logs of the cored intervals are presented in Appendix A. Figure 5.4 illustrates the facies associations from Table 5.3 related to gamma ray -, density- and neutron readings.

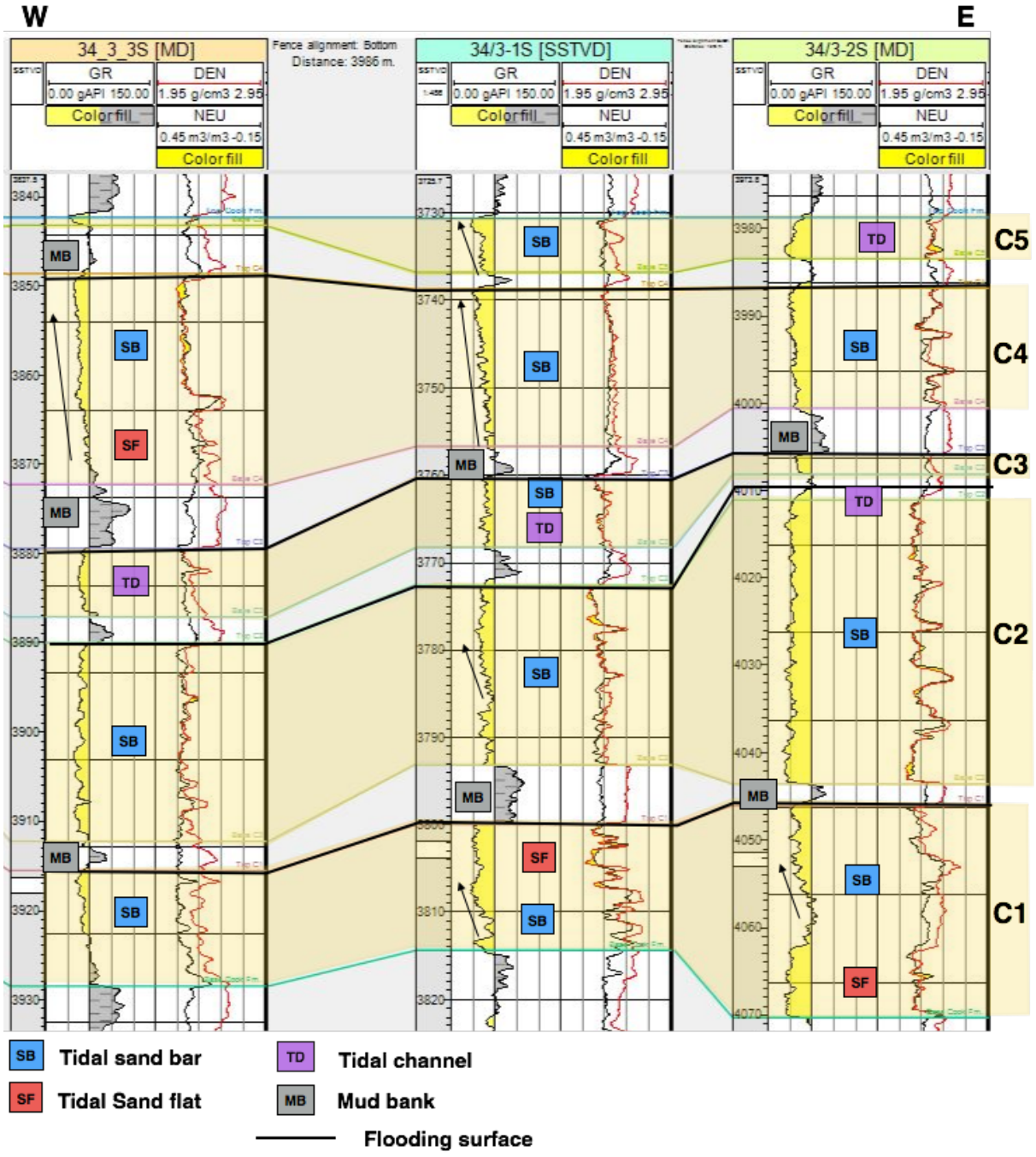

Figure 5.4 Neutron, density and gamma ray logs for the entire Cook Formation from all three wells. Note the common upward coarsening trends. Facies associations are also described with abbreviated names.

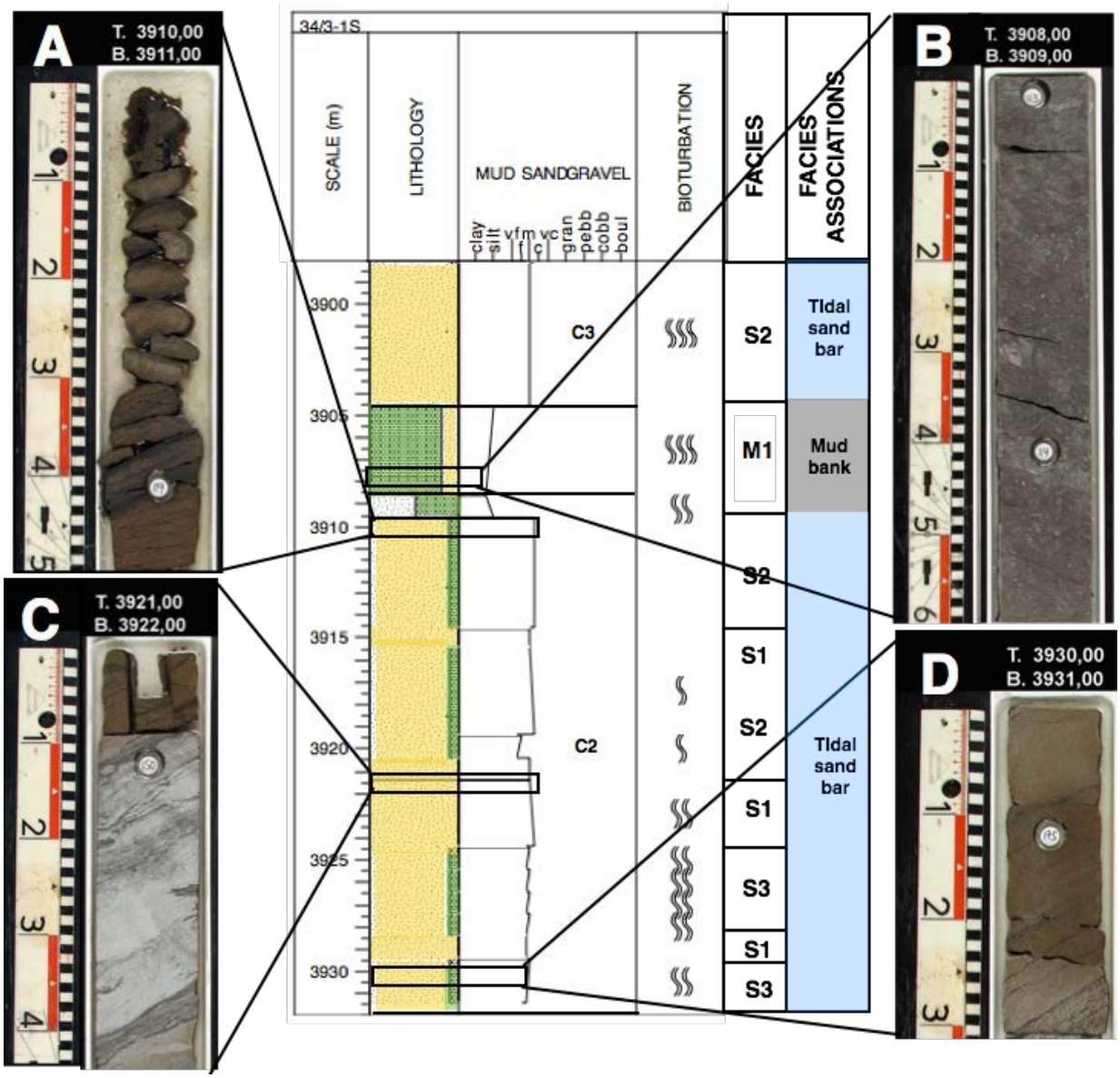

Figure 5.5 Sedimentological log from C2 sandstone unit in well 34/3-1 S. A) Brown sandstone with oil suggested associated with tidal sand bar deposits. B) Intensely bioturbated mudstone and sandstone associated with mud bank deposits. C) Cemented sandstone. D) Relatively clean sandstone with oil and some mudstone associated with tidal sand bar deposits.

6 Petrographic results

6.1 Introduction

To obtain a detailed description of the Cook Formation a petrographic analysis were performed. The petrographic analysis includes investigation of mineral composition, chemical composition and texture of sandstone units of interest. The objective is to investigate if the chlorite coatings are restricted to a certain facies or depositional environment. Composition and texture of sand units is helpful for determining the amount of chlorite coatings present, what types and how the grain was covered. To achieve this, an understanding of the controlling factors during development of authigenic chlorite is needed. Knowledge about the limitations of chlorite can be of high importance for predicting the reservoir quality in deeply buried reservoirs in future exploration.

6.2 Composition and texture

Based on point counting results (Table 6.1) the sandstone within the Cook Formation is classified with an average composition of $Q_{82}F_{16}L_2$, meaning 83% quartz grains, 16% feldspar grains and 2% lithic rock fragments. Thus, the sands are determined to be mainly subarkosic, while a few classifies as quartzarenite and lithic arkose (Figure 6.1).

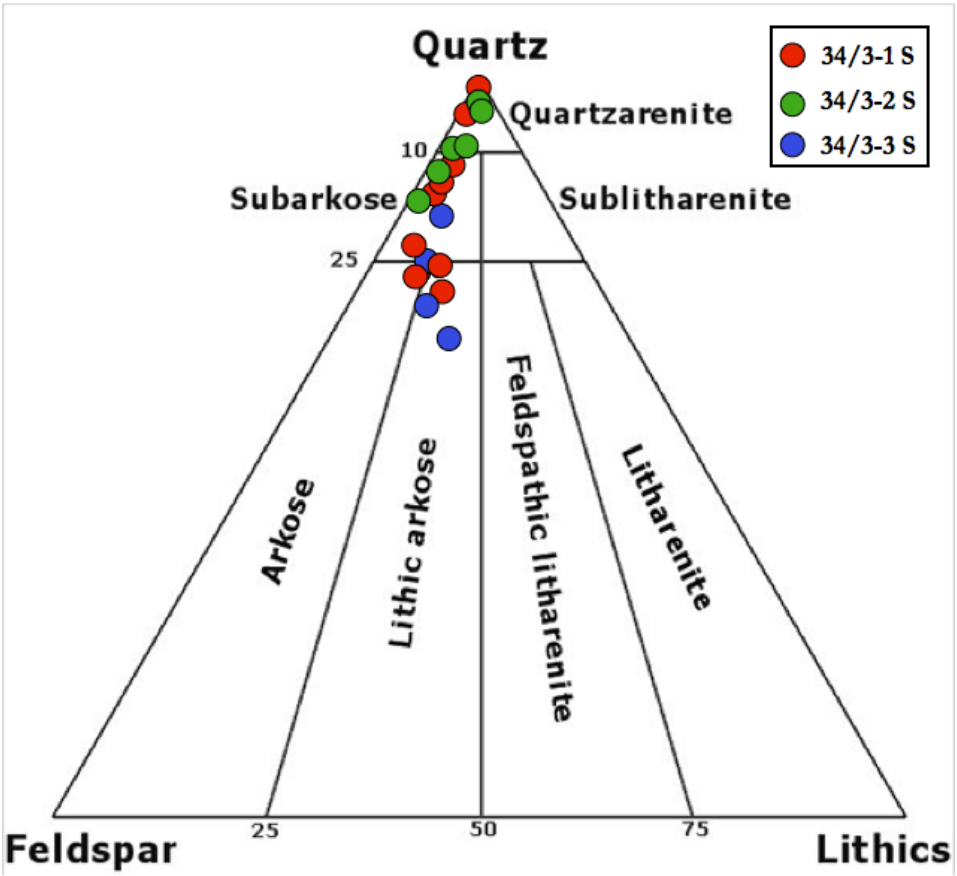

Figure 6.1 Sandstone unit C1, C2, C3, C4 and C5 classified in Folk's classification of sandstones (Folk, 1980). Most of the sandstone classifies as subarkose.

Mineral composition of the sandstone units in the Cook Formation was investigated from thin section analysis. In the following grain size, XRD data, point counting and a brief description of observed minerals are presented.

6.2.1 Grain size and porosity

Generally, the grain size of sandstone ranges from 0.0625–2.00 millimetre (Wentworth, 1922). Grain sizes of the sandstone samples from the Cook Formation ranges between 0,055 –0,877 millimetres (Table 6.1 and Figure 6.2&6.3), some silt are therefore present within in the sandstone units. The coarsest sands are found within well 34/3-3 S and in the deeper parts of well 34/3-2S (Table 6.1 and Figure 6.3A).

A normal distribution of the grain sizes within the sandstone units in the three studied wells can be observed (Figure 6.2A). Grain size measurements versus porosity (Figure 6.2B-D) show a good statistical linear correlation, where increasing grain size corresponds to increasing porosity. However, well 34/3-2 S (Figure 6.2D) plots more scattered.

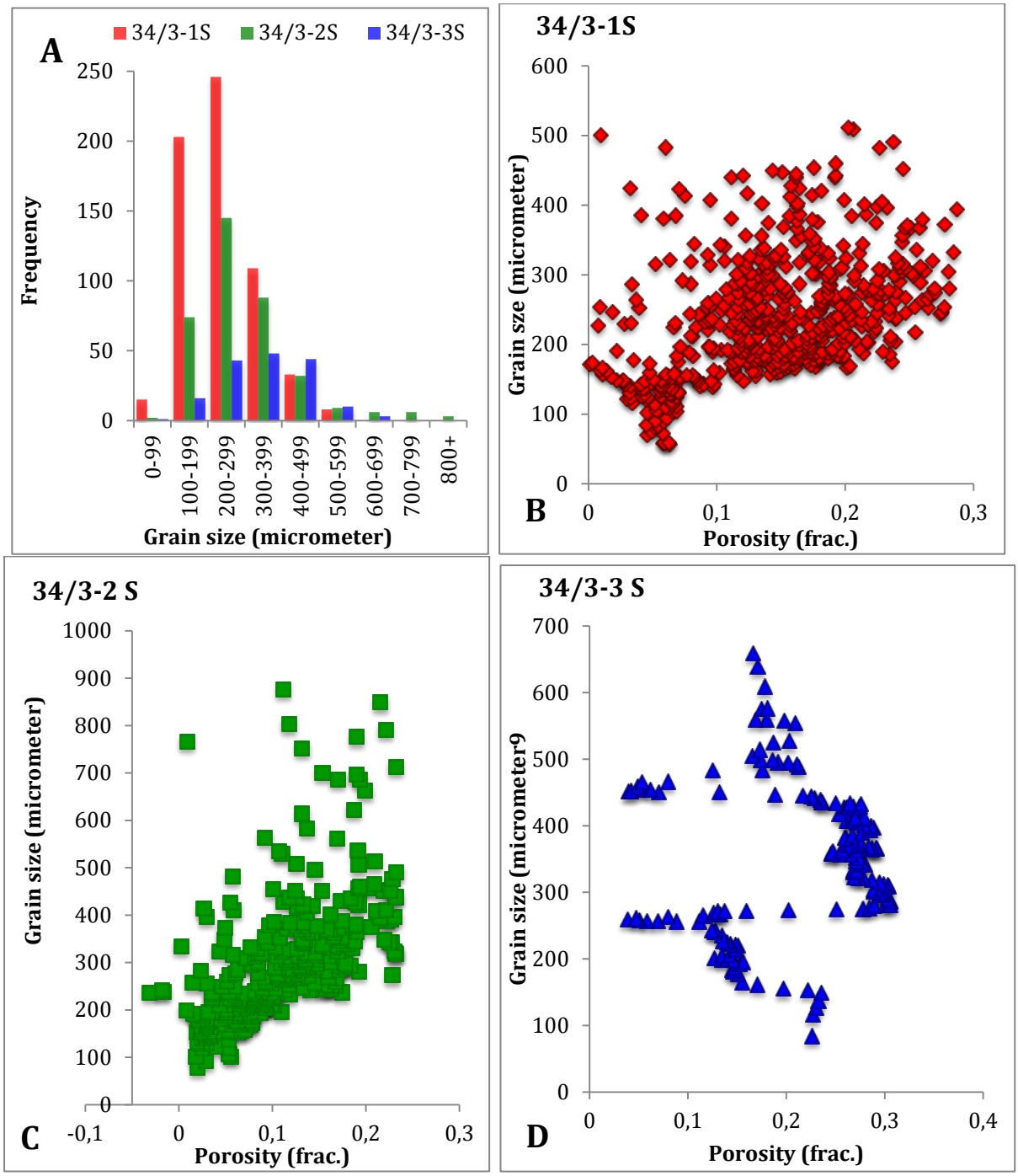

Figure 6.2 A) Distribution of grain size in the three studied wells. Note the normal distribution. B-D) Grain size vs. porosity. Observe how the porosity increases with increasing grain size. Examples of grain sizes from all three wells are shown in Figure 5.3.

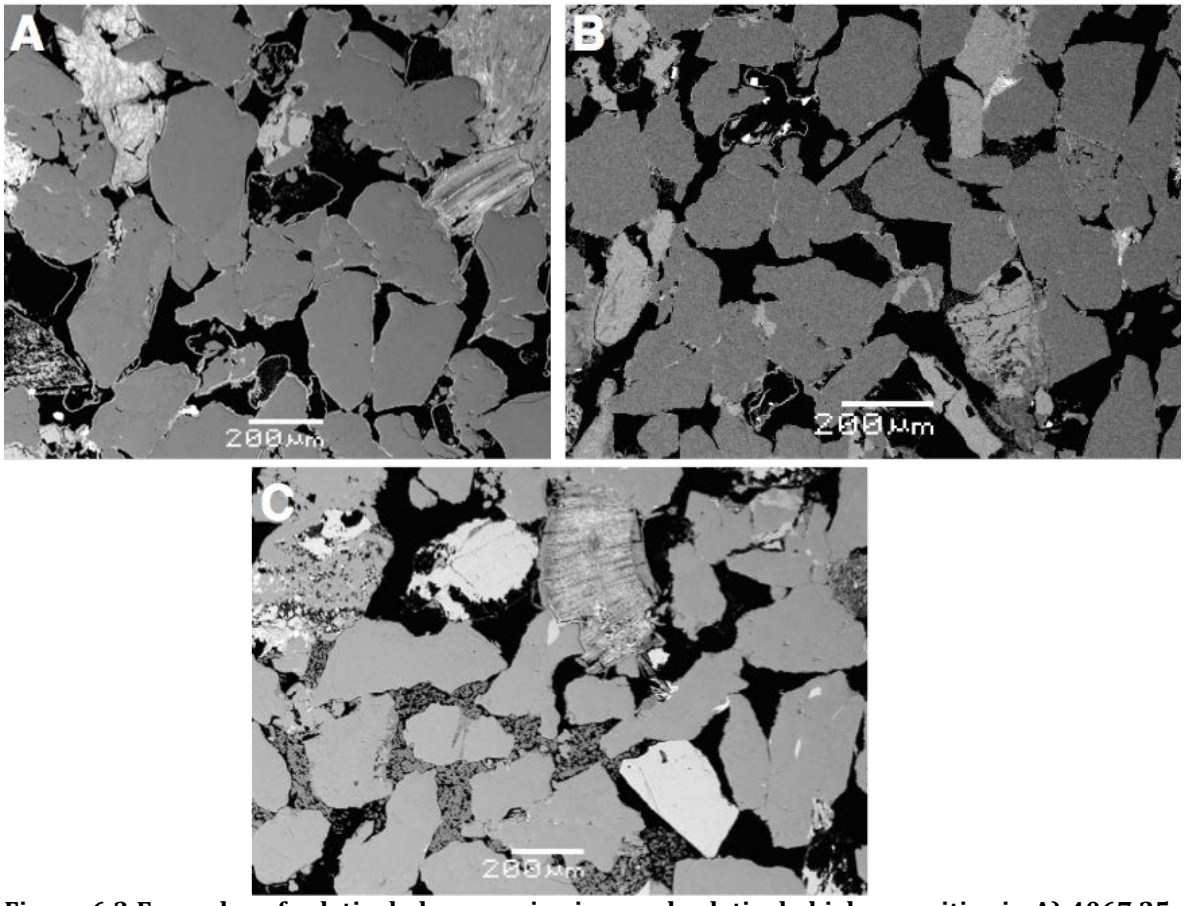

Figure 6.3 Examples of relatively large grain sizes and relatively high porosities in A) 4067.25 well 34/3-2S, B) 3927.81 in well 34/3-1S and C) 3959.06 in well 34/3-3S.

6.3 XRD results

Bulk XRD-data where obtained for selected samples in all three wells from well reports provided by BG Norge (Figure 6.4A). For well 34/3-2 S samples do not fit exactly with the studied samples, however, it involves quantitative determination of the rock forming minerals and total amount of clay. Figure 6.4B illustrates XRD clay fraction for all available samples throughout the Cook Formation, indicating which minerals are present.

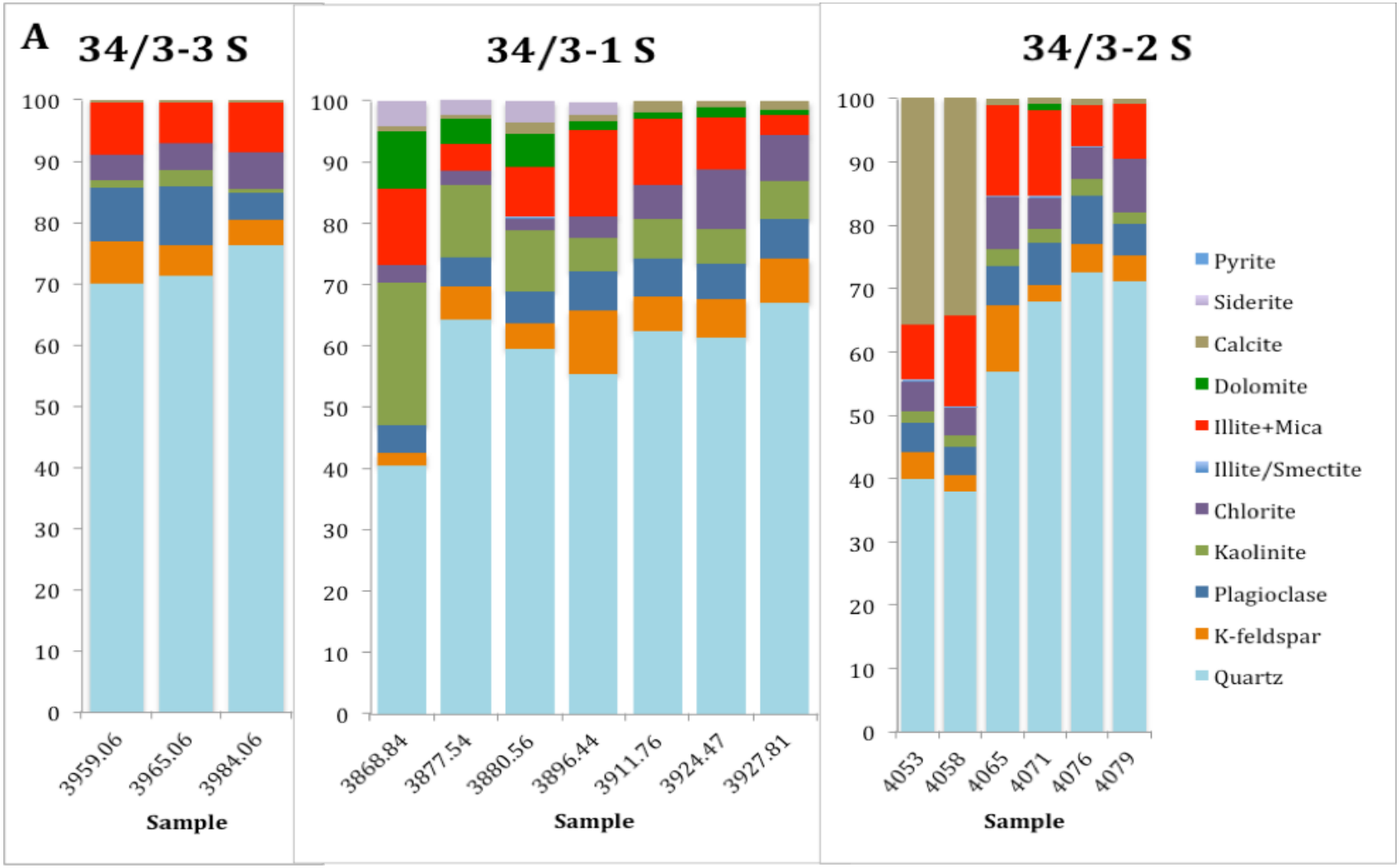

Figure 6.4A) XRD bulk analysis obtained from well reports from all three wells for selected samples.

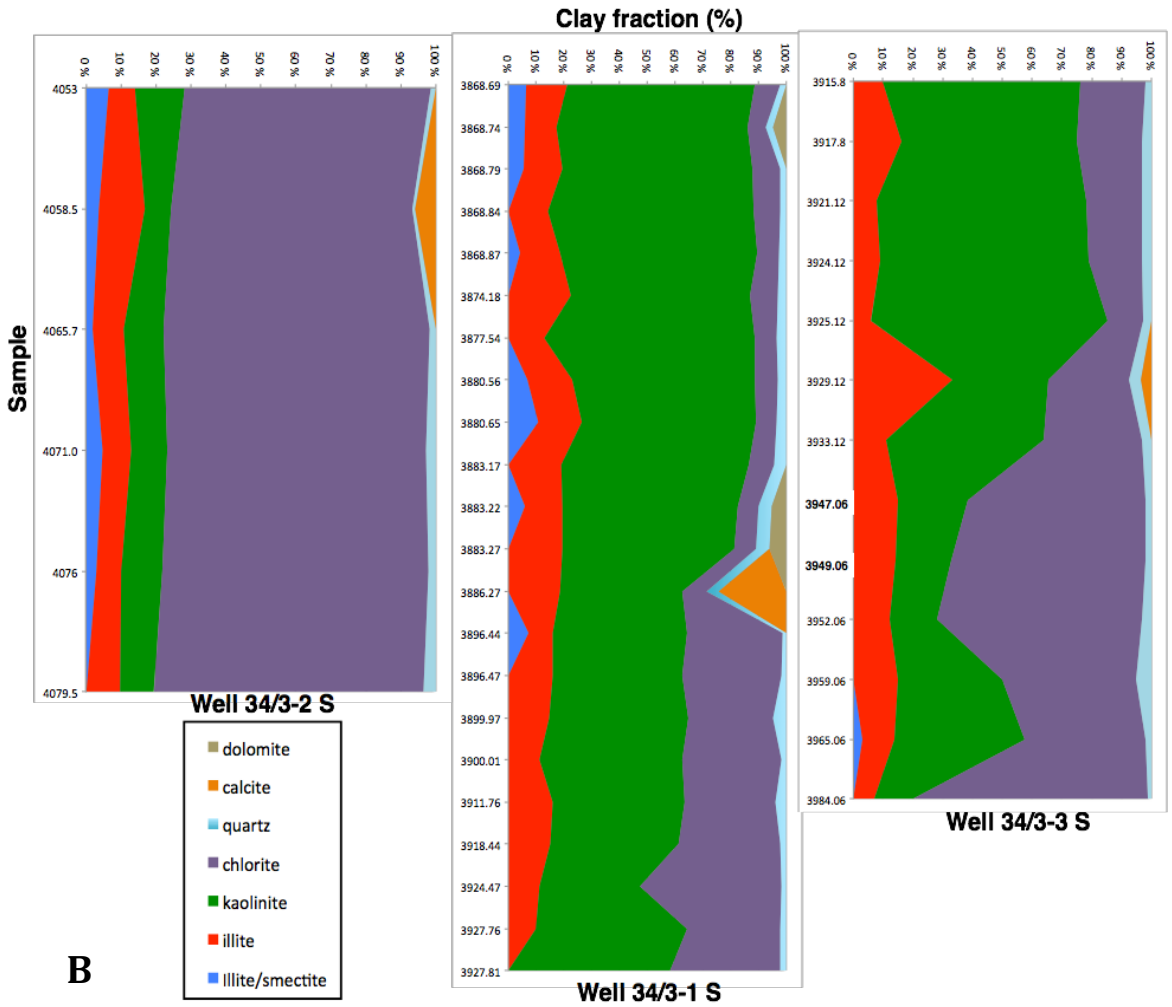

Figure 6.4B) XRD clay fraction obtained from well reports from all three wells for all samples available in the Cook Formation. Note huge amount of chlorite in well 34/3-2 S.

Table 6.1 Point counting results (in %). Sorting, IGV and average grain size are also presented. M-w is moderate to well sorted.

Sample information			Mineralogy												Texture			
			Framework minerals				Matrix			Cement					Depositional texture			
Well	Depth	Unit	Quartz	Feldspar	Heavy minerals	Rock frag.	Mica	Chlorite	Other	Kaolinite	Illite	Quartz	Carbo-nate	Chlorite	Sorting	Porosity	IGV	Average grain size(mm)
34/3-1S	3868,84	C5	42,3	6,3	0,7	0,0	9,0	8,0	0,0	1,0	0,0	7,7	8,7	4,7	Well	11,7	37	0,1614
34/3-1S	3877,54	C4	48,7	10,3	0,7	0,0	5,0	8,0	0,3	0,7	0,0	9,3	4,7	2,7	Well	9,7	33	0,3188
34/3-1S	3880	C4	48,0	17,3	0,3	0,0	2,0	12,7	0,0	0,3	0,0	8,0	0,7	1,3	Well	9,3	31	0,2653
34/3-1S	3890,5	C4	46,3	6,7	0,0	0,0	8,3	22,7	0,0	0,0	0,3	10,0	0,0	0,0	Well	5,7	39	0,2233
34/3-1S	3896,35	C3	41,7	14,0	0,3	0,0	4,0	13,7	0,0	0,0	0,7	3,7	0,0	4,0	Well	18,0	36	0,2438
34/3-1S	3896,44	C3	36,7	12,7	0,7	0,0	6,0	17,7	1,0	0,0	0,0	2,7	0,3	5,7	Well	16,7	38	0,135
34/3-1S	3898,7	C3	44,7	10,7	0,0	0,0	5,7	13,7	0,3	0,0	0,0	6,3	0,7	5,7	M-w	12,3	33	0,2431
34/3-1S	3911,76	C2	45,0	13,7	0,7	0,0	2,7	10,7	0,3	0,0	0,0	5,7	0,0	3,3	Well	18,0	35	0,2196
34/3-1S	3915,6	C2	60,3	0,0	1,7	0,0	9,3	1,3	0,0	0,3	0,0	0,0	26,0	0,0	Well	1,0	29	0,2529
34/3-1S	3918,85	C2	46,7	16,0	1,0	0,0	4,0	7,7	0,7	0,0	0,0	4,7	0,3	5,3	Well	13,7	27	0,3382
34/3-1S	3924,47	C2	42,0	14,0	0,0	0,0	5,3	13,7	0,0	0,0	0,0	7,7	0,7	5,3	Well	11,3	33	0,2219
34/3-1S	3927,81	C2	57,0	1,7	2,7	0,0	5,3	6,0	0,3	0,3	0,0	1,7	0,0	6,7	Well	18,3	27	0,18
34/3-2S	4055,5	C2	60,7	0,7	0,0	0,3	9,3	19,0	0,0	0,7	1,0	5,3	0,0	0,3	Well	2,7	29	0,2535
34/3-2S	4057,75	C2	56,3	1,0	2,3	1,0	3,0	2,3	0,0	1,3	0,0	3,0	3,7	5,3	Well	20,7	31	0,2329
34/3-2S	4061,75	C2	62,0	1,0	0,3	0,0	3,3	1,7	0,0	4,7	0,0	4,3	2,3	6,7	Well	13,7	27	0,2447
34/3-2S	4065,7	C2	55,3	12,7	1,0	0,0	5,3	10,0	0,0	0,3	0,0	3,7	0,7	2,0	Well	9,0	24	0,2785
34/3-2S	4067,25	C2	59,0	3,3	0,0	0,0	5,3	16,7	0,0	1,0	0,0	8,0	2,3	0,7	Well	3,7	32	0,2917
34/3-2S	4073,25	C2	62,0	6,0	0,3	0,7	4,7	12,3	0,3	0,0	1,0	2,3	3,3	0,7	M-w	6,3	26	0,3785
34/3-2S	4079,5	C1	56,7	7,0	0,7	0,0	4,0	16,0	0,0	0,0	0,0	5,3	0,0	3,3	M-w	7,0	28	0,3994
34/3-3S	3959,06	C2	46,7	18,0	1,0	1,7	2,3	4,7	0,0	3,0	0,7	2,3	0,0	3,7	Well	16,0	27	0,4152
34/3-3S	3965,06	C2	49,7	16,0	0,7	0,7	3,7	6,3	0,0	3,3	0,0	2,3	0,0	4,0	Well	13,3	25	0,3029
34/3-3S	3975,06	C2	40,7	18,0	0,7	0,7	2,3	9,3	0,0	2,7	1,3	1,7	0,7	4,7	Well	17,3	33	0,34
34/3-3S	3984,06	C1	53,3	11,7	0,0	0,7	0,7	6,0	0,3	2,7	4,7	2,7	2,3	5,7	M-w	9,3	28	0,3761

6.3.1 Detrital mineralogy

The framework grains of the subarkosic sandstone within the Cook Formation mainly contain quartz and feldspar (Table 6.1 and Figure 6.4). Other detrital mineralogy observed in this sandstone includes heavy minerals, carbonate grains and minor amounts of lithic rock fragments. Detrital mineralogy is important regarding facies and depositional environment. In the subsequent section the main framework grains are described.

Quartz (SiO_2)

Quartz dominates the framework mineralogy in the studied wells. Grains are mainly angular to subangular in shape and colourless (Figure 6.3 and 6.5A). Additionally, the quartz appears as authigenic quartz overgrowths as well (Section 6.7).

K-feldspar ($KAlSi_3O_8$) and Albite ($NaAlSi_3O_8$)

The feldspar is dominated by K-feldspar and plagioclase (Figure 6.4A). K-feldspars observed in thin section commonly show clear, parallel lines of cleavage planes. However, K-feldspar grains are commonly dissolved and appear as secondary pores within the Cook Formation (Figure 6.5A&B). Albitisation of plagioclase grains is commonly observed throughout the samples, resulting in the albite to be authigenic and notably fresher than the K-feldspar, as it has not dissolved (Figure 6.5C).

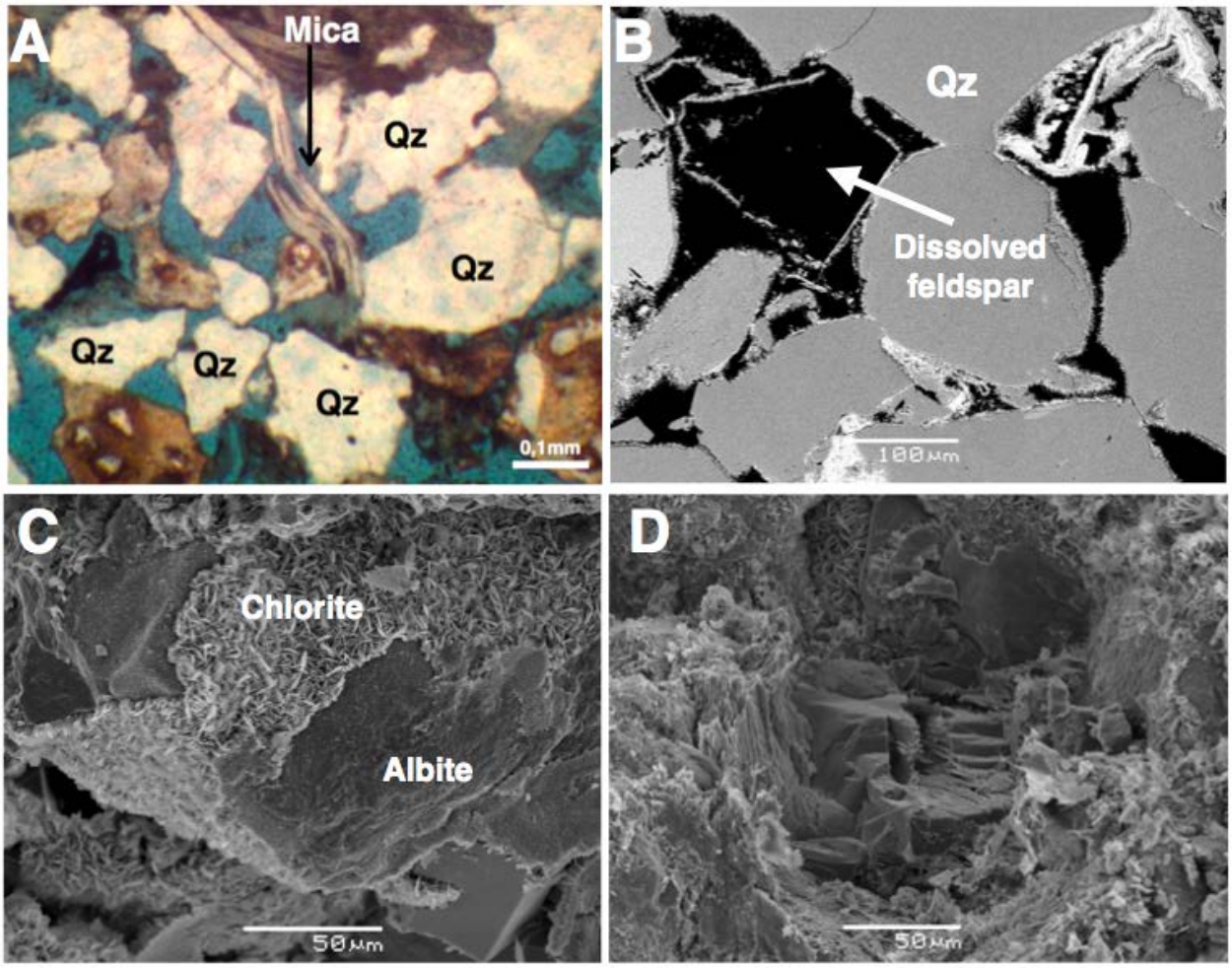

Figure 6.5 A) Quartz grains and mica grain within sample 3918.85 in well 34/3-1S. B) Dissolved K-feldspar with only chlorite coating left. C) Chlorite partially covering an albite grain from sample 4057.75 in well 34/3-2S.. D) Partly dissolved K-feldspar from sample 4057.75 in well 34/3-2S.

Mica

Mica, mainly as muscovite, is prominent through all samples studied. Some plates are fresh, while others are replaced by authigenic phases, like chlorite (Figure 6.5A). In thin section, the colour of the mica grains was colourless, however, the birefringence colour were mostly first order colours. A crystal structure of thin sheets and a well-developed platy cleavage were observed. However, due to this platy cleavage the crystals seemed to have broken up into thin grains (Figure 6.5A). According to the point counting results (Table 6.1) the abundance of mica seem to be relatively similar throughout the Cook Formation.

Heavy minerals

Heavy minerals observed are pyrite (FeS_2) (Figure 6.5A), barite ($BaSO_4$), rutile (TiO_2), zircon ($ZrSiO_4$) (Figure 6.6B) and siderite ($FeCO_{3)}$. They appear scattered and in rather

small quantities. The grains, especially zircon, were colourless and easily recognised by their very high relief.

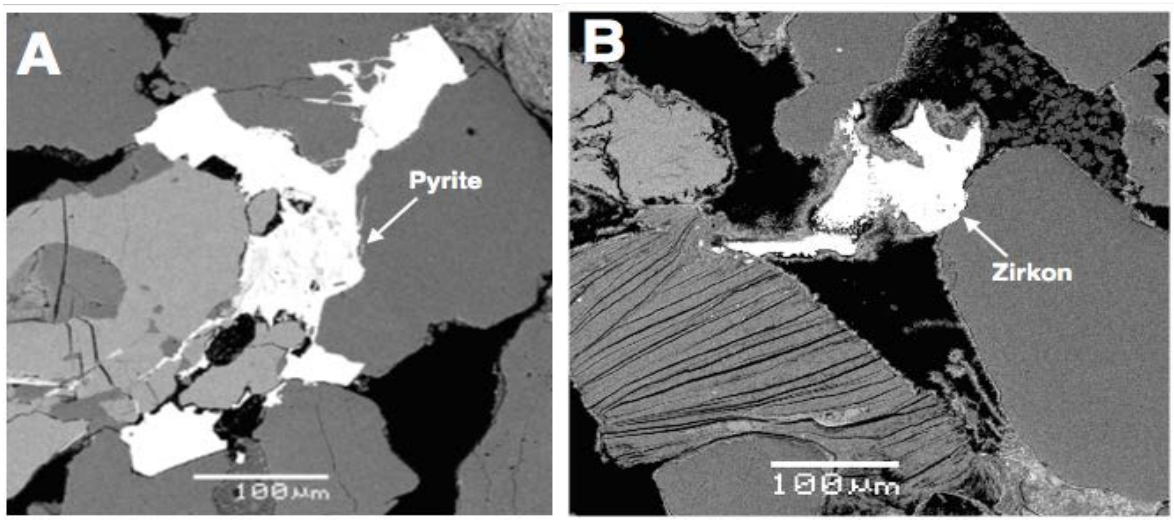

Figure 6.6 A) Pore-filling pyrite at depth 3959.06 in well 34/3-3S. B) Zirkon from 4061.75 in well 34/3-2S.

Detrital clay rims

Detrital clay rims were observed as a discontinuous, thin grain rims (Figure 6.14A). It is extremely difficult to determine the composition of the detrital clay, because the rims are so thin and difficult to locate with SEM. Furthermore, the XRD-data cannot distinguish between detrital and authigenic clay. However, various evidence from the SEM suggest that the detrital clay may have a mixed composition of potentially illite (Figure 6.8C), smectite, chlorite and kaolinite.

6.3.2 Authigenic mineralogy

The most common authigenic mineral in the Cook Formation in the Knarr area is chlorite, together with kaolinite (Figure 6.4A&B). Other minerals observed are illite, and albite (see Detrital mineralogy) and minor amounts of carbonate and quartz cement.

Chlorite

The morphology of chlorite is very variable, however, chlorite commonly occurs as grain coating with the chlorite crystals attached perpendicular to the grain surface (Worden and Morad, 2003). The authigenic chlorite observed in the Cook Formation seems to occur mainly as chlorite coatings. Chlorite was in addition observed as pore filling and rosette-like features (Figure 6.7). According to XRD results well 34/3-2 S

encountered the highest percentage of chlorite (Figure 5.4B), whereas the amount of chlorite is more scattered in the point counting results (Table 6.1).

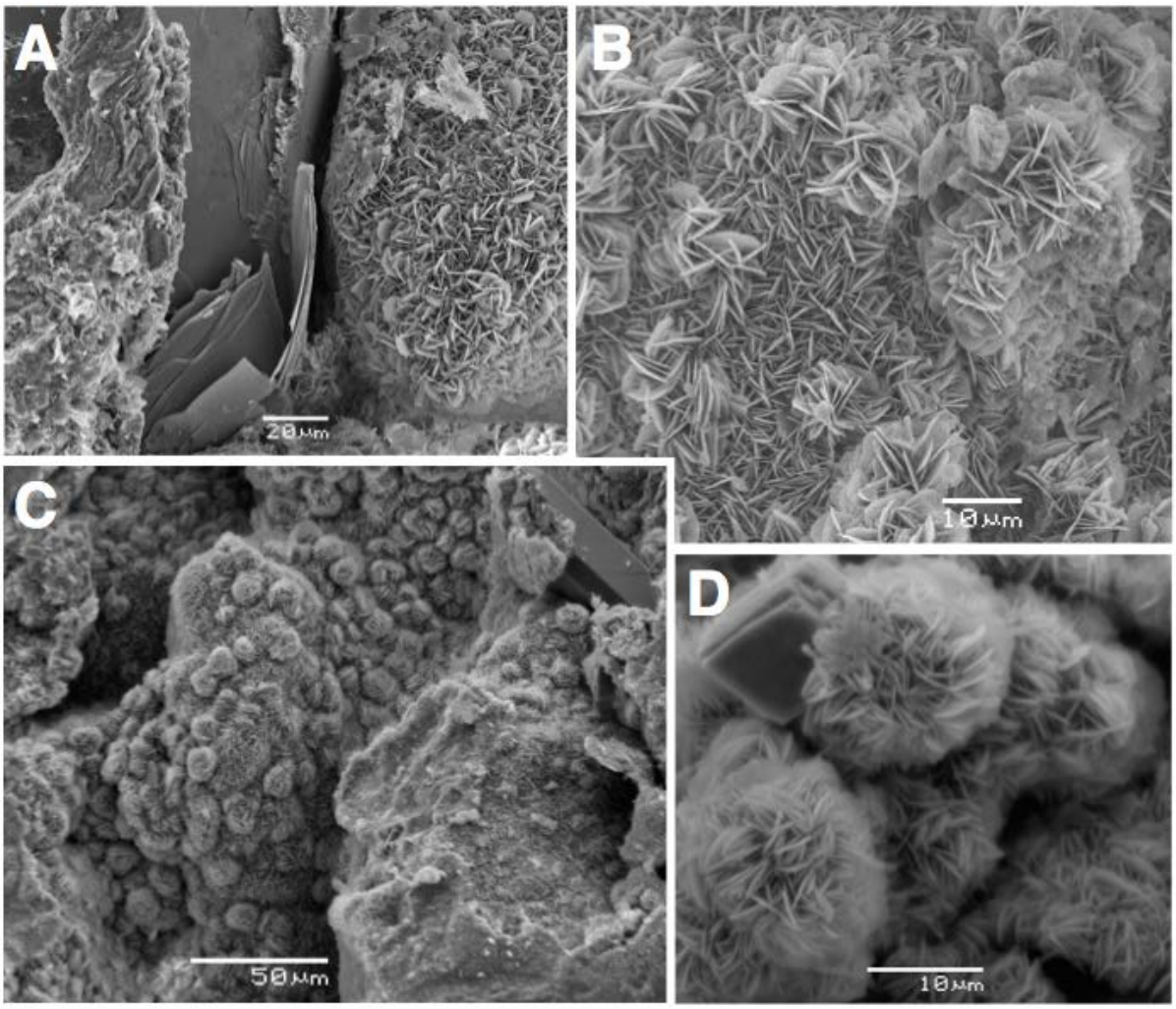

Figure 6.7 A&B) Grain coating chlorite from sample 4057.75 and 4079.50 in well 34/3-2S. C&D) Chlorite rosettes from sample 3984.06 in well 34/3-3S.

Kaolinite

Stacked books of kaolinite occur locally in almost all samples (Figure 6.8A). The blocky, pore-filling kaolinite has booklets with a thickness of approximately $1\mu m$. Micropores are visible within the pore-filling kaolinite. Comparing point counted results (Table 6.1) with XRD results (Figure 6.4) for well 34/3-2S it seems like there is more kaolinite present than has been encountered during point counting. However, the small amount of kaolinite detected in the sandstone intervals implies that it is of authigenic origin.

Illite

Authigenic illite was observed as a fibrous and pore-filling mineral, occurring scattered and in minor amounts (Figure 6.8C). In thin sections the illite appeared as a brown pore-filling matrix.

Carbonate

Carbonate cement, as calcite ($CaCO_3$), was observed in a few of the samples (Figure 6.8B, Table 6.1 and Figure 6.4). Calcite appears as colourless, but with high order green and pink birefringence colours. The relief is high, and their cleavage planes are commonly very distinct (Figure 6.8B). Additionally, scattered and minor amounts of carbonate grains were observed at several depths. In thin sections, the carbonate had blue staining to make it possible to distinguish between ferroan calcite and non-ferroan forms of the mineral.

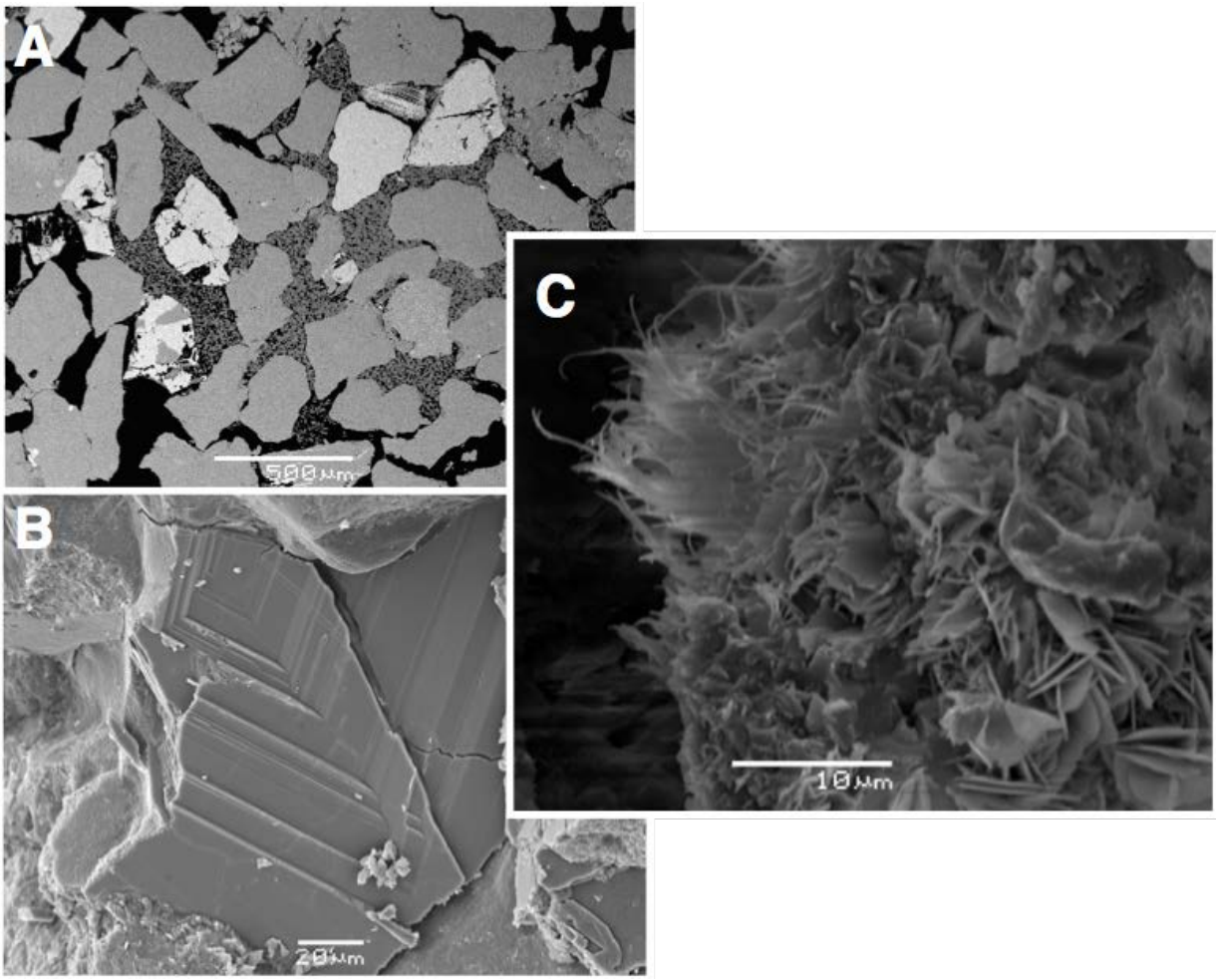

Figure 6.8 A) Pore-filling kaolinite in sample 3959.06 in well 34/3-3S surrounded by mainly quartz grains B) Calcite cement in sample 3915.60 in well 34/3-1S. C) Fibrous and pore-filling illite in sample 4073.25 in well 34/3-2S.

Ooids

Ooids are very rare, and only noted within sample 3984.06 in well 34/3-3 S. They are comprised of a quartz grain at the centre, encased with multiple concentric rings of finely crystalline clay, commonly replaced by chlorite (Figure 6.9).

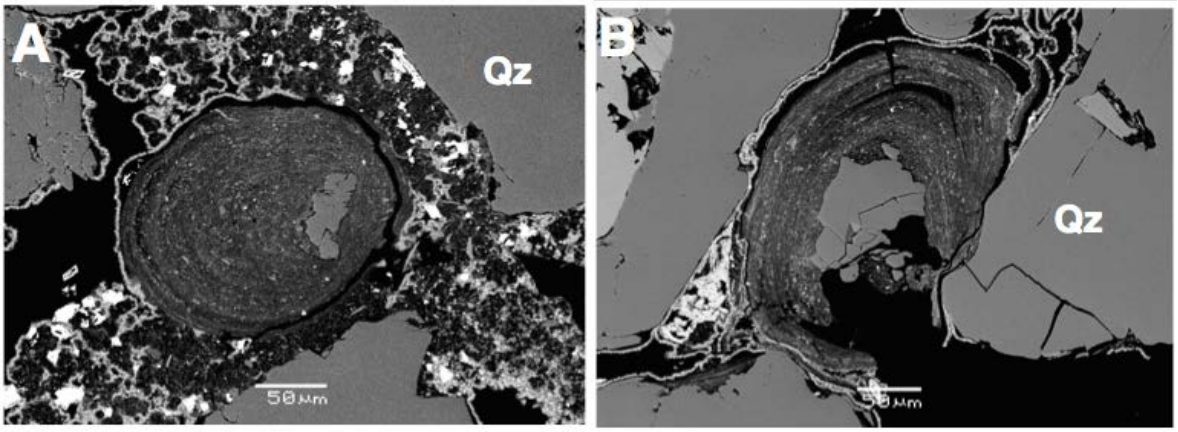

Figure 6.9 Ooids from sample 3984.06 in well 34/3-3S. Note the finely crystalline clay enclosing the small quartz grain.

6.4 Intergranular Volume (IGV)

The intergranular volume (IGV) calculated from the petrographic analysis (Table 6.1) is plotted in Figure 6.10. Values ranges from 23-39%, whereas the highest values from 36-39% represents carbonate cement, which in this case is in the form of calcite (Figure 6.10A). The porosity at deep burial and the volume of quartz cement will be a direct function of the intergranular volume at the onset of chemical compaction. IGV is also a function of grain size (Figure 6.10B).

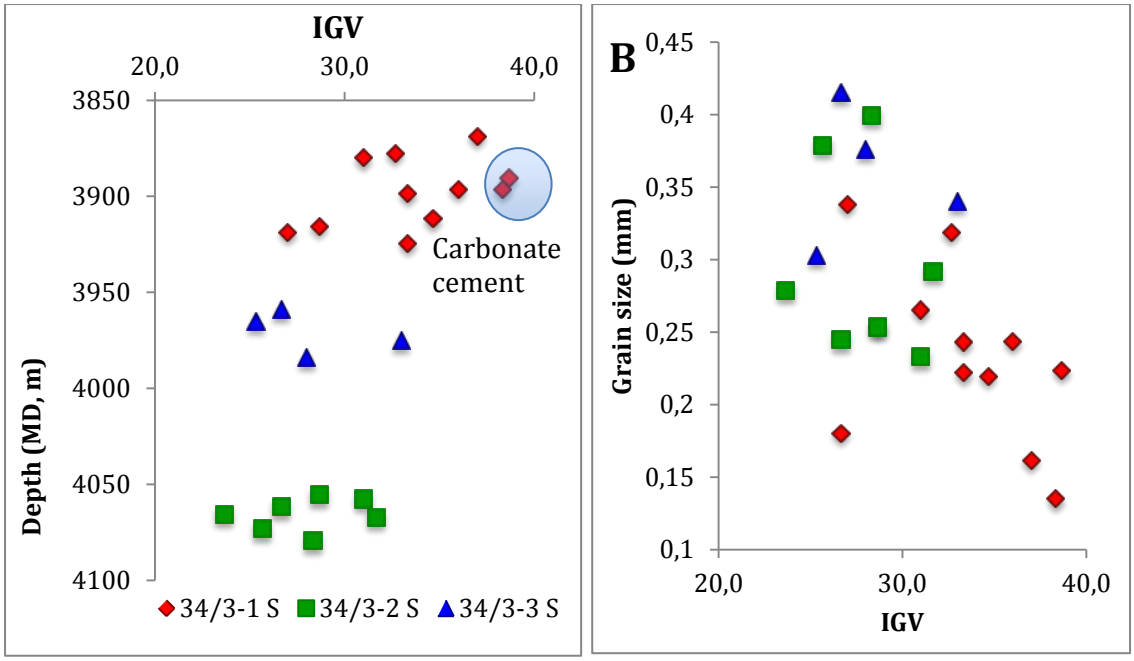

Figure 6.10 A) IGV versus depth (MD) for the three wells. Points with high IGV values indicate the presence of carbonate cement. B) IGV vs. grain size shows a trend where high IGV values correspond to small grain sizes, and vice versa. Same colour legend as in A).

6.5 Composition of chlorite

Chlorite grains (Figure 6.13) from sandstone sequence C2 were investigated from well 34/3-2, 34/3-1 and 34/3-3 at depth 4061,75m, 3927,47m and 3975.06, respectively (Table 6.2). An example of energy dispersive X-ray spectrum of the chlorite is shown in Figure 6.11, while the average composition of the chlorite is presented in Table 6.2, whereas all results are presented in Appendix B.

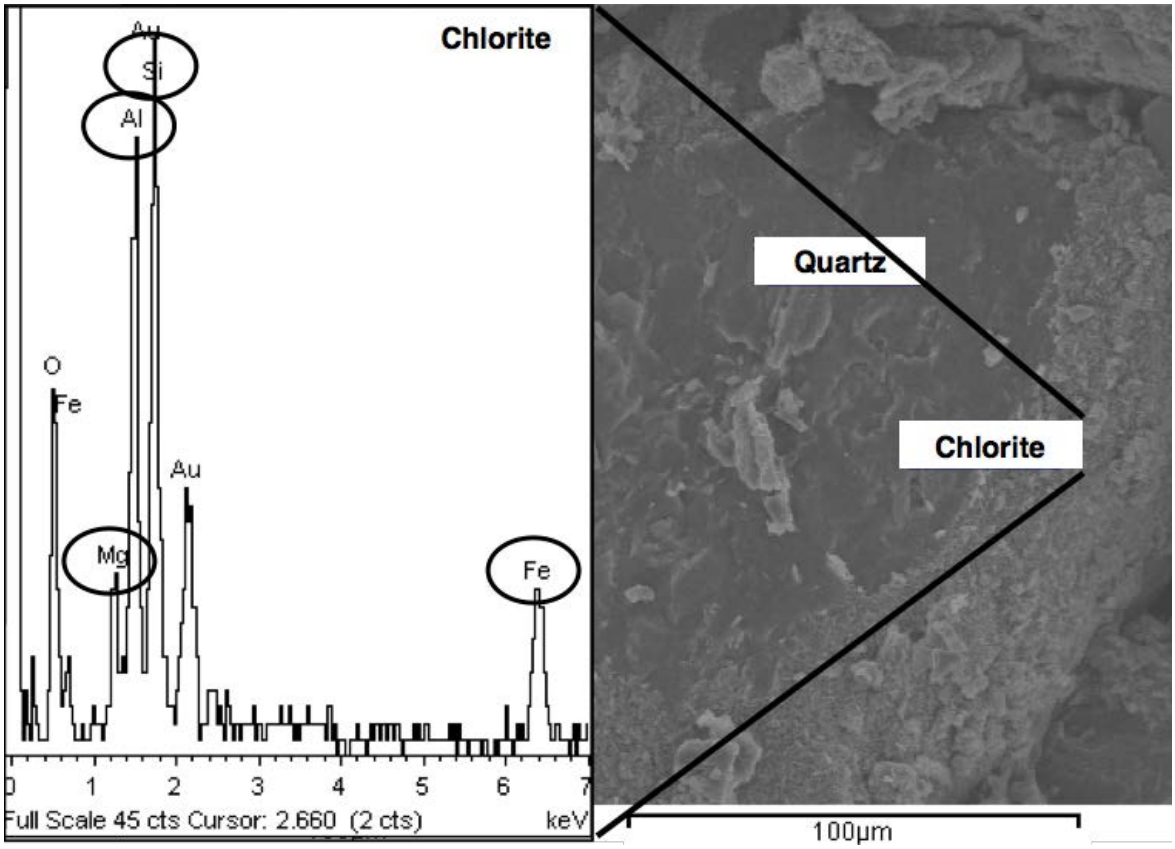

Figure 6.11 Energy dispersive X-ray spectrum (EDX) of chlorite at 3924.47 in well 34/3-1S. Note the high iron peak, indicating a Fe-rich chlorite.

Table 6.2 Average composition of the chlorite from sequence C2.

Well	Sample	Average composition of chlorite
34/3-2 S	4061.75	$(Mg_{0,83}Fe_{3,49}Al_{1,49})_6(Al_{1,12}Si_{2,88})_4O_{10}(OH)_{8.}$
34/3-1 S	3927,47	$(Mg_{0,80}Fe_{2,63}Al_{1,96})_6(Al_{0,71}Si_{3,26})_4O_{10}(OH)_{8.}$
34/3-3 S	3975.06	$(Mg_{0,75}Fe_{2,36}Al_{2,10})_6(Al_{0,55}Si_{3,45)4}O_{10}(OH)_{8.}$

Figure 6.12A illustrates the consistently composition of the chlorite in all samples, where high content of tetrahedral Al corresponds to high content of Fe. Classification of the chlorite is shown in Figure 6.12B, whereas the points plot close to diagenetic chlorite and bertherine.

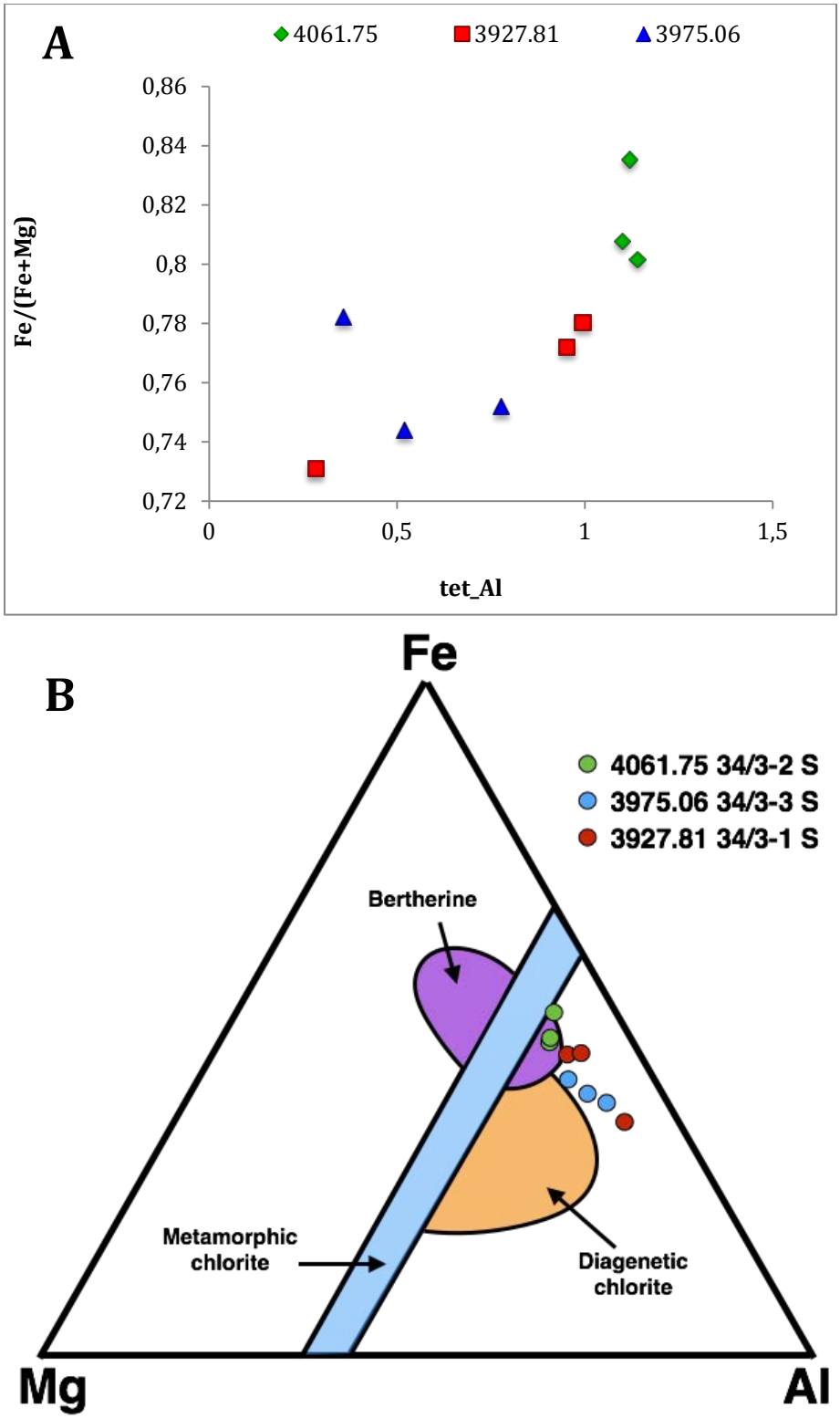

Figure 6.12 A) Fe/(Fe+Mg) versus tetrahedral Al illustrates a consistently composition of the chlorite. B) Classification of the chlorite at different depths in the C2 unit from all three wells plotted in a diagram from Velde (1985). Note how the chlorite is plotted close to bertherine.

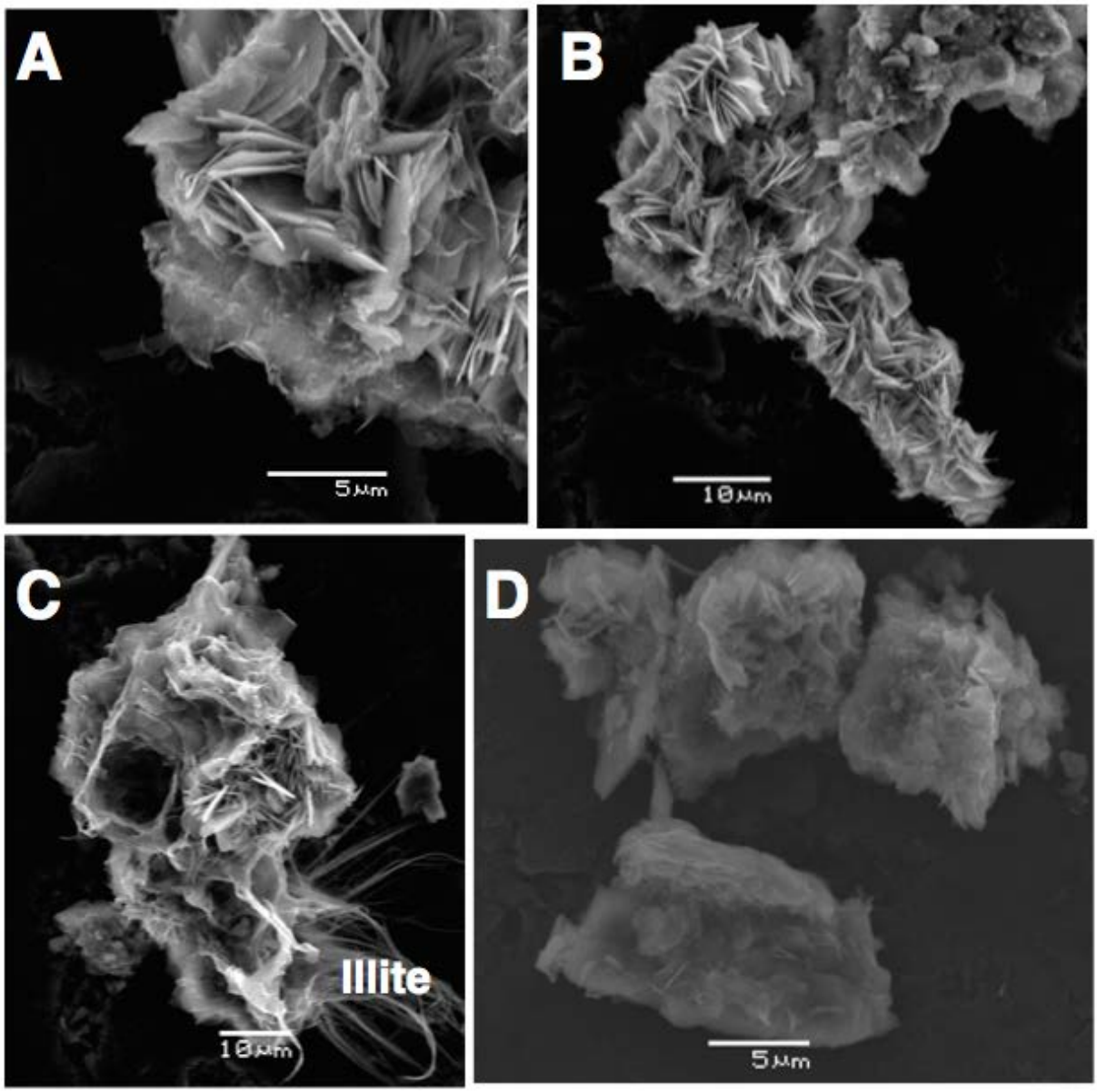

Figure 6.13 SEM images of chlorite. A) Close-up of the chlorite grain in B) found in sample 4061.75 in well 34/3-2S. Note the clay rim around the grain. C) Chlorite grain with fibrous illite from sample 4061.75. D) Chlorite cluster from sample 3927.81 in well 34/3-1S. Note how small this grain is compared to sample 4061.75.

6.6 Grain coating chlorite

Observations show that chlorite coating is not present at grain-to grain contacts (Figure 6.14B). However, the precursor clay seems to be present at grain-to grain contacts as a thin dust rim. Precursor clay is also present between grains and chlorite coating (Figure 6.14A). Chlorite rosettes (Figure 6.7C&D) are isolated and appear more or less on top of the chlorite coating. Samples with extensive carbonate do not contain significant amounts of chlorite coating (Figure 6.14C).

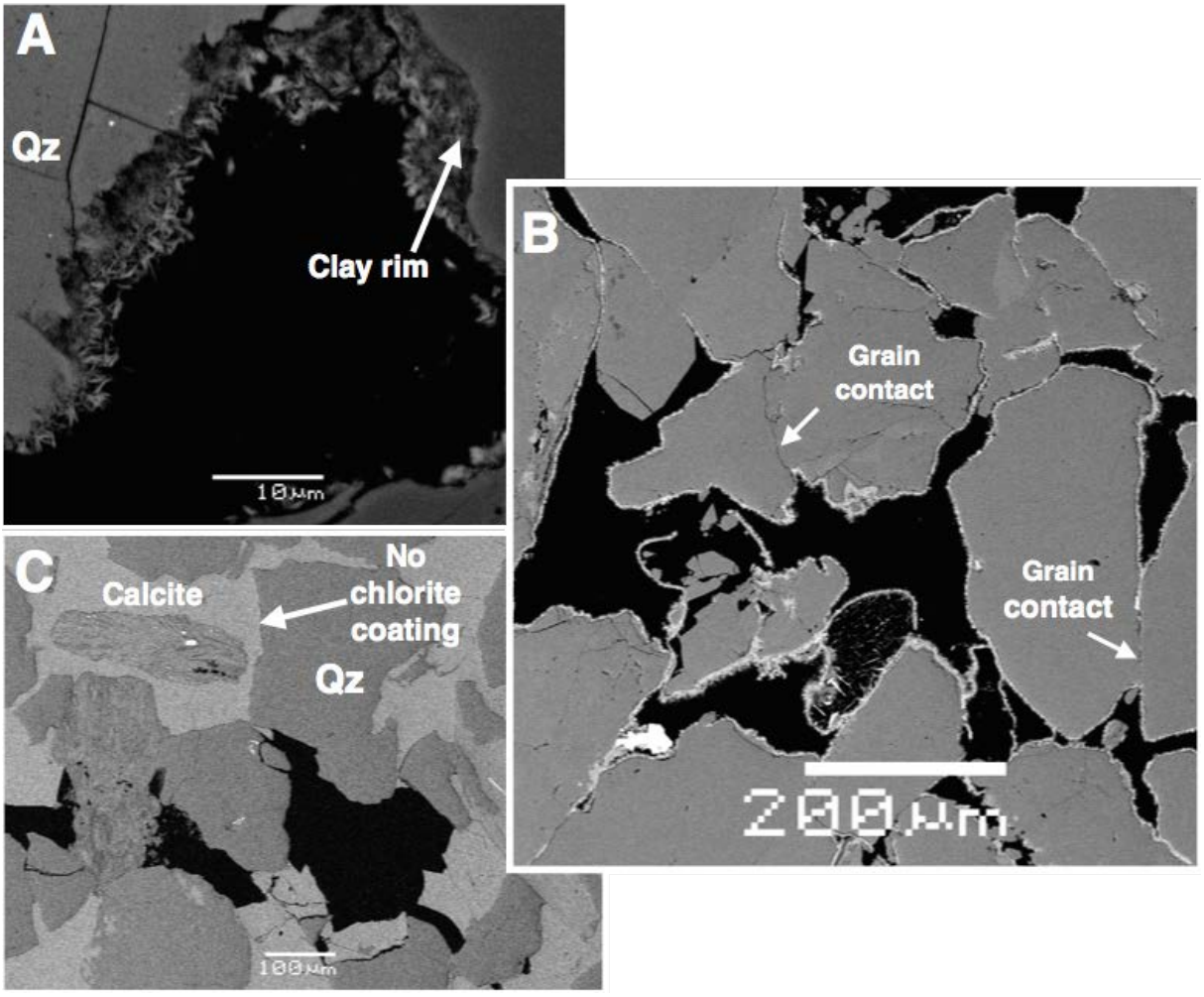

Figure 6.14 A) Chlorite coated quartz in sample 3915.60 in well 34/3-1S, a clay rim between the grain and the coating is observed. B) Extensive chlorite coating in sample 4067.25 in well 34/3-2S. However, chlorite coating is not present at grain-to- grain contacts. C) Intensively carbonate cemented area in sample 3915.60 where there are no chlorite coating between the grain and the carbonate cement.

Porosity versus chlorite coating plot (Figure 6.15A) where increased chlorite coating corresponds to increased porosity. Furthermore, chlorite versus grain size gives a scattered plot with no significant trend (Figure 6.15B).

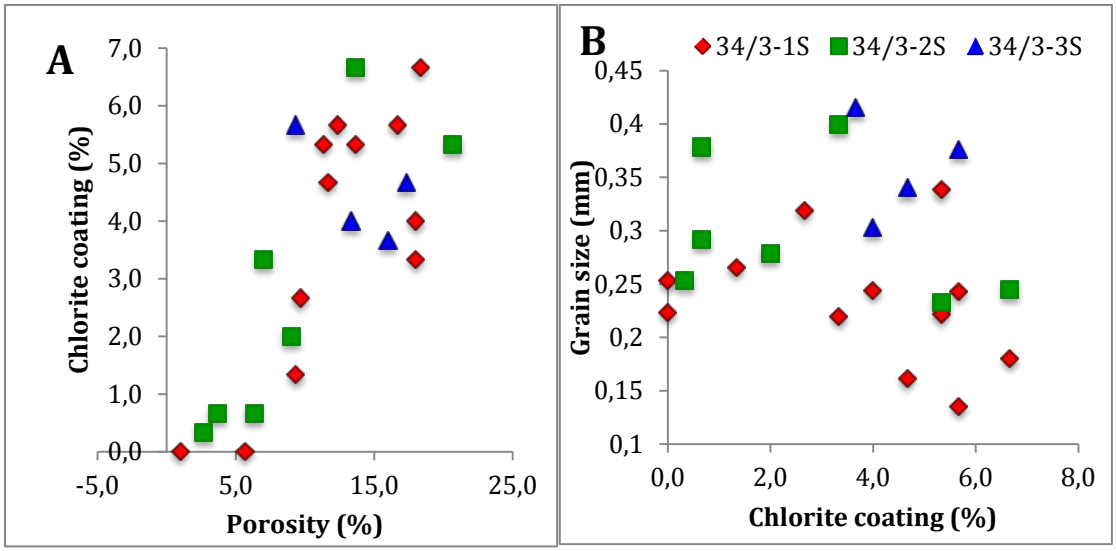

Figure 6.15 A) Chlorite coating vs. point counted porosity shows a nearly linear trend with increasing chlorite coating with increasing porosity. B) Chlorite coating vs. grain size plots scattered with no significant trends.

6.7 Quartz overgrowth

The studied samples are situated at temperatures > $65C^o$ and the amount of quartz cement tends to increase as a function of temperature. Point counting results (Table 6.1) do not show any significant trend where quartz cement is increasing with depth. Small amounts of quartz overgrowths have been detected in the studied samples, both in the XRD – and point counting results (Figure 6.4B and Table 6.1). Quartz cement varies according to grain size, quartz clast content and degree of coating within the sandstone of interest (Figure 6.16).

Plotting quartz cement with chlorite coating gives a scattered plot with no prominent trend (Figure 6.17A). Likewise, quartz cement versus density plot gives a more or less scattered plot (Figure 6.17B).

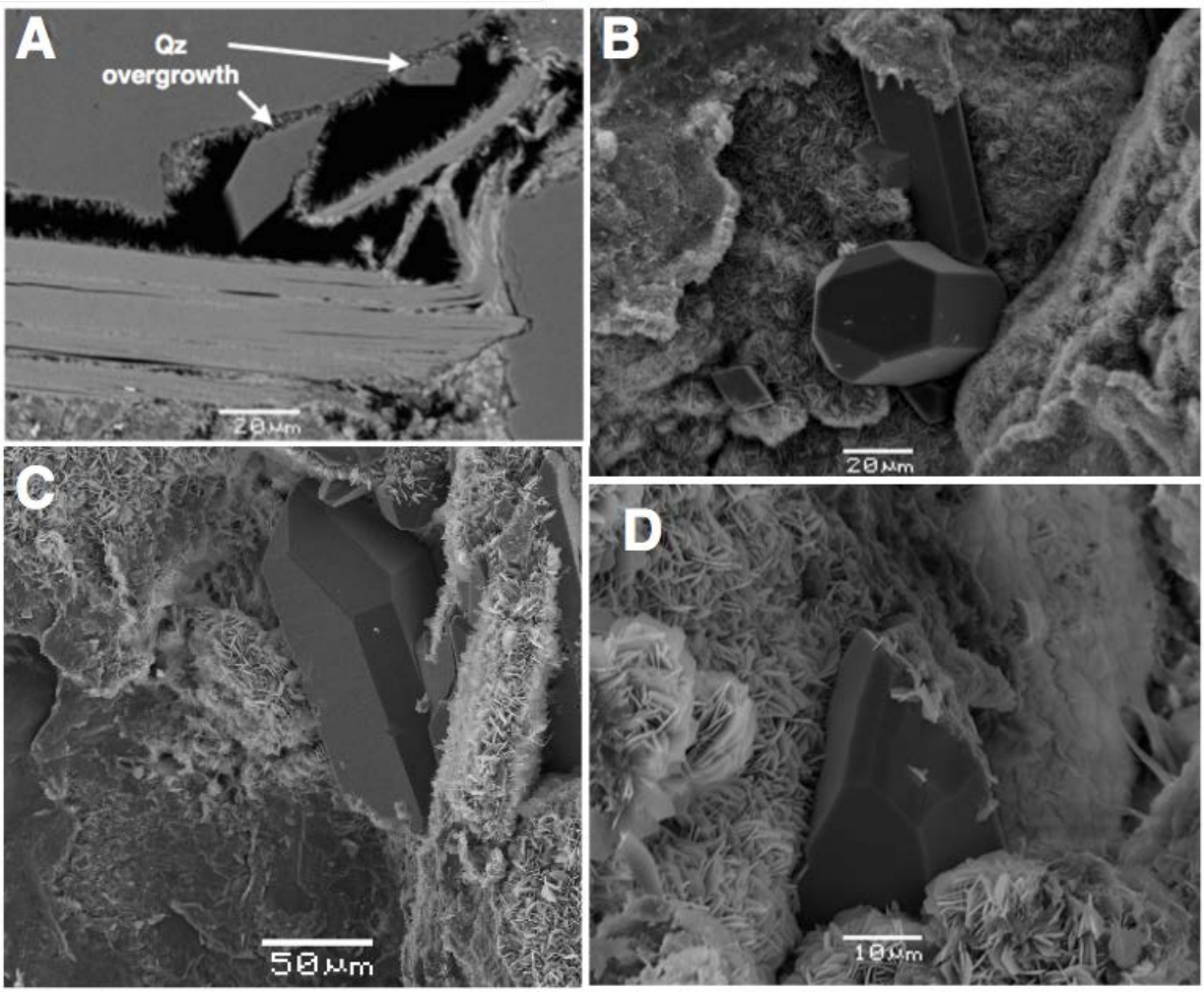

Figure 6.16 A) Only small breaks in the chlorite coating will cause development of quartz overgrowths from sample 3915.60 in. well 34/3-3S. Prismatic quartz crystals from sample 3984.06 in well 34/3-3S (B), sample 4057.75 and 4073.25 in well 34/3-2S (C&D).

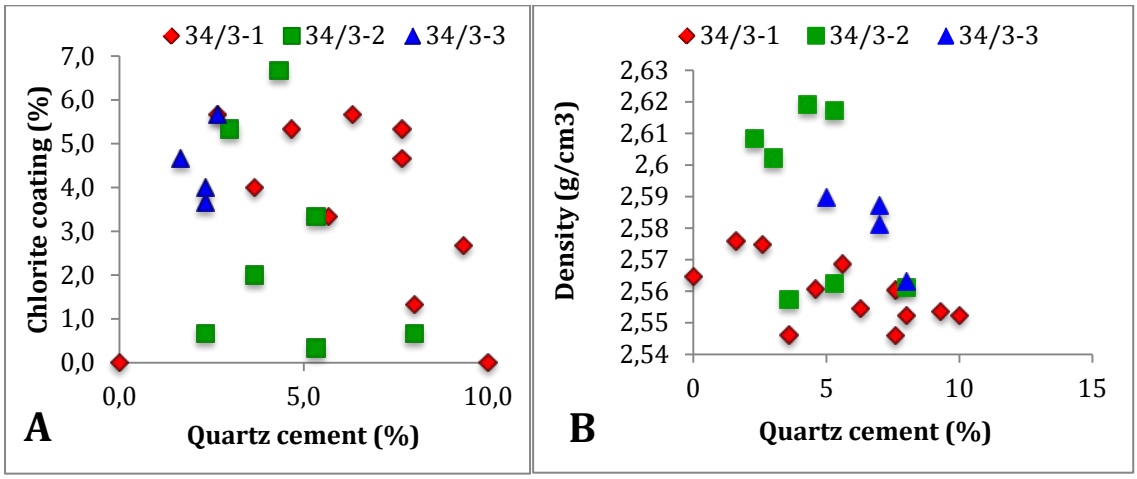

Figure 6.17 A) Quartz cement versus chlorite coating gives a scattered plot, however, a slight trend with increasing quartz cement and decrease in coating is seen. B) Quartz cement versus density also gives a scattered plot.

7 Petrophysical results

7.1 Well correlation

In order to clearly see the genetic sequences of sandstone a well correlation between the four wells (34/3-1 S, 34/3-2 S, 34/3-3 S and 34/5-1 S) were performed (Figure 7.1 and 2.4). The entire Cook Formation was penetrated and wire-line logs were run in all wells. The individual sandstone units (C1, C2, C3, C4 and C5) were correlated based on electrical logs were the curves where scanned for similarities in shape and magnitude, all this with contribution from NPD Factpages and core logs (Kjølstad, 2014). The genetic sequences with their corresponding depth are shown in Table 5.1 (Chapter 5), whereas the resulting well correlation is illustrated in Figure 7.1. Table 7.1 presents the database, whereas the average temperature where calculating assuming a temperature gradient of 0,03 C^o/m and a sea water temperature of $4C^o$ at the sea floor.

Table 7.1 Table of well database used in the petrophysical evaluation (obtained from NPD Factpages). Average temperature data is calculated in Interactive Physics.

Well	Total depth, MD (mRKB)	TVD (mRKB)	Kelly Bushing elevation (m)	Bottom hole temp. (C)	Water depth (m)	Top Cook Fm. (MD)	Average temp. (C^o) in Cook Fm.
34/3-1S	4221	4081	25	142	410	3866	113,38
34/3-2S	4331	4315	18	148	409	4012	116,76
34/3-3S	4063	4012	18	141	400	3908	107,94
34/5-1S	3900	3737	25	135	387	3629	99,87

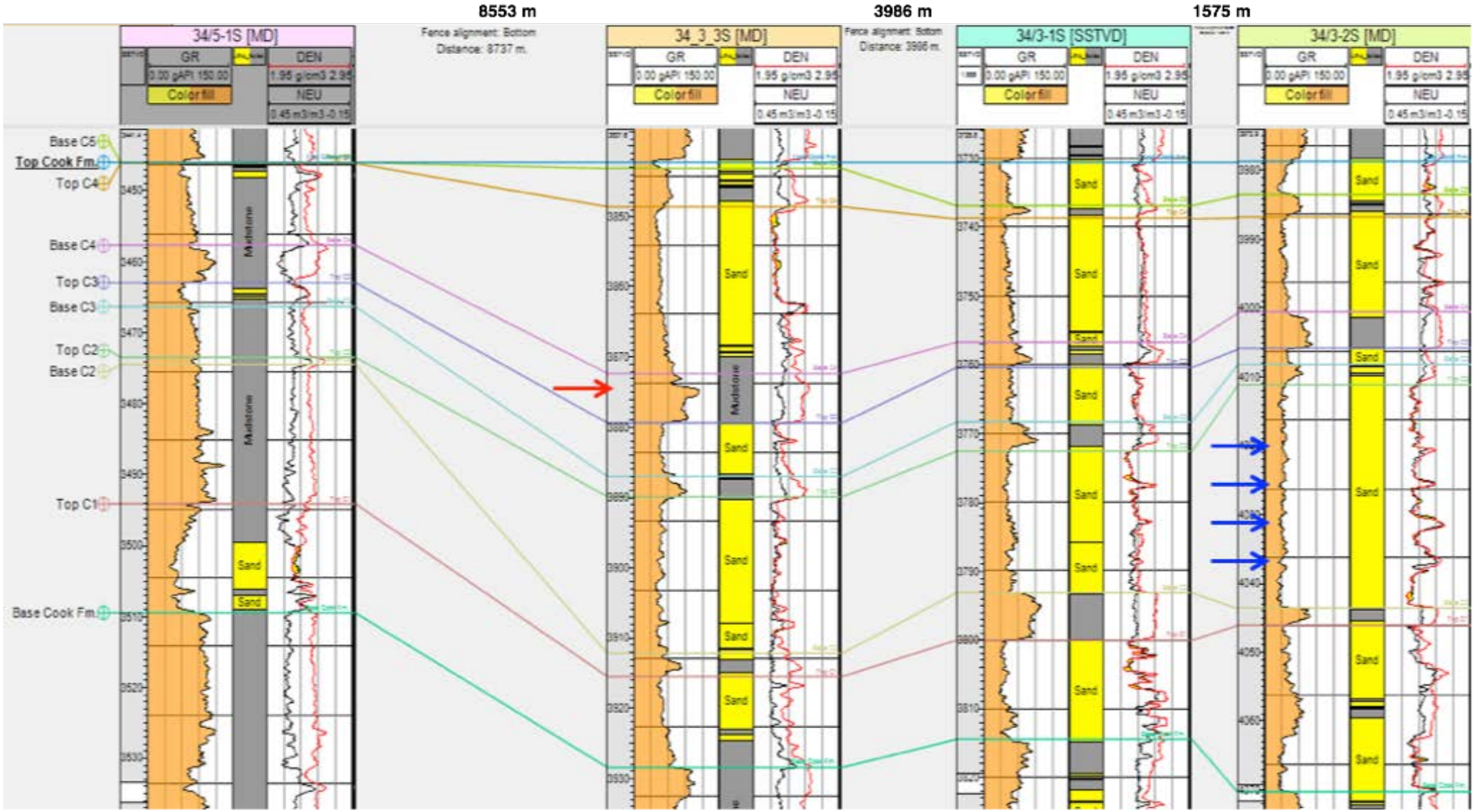

Figure 7.1 Well correlations between all four wells with lithology, gamma ray, neutron, density and travel time (sonic). Examples of cemented intervals within well 34/3-2S are illustrated with blue arrows. Red arrows in well 34/3-3 S illustrate organic rich mudstone.

7.2 Petrophysical evaluation

The shale-sand boundary was set at a gamma ray value of 60, with shale above 60 and sand below 60 (Figure 7.2B). As sand becomes shalier, the bulk density increases as the gamma ray readings increases (Figure 7.2A). Carbonate forming cement within the intergranular pore spaces will increase the density while the gamma ray remains constant. Density readings for the shale remain constant as the clay volume displaces quartz, because they have a similar density (Figure 7.2).

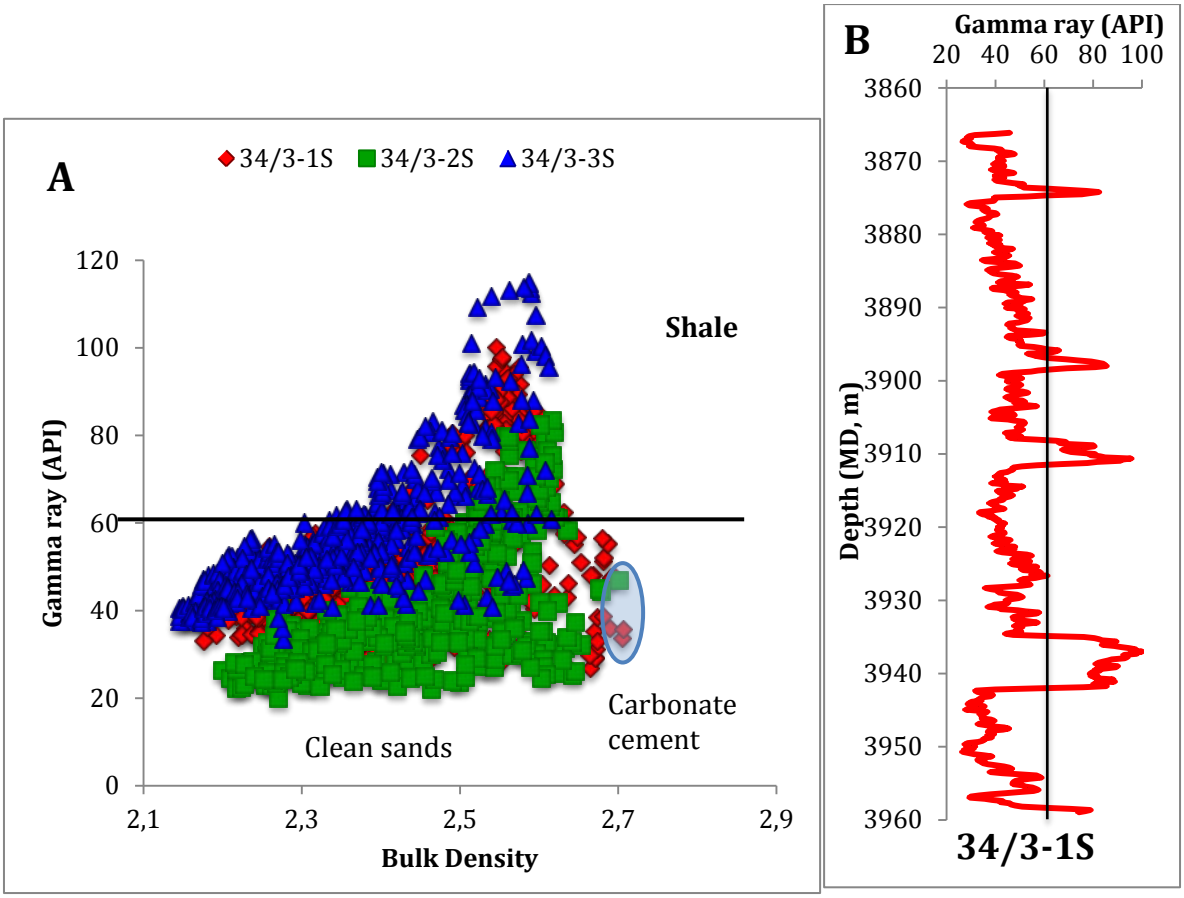

Figure 7.2 A) Gamma ray vs. bulk density for the three wells. Note the carbonate cement shifting towards right in the plot. B) Gamma ray log illustrating the shale-sand boundary at 60 API in well 34/3-1S.

The neutron density plot (Figure 7.3) is commonly used for lithology and porosity determination in simple lithologies. It is important to determine the effect of shale upon porosity, permeability and fluid saturations (Rider and Kennedy, 2011). Due to the lack of permeability data, the emphasis for this thesis will mainly be to determine the effect of shale upon porosity. Between the quartz point at 0 neutron porosity and 2,65g/cm^3 and the water point at 1 neutron porosity and 1g/cm^3 the "clean sand line" can be drawn (Heslop and Heslop, 2003) (Figure 7.3).

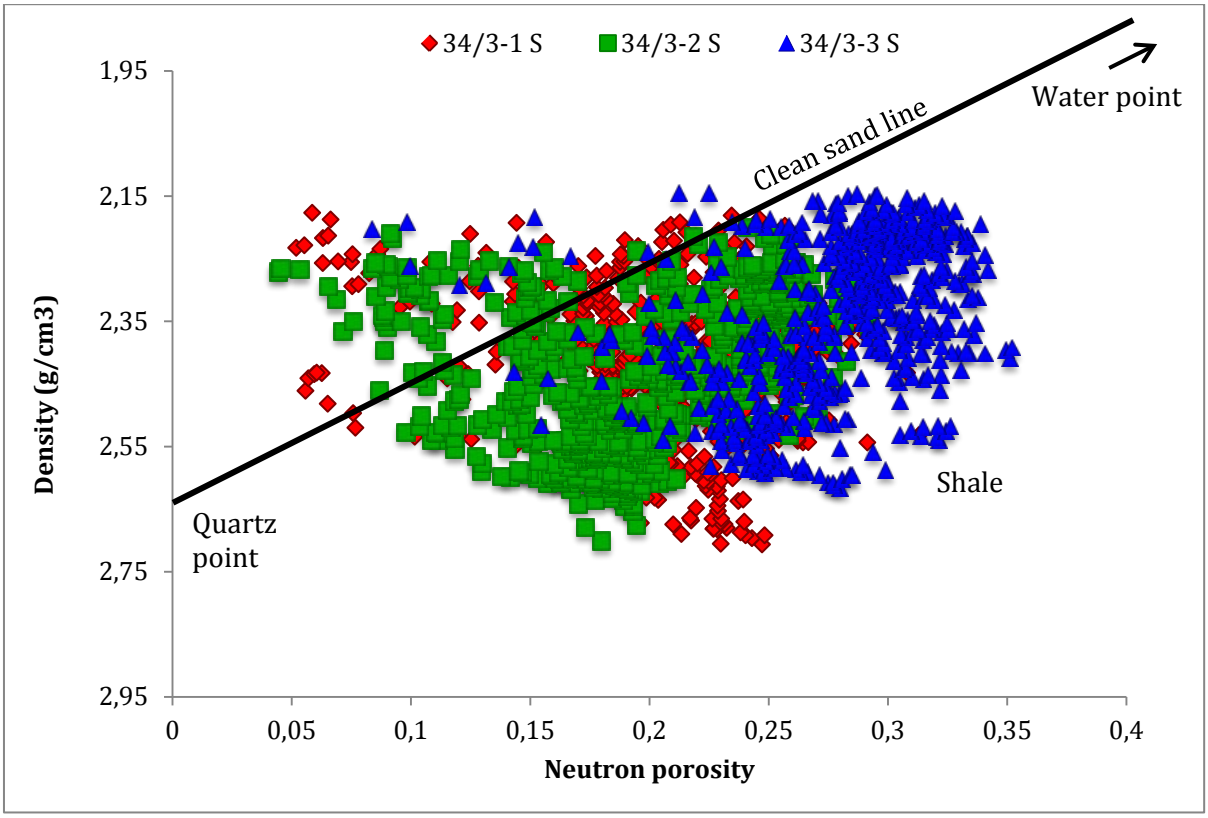

Figure 7.3 Neutron porosity versus density for all three wells. The measurement plots scattered and the porosity ranges from 0 to about 0,35.

Plotting the gamma ray log values against the neutron log values a consistent, straight-line relationship between the two can be observed (Figure 7.4). At this point, the gamma ray and the neutron logs are reacting to a shale-sandstone mixture. Through this straight-line region, changes in neutron porosity typically involve changes in shale content. In very clean sandstones there are variations in porosity that do not involve shale and the relationship between the two logs changes (Rider and Kennedy, 2011). The changes in porosity significantly affect the neutron readings while the gamma ray is unaffected. Neutron tools react to all hydrogen present, resulting in a response with the hydrogen combined with carbon in organic matter. This relationship break can be observed at high gamma ray and neutron values (Heslop and Heslop, 2003) (Figure 7.4).

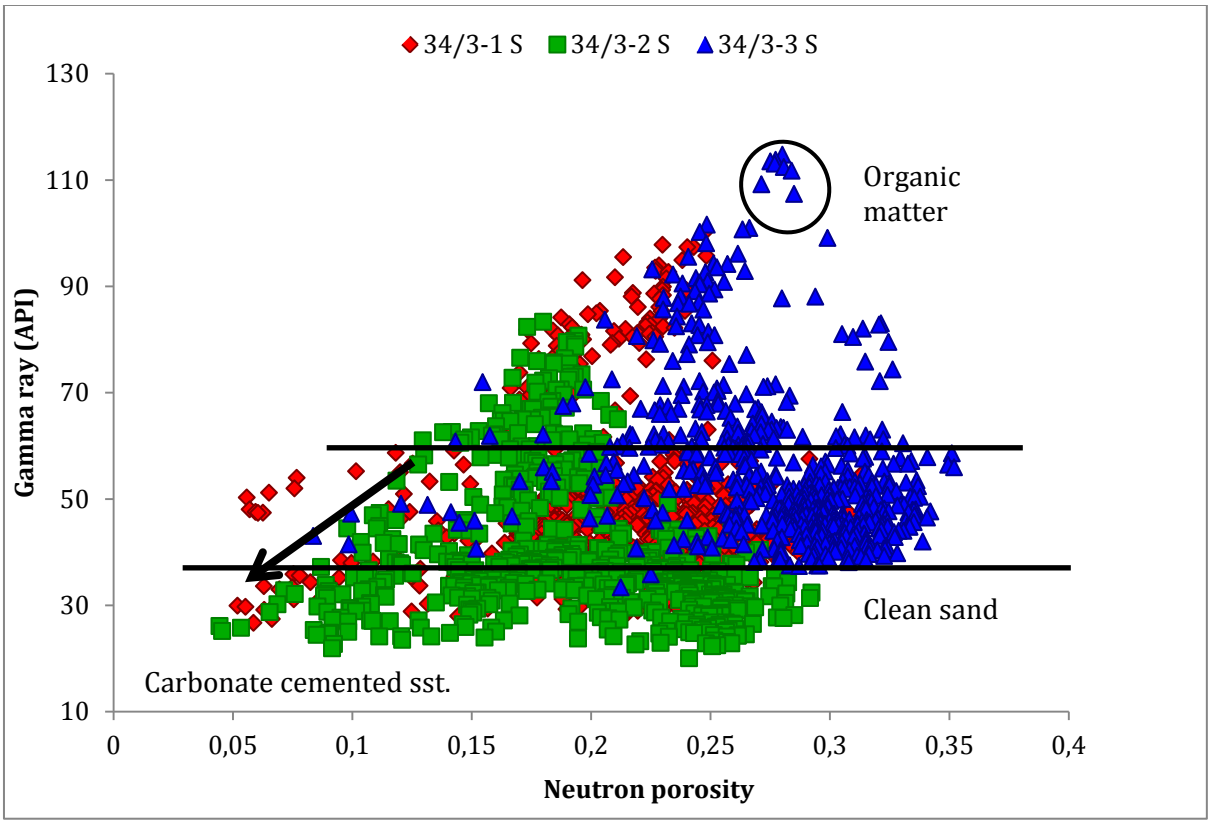

Figure 7.4 Neutron versus gamma ray cross plot with all three wells. Note the almost straight line through the plot that indicates a mixture of shale and sandstone.

The resistivity for shales of common depositional environments is generally constant (Figure 7.5). Inclusions of quartz and other minerals within the shale will have higher resistivity readings than the clay matrix (Heslop and Heslop, 2003). However, these inclusions do have very little effect on the total resistivity of the shales.

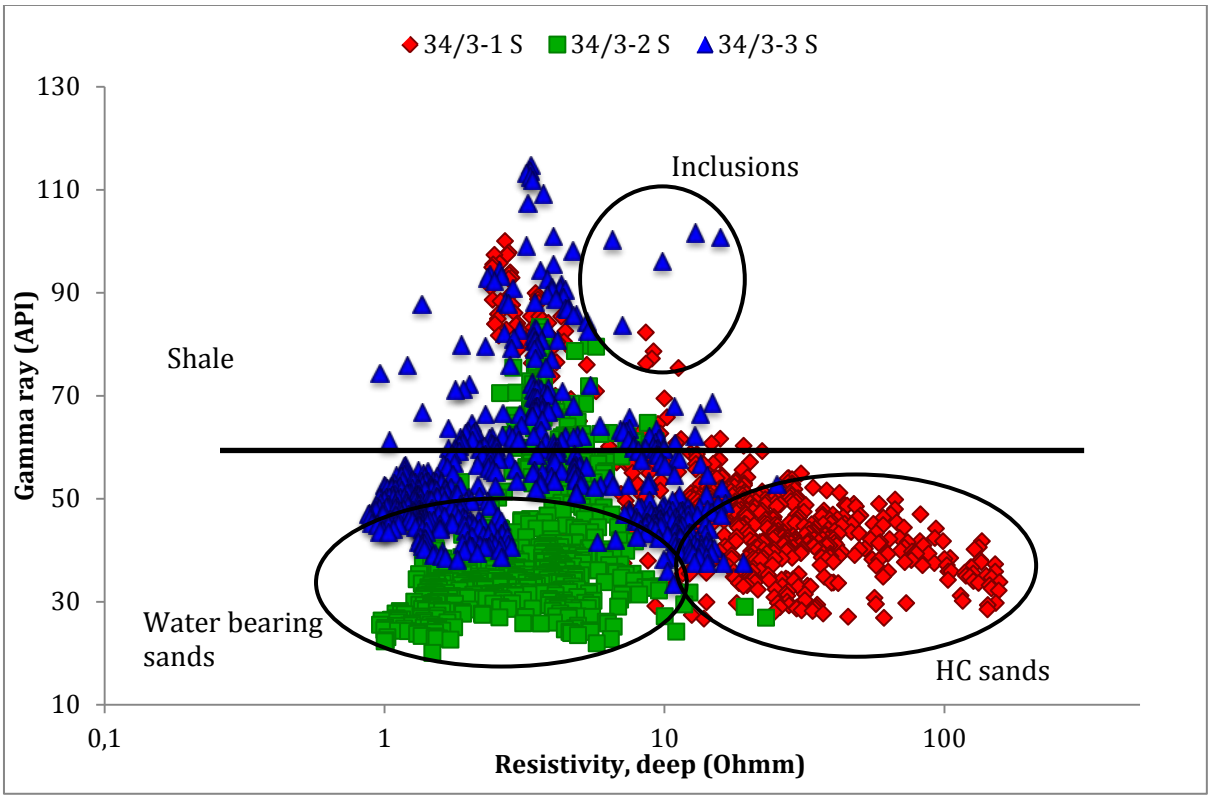

Figure 7.5 Resistivity versus gamma ray for all three wells. Note the constant resistivity values for the shales.

The acoustic travel time (sonic) in shales and sandstone can be similar. For this reason, it is difficult to distinguish between sand and shale responses. Figure 7.6B illustrates the acoustic travel time versus gamma ray in all three wells, Figure 7.6A illustrates a typical calcite cemented interval within well 34/3-1 S. The acoustic travel time is sensitive to cement, resulting in low travel times and moderate gamma ray readings for quartz and carbonate cement (Figure 7.1 and 7.6B). The porosity can be calculated from the sonic log, whereas the travel time recorded on the log is the weighted average of the travel time in the compact rock matrix and through the fluid in the pores (Desbrandes, 1985). The empirical Wyllie time-average equations neglect the variability in important parameters such as mineralogy, texture, pore shape and pore size distribution (Jian et al., 1994). This method is therefore mainly used if there is no other alternative. For this study, the density log was another alternative and has been used for porosity calculations.

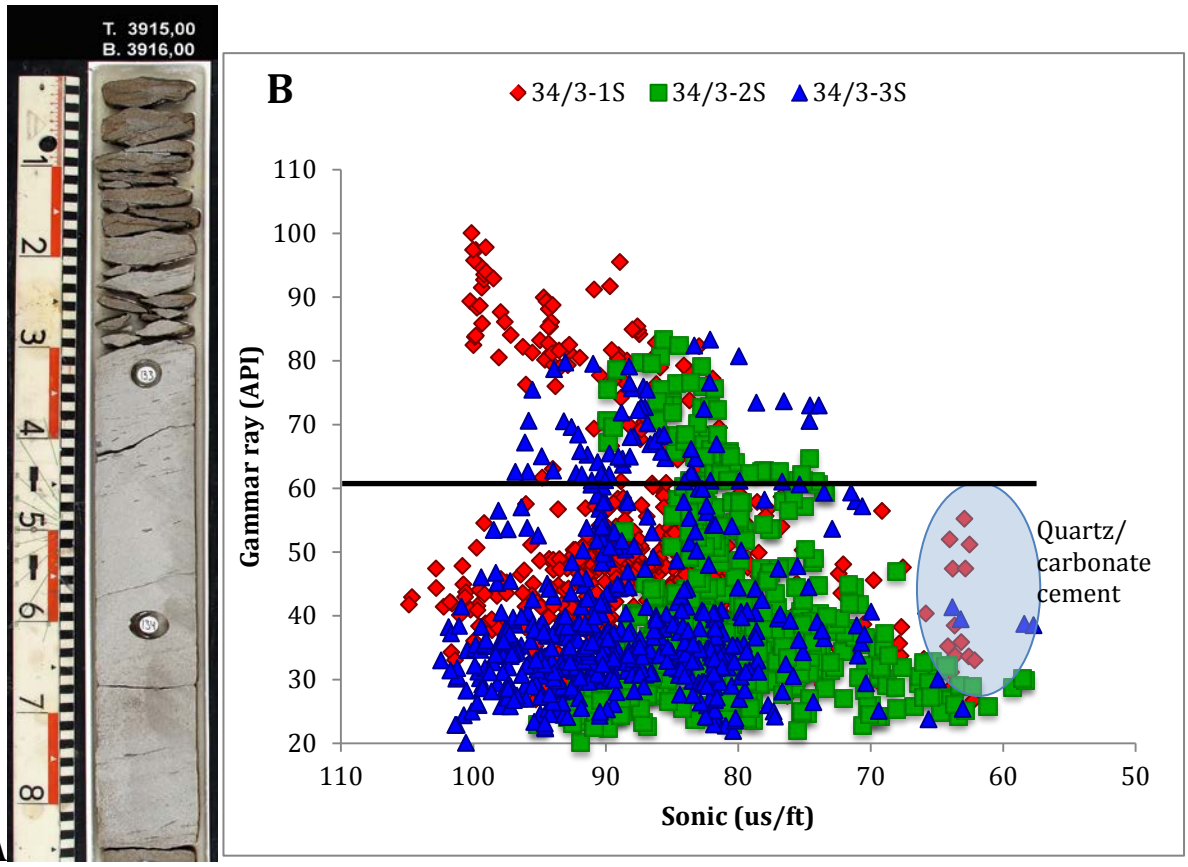

Figure 7.6 A) At 3915-3916 m (MD) in well 34/3-1 S a typically calcite cemented interval is observed. B) Sonic vs. gamma ray for all three wells. Note the carbonate-cemented intervals in well 34/3-1S.

7.2.1 Porosity distribution within the Cook Formation

Porosity distribution of the Cook Formation in the three studied wells are shown in Figure 7.7. The porosity is calculated from Eq. 4.8 ($\phi = \frac{(V_{sh}(\rho_{sh}-\rho_{qz})+\rho_{qz}-DEN}{(\rho_{qz}-\rho_f)}$) and Eq. 4.5 ($\phi = \frac{(\rho_{qz}-\rho_b)}{(\rho_{qz}-\rho_f)}$) (see Chapter 4). Density for rock matrix and shale are not constant for the entire reservoir, and it is therefore difficult to estimate accurately. Equation 4.8 resulted in some negative values (Figure 7.7A), indicating the presence of cemented intervals. Equation 4.5 results in less negative values (Figure 7.7B) compared to Eq. 4.8 (Figure 7.7A).

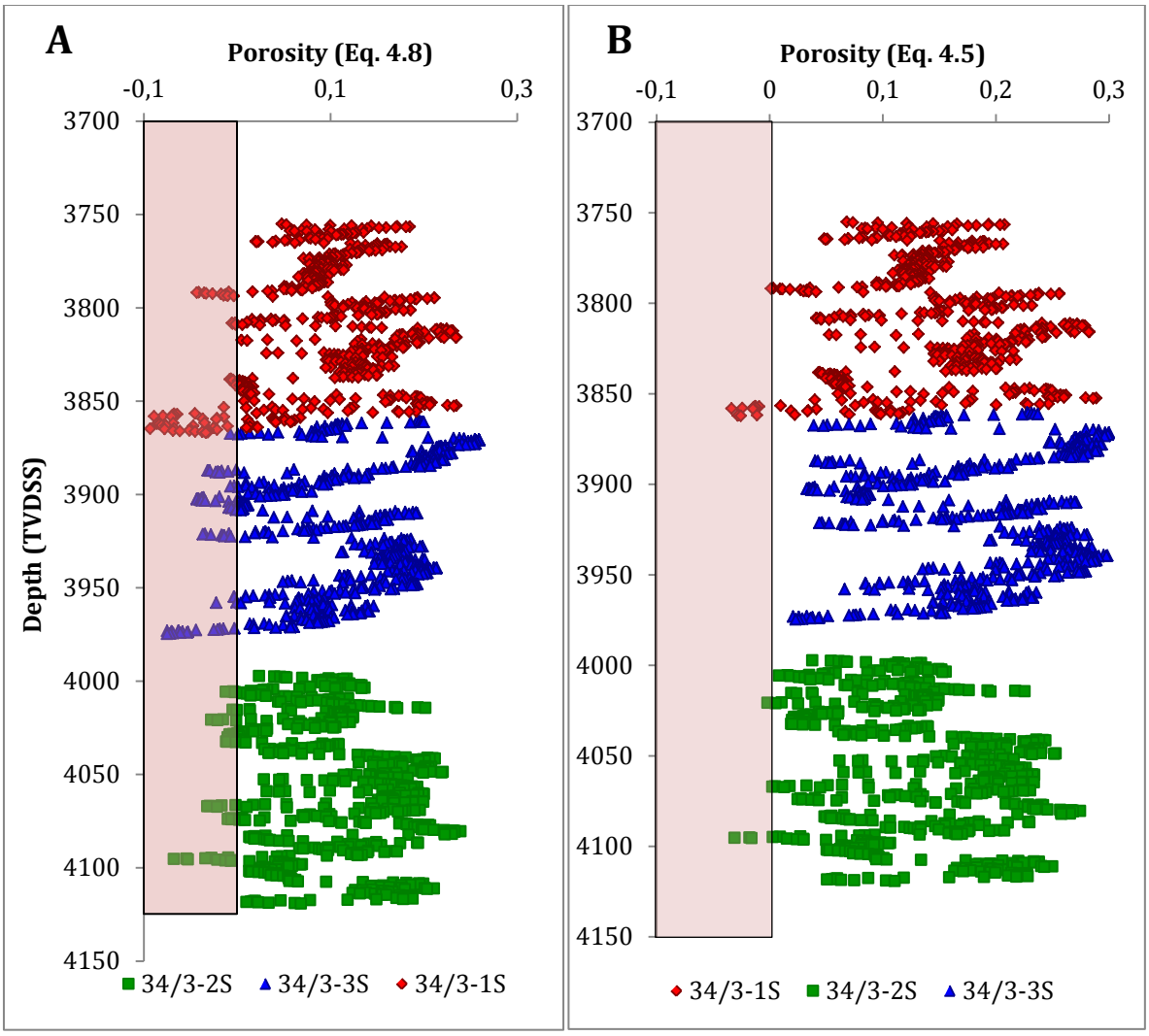

Figure 7.7 A) Density porosity versus depth for all three wells using Eq. 4.4. Note the number of negative values. B) Density porosity versus depth for all three wells using Eq. 4.5. This equation do not result in that many negative values.

Porosity distribution of the five sandstone units within three wells is shown in Figure 7.8, whereas the porosity is calculated from Eq. 4.5, assuming that shale and quartz has the same density. Sandstone unit C2 seem to have the overall highest porosities. However, high porosities are detected within all units and indicate that a porosity preserving mechanism must be present.

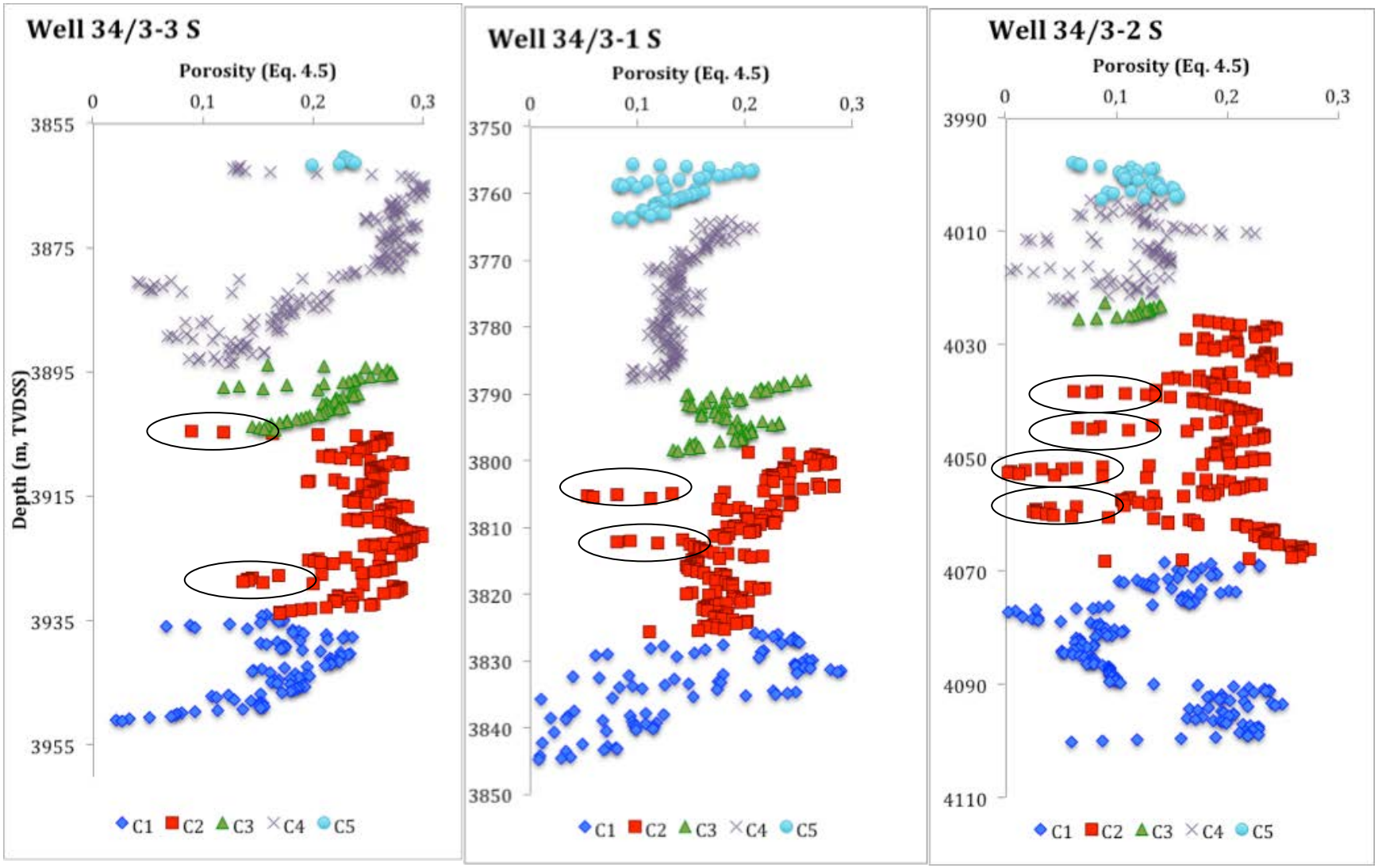

Figure 7.8 Density porosity of all five sandstone units in three wells within the Cook Formation. Note how the porosities are consistently very high in all three wells. C2 generally have the highest porosities (red squares), however, very low porosities are encountered (black circles).

In sandstone reservoirs empirical data indicate that porosity values at a given depth display either an approximately normal distribution or a lognormal distribution (Bloch et al., 2002). Frequency plots of both point counted and calculated porosities and a porosity grain size plot is shown in Figure 7.9. Well 34/3-3S is right skewed and shows anomalous high porosities within the 25-29% and 30+ interval, indicating occurrence of extensive chlorite coating. A right skewed porosity distribution may also indicate sampling problems or reflects diagenetic effects. Both well 34/3-1S and 34/3-S have lognormal porosity distributions. Extensive cementation and/or compaction may result in a shift from normal towards lognormal porosity distribution (Bloch et al., 2002). About the same trends appear in the point counted porosities (Figure 7.9A) as in the calculated porosities (Figure 7.9B), which can work as a quality check for the point counting.

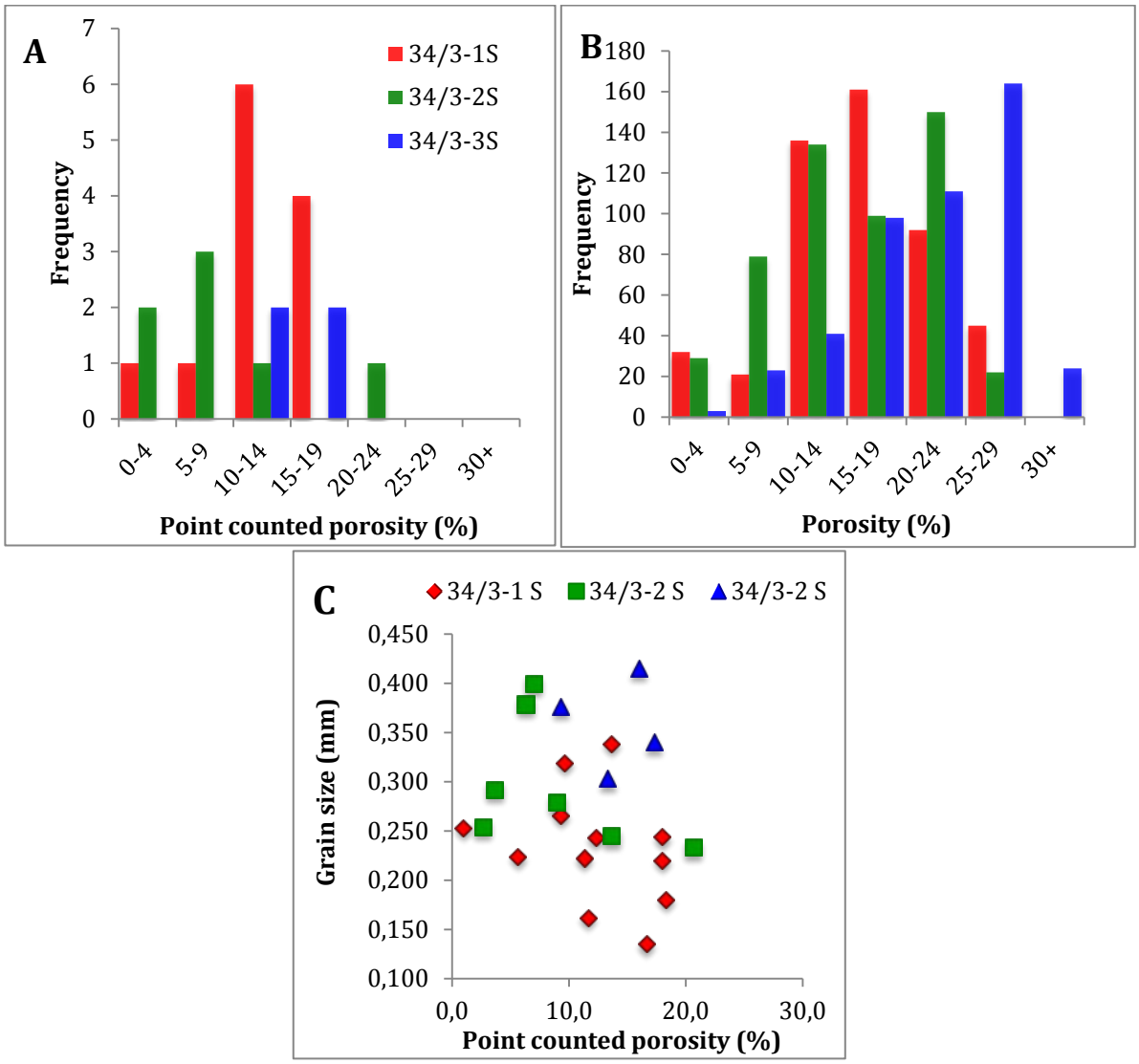

Figure 7.9 A) Point counted porosity distribution for the Cook Formation for all three wells. B) Calculated porosity (Eq. 4.5) distribution for the three wells. Note how the two plots have similar trends. C) Porosity versus grain size results in a relatively scattered plot.

7.2.2 Quartz cementation

A simple kinetic model that simulates quartz cementation and the resulting porosity loss was proposed by (Walderhaug, 1996). This model includes burial and temperature history as important factors regarding modelling of quartz cementation. Consequently, a depth versus quartz cement plot does not adequately represent the effect of temperature history on quartz cementation because sandstones presently at the same depth may have reached this depth by a variety of burial paths, and geothermal gradients may vary both in space and time.

Furthermore, the grain size and mineralogy affects the quartz cementation. Finer grained intervals have been observed to be more quartz cemented than coarser grained intervals. However, McBride (1989) also discusses the opposite trend where there is a higher degree of quartz cement within coarser intervals. Observations for this study, indicates a slight trend with increasing quartz cement with increasing grain size, however, well 34/3-3S do not indicate this trend (Figure 7.10).

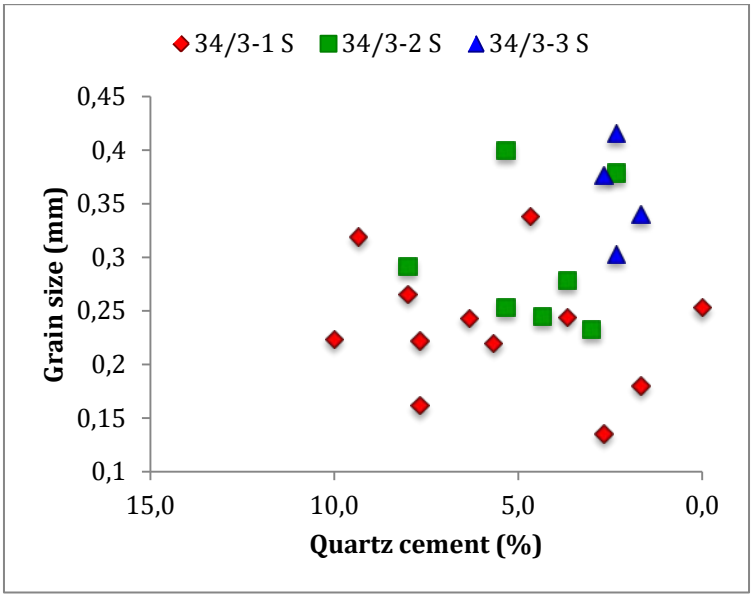

Figure 7.10. Quartz cement versus grain size. Note the slight trend where increasing quartz cement corresponds with increasing grain size.

8 Discussion

8.1 Introduction

Results (Chapter 5-7) presented in this study have shown that the intermediate to deeply buried Cook Formation contains chlorite-coated grains resulting in anomalously high porosities. Sedimentological, petrographic and petrophysical findings suggest a shallow marine setting influenced by both tides and fluvial processes. As a result, the reservoir quality of the Cook Formation in the Knarr area is determined as very good.

8.2 Depositional environment

Cook Formation has been subdivided into five sandstone units, separated by layers of mudstone (Figure 2.4). The five individual, commonly medium-coarse grained and bioturbated, sandstone units contains sedimentary structures indicating a marine setting influenced by tides (Table 6.2). Mud cracks or other features indicating subaerial exposure of sediments were not encountered within the cores, and the sandstones are therefore considered to be deposits without subaerial exposure.

Facies are associated with tidal channel deposits, tidal flat deposits, tidal sand bar deposits and mud bank deposits. Stacked tidal sand bar deposits make up most of the Cook Formation within the three studied wells (Figure 5.4), indicating a large lateral extent of the sand bars. Tidal sand bars forms in a variety of depositional environments, such as deltas, estuaries and more distal marine settings. Evidence suggests that the observed tidal sand bars seem to grade into a more offshore environment. This is indicated by prograding and aggragating structureless sandstones (Facies S1) and sandstones with dune structures (Facies S3) (Figure 5.4). Additionally, a lack of plant evidence within both the mudstone and sandstone are evident, confirming a more or less distal setting from the shore. Tidal channel deposits are considered to develop on the crest of the tidal sand bars (Figure 8.1). Tidal sand flat deposits are related to more proximal parts of the delta, however, similar features might be observed on the flank or crest of tidal bars with tidal channels. Ooids were observed in sandstone unit C4 in well 34/3-1 S (Figure 6.8), indicating a high-energy environment with wave activity during deposition. Mud bank deposits separating the five sandstone packages are most likely deposited over the sandstone surface during relative sea level rise. Sharp boundaries separate the sandstone from the mudstone, indicating rapid sea level rise or erosion.

Regression and transgression are the common control on facies and accumulation rates within the Cook Formation. Under conditions of shoreline regression, one would expect certain variables to change over time and space: water depth to decrease and grain size to increase. Under conditions of shoreline transgression, one would likewise expect certain variables to change over time and space: water depths to increase and grain sizes to decrease (Wood, 2004). This is well illustrated in the Cook Formation with cycles of coarse-grained sandstone deposited during regressive events, separated by fine-grained mudstone intervals deposited during transgressive events (Figure 5.4). Cycles of regression and transgression during the deposition of the Lower Jurassic rocks have been identified in several other basins in Western Europe (Parkinson and Hines, 1995), confirming the observed cyclic pattern of the Cook sandstones.

Previous interpretation of the Cook Formation in other fields in the North Sea, presented in Table 2.2, provides additional insight into the mode of deposition in the Knarr area. Facies associations suggested in these fields seem to be both similar and different from what is presented in the present study. Due to the lateral extent of the Cook Formation, it is likely to include several depositional environments (Figure 2.5A). In the Oseberg area the Cook Formation is interpreted to be deposited as offshore sand ridges (Livbjerg and Mjøs, 1989), similar to what is presented herein. The Oseberg and the Knarr areas are located at almost the same longitude, on a structural high at the margin of the Viking Graben (Figure 2.5A), which may result in similar depositional environments. The shaly Burton Formation is underlying the Cook Formation in the Knarr area, whereas the shaly Drake Formation is overlying (Table 2.1 and Figure 2.3). Both formations are interpreted as offshore/shelf deposits (Table 2.1), and the Cook Formation could be interpreted as a large-scale prograding-retrograding unit.

As a result, the Cook Formation consists of series of stacked prograding and aggragating tidal sand ridges close to a deltaic setting within the dynamics of the tides (Figure 8.1). Westerly thinning of sandstone packages towards well 34/5-1 S indicates prograding from the east (Figure 2.4). The dimensions and architecture of the Cook sandstone is difficult to predict whit only three wells studied.

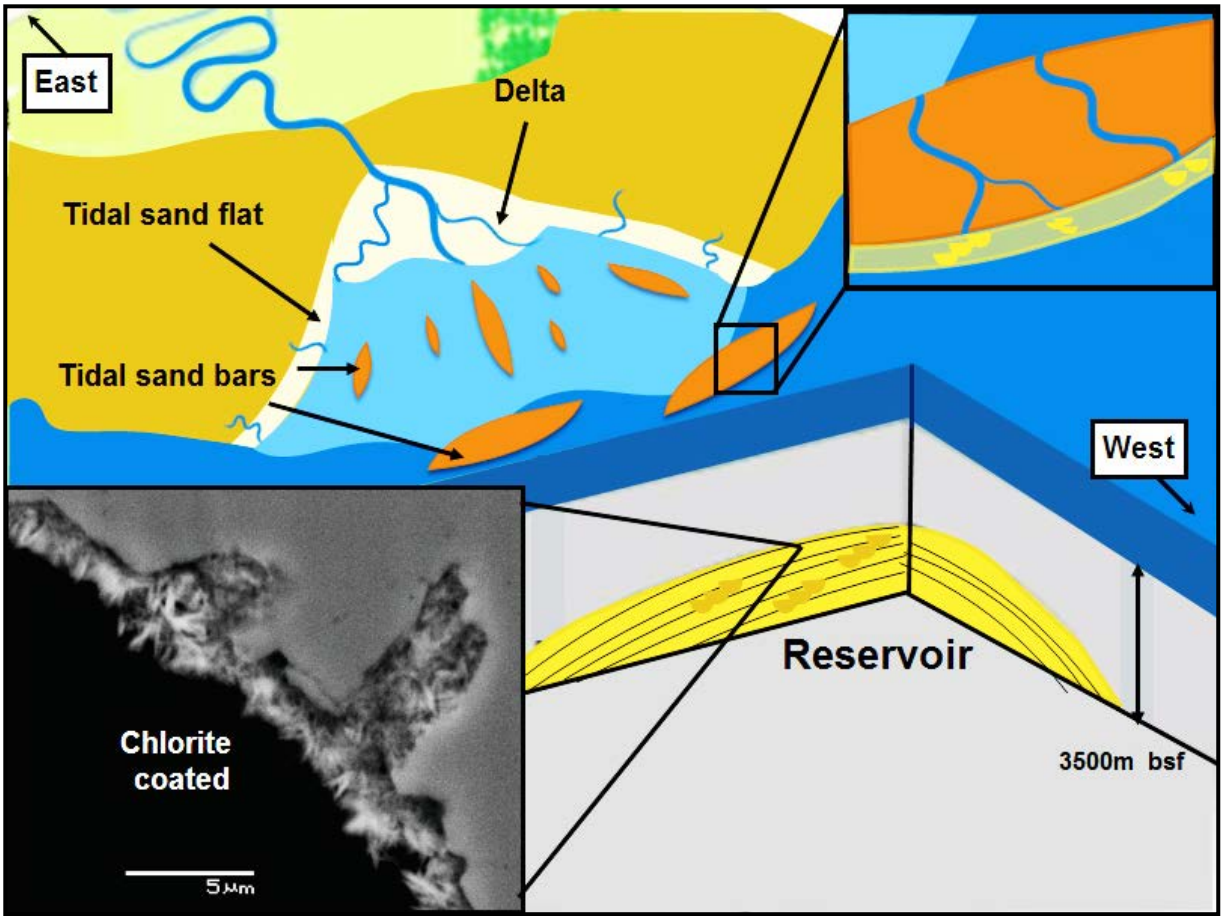

Figure 8.1 Simple conceptual model illustrating the depositional environment during the time of deposition, and the chlorite coated reservoir sandstone at ~3500 m burial depth.

8.3 Detrital mineralogy

Sandstone of the Cook Formation has an average composition of $Q_{82}F_{16}L_2$ and classifies as subarkosic (Figure 6.1). The framework composition of the sandstone does not vary much over the studied samples and significant variation from facies to facies is not observed. The overall subangular shape of the quartz grains indicates generally texturally immature sandstones. The grain sizes of the sandstone ranges between 0,055-0,877 mm and the degree of sorting is moderate to well (Table 5.1). Porosity is independent of grain size (Figure 7.9C), but is strongly controlled by sorting. Porosity decreases progressively from very well sorted to poorly sorted sandstone (Beard and Weyl, 1973). Sandstone of the Cook Formation consists of overall well-sorted sandstone (Table 6.1), corresponding with relatively high and constant porosity measurements throughout the sandstone within the formation (Figure 7.8).

8.4 Burial diagenesis

A quantitative identification of the clay minerals present may contribute to a better understanding of the burial diagenesis of the Cook Formation.

SEM observations suggest that albitization of plagioclase and K-feldspar was significant during burial diagenesis. If the albitisation process is active from 65-105C^{o} the temperature data of the Cook Formation (Table 7.1) indicate that the process has just ended and/or is still on-going. Consequently, the feldspar compositions in the Cook Formation sandstones can be considered to be of both authigenic and detrital origin. The commonly dissolved feldspar grains indicate that the Cook sandstone has been subjected to meteoric water flushing (Figure 6.5B and 6.14B).

XRD results (Figure 5.4A and B) indicate quite large amounts of kaolinite, and less illite. Kaolinite precipitate from dissolved feldspar, and the large amount detected indicate a high degree of meteoric water flushing and feldspar dissolution. Small amounts of illite could indicate that the reaction between kaolinite and K-feldspar has not occurred at the burial depth and temperature interval of the Cook Formation (Table 7.1).

Chlorite coating forms succeeding to burial by growth outward from framework grain surfaces. The grain coating chlorite, pore-filling chlorite and chlorite rosettes seems to occur during early diagenesis, predating the development of secondary porosity (Figure 5.5B&D) and the precipitation of quartz overgrowths (Figure 5.16 and 8.2). Chlorite coating is commonly not observed to be growing on quartz overgrowths, confirming that it formed during early diagenesis (Figure 6.16).

Carbonate cement probably formed during early diagenesis from marine organisms composed of aragonite that have dissolved and precipitated as carbonate cement in the pore spaces. The range and extent of the carbonate cement is difficult to predict from thin sections, and a more comprehensive study is needed to map the carbonate cement in more detail.

Authigenic quartz cement was not encountered frequently, and at sites observed it appeared as overgrowths. The Cook Formation is buried to a depth with a temperature interval were quartz cementation is expected (Table 7.1). Extensive chlorite coating has limited the growth

of authigenic quartz within the Cook Formation. Examples were quartz overgrowths were interpreted to grow despite the existence of chlorite coating reflects a thin or weak chlorite coating at that site (Figure 6.16). Where the chlorite coating appeared to be discontinuous quartz overgrowths were present (Figure 6.16). From SEM analysis the quartz seem to precipitate as syntaxial quartz overgrowths on surfaces of detrital quartz grains (Figure 5.16), and is therefore considered to be precipitation controlled. Stylolites were observed in a few samples during petrographic analysis, and they can be observed in core photos (black squares in Figure 5.2). Stylolites are regarded as the dominant source for quartz cement. Due to a lack of burial history data and pressure data for the Cook Formation in the Knarr area, the distribution of the quartz cement was difficult to predict. A more detailed study of the quartz distribution should be performed.

8.4.1 Chlorite

Composition

Published chemical compositions show that chlorite-coated sandstones can have a range of Fe-Mg ratios (Table 8.1). For coastal settings, the majority appear to be Fe-rich, whereas arid climates and eolian sandstones seem to contain Mg-rich chlorite.

Comparing average compositions of chlorite coating from other studies, similarities can be drawn (Table 8.1). Mg-values range from 0,48-0,80, whereas the synthesised chlorite composition seems to have the lowest values. The Fe-values range from 2,83 – 3,47, indicates that the present study and the published studies include Fe-rich chlorites. Silica tetrahedral occupancy ranges from 2,74 – 3,20. The average composition of the chlorite within the Cook Formation is within the normal range of Fe-rich diagenetic chlorites, and corresponds with earlier research (Table 8.1). In more detail, the chlorite composition recorded in this study is considered as chamosite.

Table 8.1 Average composition of chlorite from different locations. Note how the present results are similar with earlier studies.

Formation	Field/location	Average composition of chlorite	Reference
Cook Fm.	Knarr	$(Mg_{0,80}Fe_{2,83}Al_{1,85})_6(Al_{0,81}Si_{3,20})_4O_{10}(OH)_8$	Present study
Tilje Fm.	Smørbukk	$(Mg_{0,75}Fe_{3,31}Al_{1,70})_6(Al_{1,21}Si_{2,79})_4O_{10}(OH)_8$	Jahren et al. (1998)
Garn Fm.	Smørbukk	$(Mg_{0,88}Fe_{2,89}Al_{1,88})_6(Al_{1,17}Si_{2,83})_4O_{10}(OH)_8$	Jahren et al. (1998)
Synthesised	Synthesised	$(Mg_{0,48}Fe_{3,47}Al_{1,73})_6(Al_{1,10}Si_{2,90})_4O_{10}(OH)_8$	Aagaard et al. (2000)
Tofte Fm.	Haltenbanken	$(Mg_{0,80}Fe_{3,31}Al_{1,68})_6(Al_{1,26}Si_{2,74})_4O_{10}(OH)_8$	Jahren and Aagaard (1992)

Texture

Grain coating chlorite is a result of authigenic processes (Wilson, 1992). The nature and texture of the chlorite coatings determine whether it has a positive or negative impact on the reservoir quality in sandstones (Bloch et al., 2002). Incomplete extensiveness of the chlorite coating may result in the development of authigenic quartz overgrowths. The pore throat diameter in the Cook Formation is controlled by grain size and the size of the chlorite crystals. Chlorite crystals are observed to have a positive effect on the medium to coarse-grained sandstone by preserving the pore network. In fine-grained sandstone and mudstone the chlorite is more detrimental because of a pore-filling behaviour. In the studied samples the chlorite coating has an extensive coverage and the coating were about 0,05mm thick (Figure 5.14A). Recent publications has shown that small chlorite crystals that cover the majority of the grain surface are more likely to preserve porosity and permeability (Ehrenberg, 1993, Berger et al., 2009).

The studied chlorite forms independently of grain size (Figure 5.15B). The coating would be expected to be more prominent in the more coarse-grained sand because it takes a smaller volume of chlorite to achieve good coat completeness in coarse-grained sand than in fine-grained sand. Small amount of data may be a reason for not observing this trend, or the fact that the chlorite is very extensive and do not favour any grain size. However, the chlorite coating in the Cook Formation is considered to have a positive impact on the reservoir quality, regarding both porosity and permeability

8.4.2 Origin of precursor clay

Chlorite is considered to be formed in an isochemical system during burial diagenesis (Chuhan et al., 2000). Within such closed systems the dominant control on the occurrence and type of chlorite is the initial mineralogy of the precursor. Consideration of the precursor mineral sources is therefore important for prediction of chlorite coatings. The chlorite coating present within the Cook Formation is most likely a product of a clay precursor, as discontinuous detrital clay rims were observed during SEM (Figure 6.13A). The systems for precursor clays to coat the grains are complex and difficult to describe. Many mechanisms for clay to coat grains are suggested in literature. Only the most probable proposals for the Cook Formation will be discussed here, including bioturbation, inherited clay coating and mechanical infiltration.

A process that may result in the formation of precursor clay coatings is the bioturbation of sediments by worms. Studies of sediment ingestion by worms reported that a range of early diagenetic clay minerals developed within this ingested sand (Needham et al., 2006). The abundant bioturbation within the studied Cook Formation may indicate that sediment ingestion by worms is the reason for the present chlorite coating. The most extensive chlorite coated facies (Facies S1), especially within well 34/3-2 S (Appendix A), do not have visible intensely bioturbation, but has most likely been bioturbated many times prior to deposition. The gel-like coating on the grain after sediment ingestion by worms does not endure high-energy near shore processes like waves. Consequently, evidence suggests that sediment ingestion by worms is of less significance within the Cook Formation.

Inherited grain coating is another potential process for developing clay coating. The process has been studied in sandstones from eolian and shelf environments, and inherited clay rims is defined as clay coats that form on framework grains prior to deposition (Wilson, 1992). Characteristics used for identifying these inherited clay coats are 1) presence at grain-to-grain contacts between framework grains; 2) widely varying thickness of coating; 3) absence on the surface of diagenetic minerals; 4) clay mineralogy similar to that of clay interbeds; 5) tendency to be developed and preserved only in selected environments (Wilson, 1992). Characteristic 1-4 fits with what is observed in the studied samples. Clay rims are present at grain-to-grain contacts (Figure 6.13B), the thickness of the coating varies (Figure 6.13A) and the clay rims are absent on the surface of diagenetic minerals (6.15A). The composition of the clay precursor is speculative, but is believed to be similar to the interbedding clay. The last

characteristic involves uncertainties and recent studies claim that clay rims are destroyed in high energy near shore environments (Wilson, 1992). High-energy and near shore processes are present within the Cook Formation, and the process of inherited grain coating is therefore unlikely for the Cook Formation.

Mechanical infiltration is the process of muddy water entering a sand body and depositing fine clay size particles on framework grain surfaces (Buurman et al., 1998). For mud water to infiltrate coarse grained sediments two factors have to be considered regarding transport of clay; 1) the state of clay in water; and 2) the nature of the contact between coarse sediments and mud water (Buurman et al., 1998). In a shallow marine setting, as suggested herein (Figure 8.1), mud water from an adjacent fluvial system may have infiltrated the sandstone and adhered to the grains mechanically. Earlier investigations of the infiltration of fine material into sandstones found that: 1) coatings on grains do form when clay suspensions passes through porous sand; 2) a significant amount of suspended material forms a filter cake on top of the sand columns; and 3) chlorite was much more effective in forming coatings than illite or smectite (Matlack et al., 1989). The proposed findings corresponds to the present study, however, the formation of filter cakes were not encountered.

The burial diagenesis of the Cook Formation suggest meteoric water flushing, a processes that the clay precursor has endured. Subaerial exposure may enhance the adhesion of clay to the sandstone grains, as the clay will dry out. As assumed earlier, the Cook Formation has not been exposed for air, and this enhancement could not be accounted for. Mechanical infiltration of clay suspensions from adjacent rivers is considered as the most likely origin of the precursor clay within the Cook Formation. However, further research should confirm this.

8.4.3 Diagenetic history of the precursor clay

During deposition of the Cook Formation it is suggested that suspended clay has infiltrated the porous sandstone and adhered to the grains. The composition of the detrital clay is speculative, however, from SEM analysis it is believed to be Fe-rich and have a mixed composition of potentially illite, smectite, chlorite and kaolinite. Too little information about the chemical composition is available for any significant classification of the precursor clay. A transmission electron micrography (TEM) analysis of the precursor clay would be helpful for classifying the early diagenetic precursor and further understand the diagenetic history. The mixed composition clay rims detected in this study formed during deposition and may have developed into other clay minerals during progressive burial and chemical diagenesis. In recent literature of chlorite-coated reservoirs, several early diagenetic precursor clays are proposed (Table 8.2). Smectite and berthierine are the most probable early diagenetic precursors for the Cook Formation and will be further discussed.

Trioctahedral smectite is proposed as an early diagenetic precursor in literature (Table 8.2). The development of chlorite from a trioctahedral smectite requires either a local source of aluminium or the loss of excess silica (Chang et al., 1986). Humphreys et al. (1989) reported chlorite coating in the Skagerrak Formation, Central Graben, and smectite was proposed as the precursor to chlorite (Table 8.2). The morphology and composition of detrital clay within the Cook Formation is hard to analyse in detail, however, it is not considered to have the flaky morphology that is characteristic for smectite.

An extensive study of Fe-rich chlorite coated quartz grains on several formations on the Norwegian Continental Shelf (Table 8.2) suggest that the chlorite has developed during diagenesis from a Fe-rich clay mineral precursor that formed at the time of deposition (Ehrenberg, 1993). The shallowest buried chlorites in these areas were shown to be a mixed layer-serpentine, whereas berthierine was identified as the most likely serpentine mineral phase. Increasing burial resulted in the mixed-layer serpentine-chlorite to become more chloritic. Simulated chlorite coats of similar morphology and chemistry to naturally occurring chlorites using berthierine-coated sandstones where performed on the Cook Formation in the Oseberg Field (Aagaard et al., 2000). Petrographic results from the present study plot the chlorites within the three studied samples close to diagenetic chlorite (chamosite) and berthierine (Figure 5.11B). Berthierine is a solution between Fe-rich serpentine and kaolinite, and can be suggested as the early diagenetic precursor for chlorite in the Cook Formation.

In the Cook Formation the clay precursor is believed to have partly developed into a berthierine precursor. The berthierine precursor appears to be a necessary requirement in the extensive chlorite coated shallow marine sandstones. Assuming a mechanical infiltration process and a berthierine precursor of the chlorite coating in the Cook Formation, the diagenetic history is summarised (Figure 8.2):

1. Mechanical infiltration results in the clay to adhere to the sand grains during deposition.
2. With increasing depth and chemical diagenesis the precursor clay transforms to berthierine between 65-100C^{o} (Aagaard et al., 2000).
3. Further burial and increasing temperature results in the precipitation of chlorite at temperatures of 80-100C^{o}.
4. Chlorite continues to grow as grain coating, pore filling and rosettes, and the formation of extensive and continuous coating preserves the porosity at great depths.

Figure 8.2 illustrates a simplified diagenetic history of four steps comparing it with a non-coated sandstone. Significant differences between the coated and non-coated sandstone, indicates how important chlorite coating is for preserving porosities in intermediate to deeply buried sandstones.

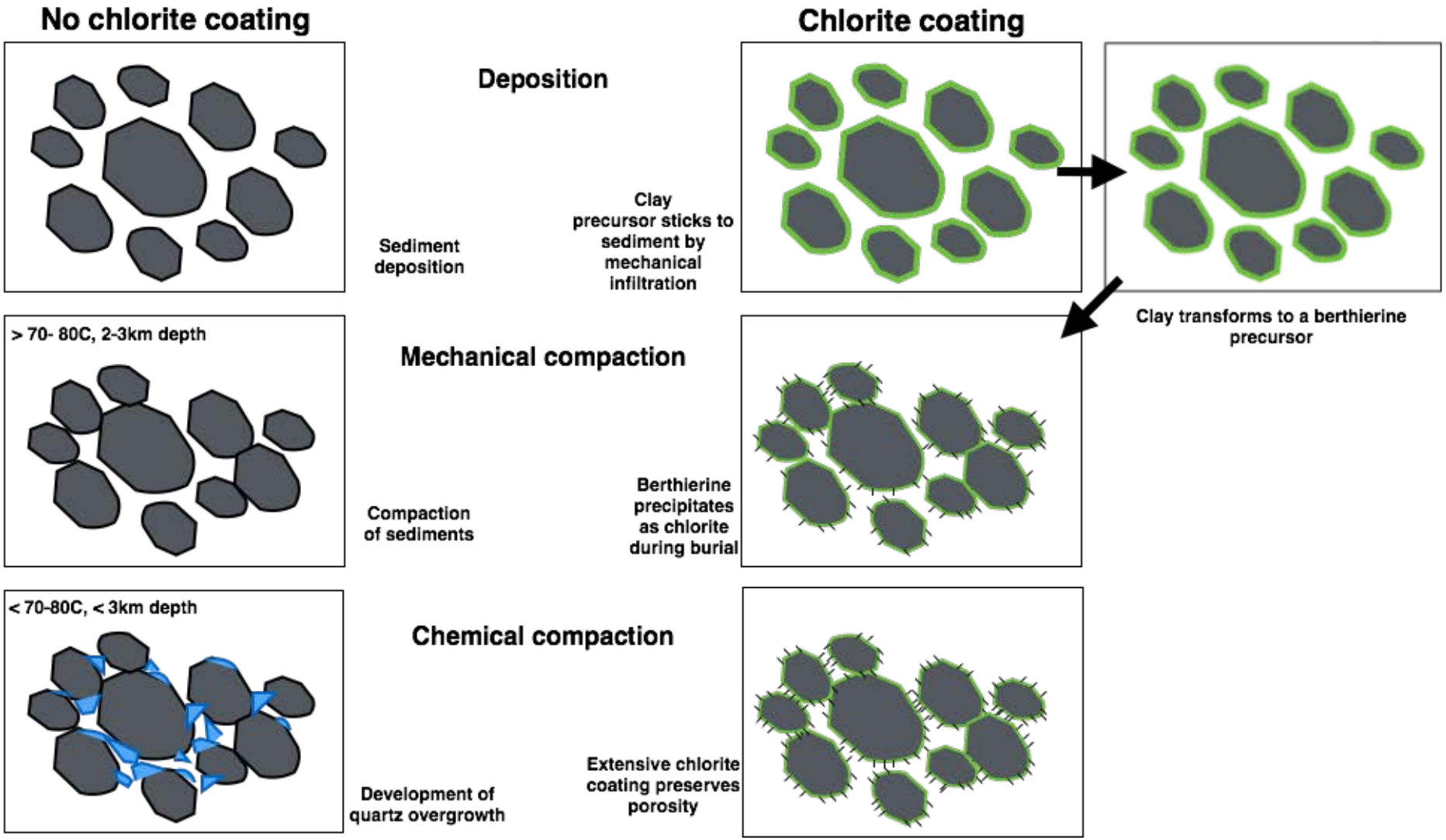

Figure 8.2 Simplified diagentic histories with and without chlorite coatings. Note how the porosity is preserved when chlorite coatings are present.

8.4.4 Depositional environment and the distribution of chlorite coating

The proposed depositional setting of the Cook Formation in the study area is a shallow marine setting within the dynamics of tides and close to a deltaic system influenced by fluvial processes (Figure 8.1). It is suggested that Fe-rich clay in suspension has infiltrated the sandstone and during burial diagenesis resulted in the present day extensive chlorite coating within the Cook Formation (Figure 8.2). This particular depositional environment and diagenetic history is not the case for all other chlorite-coated reservoir recorded worldwide. Table 8.1 summarises the depositional environment and suggested precursor for several fields with chlorite coating worldwide. Berthierine is the most frequently suggested early diagenetic precursor, especially on the Norwegain Continetal Shelf.

Comparing the present study with similar studies worldwide, similarities can be drawn. Marine and fluvial settings are consistently proposed depositional environments, indicating that processes within such environment are required for the formation of chlorite. Sandstones deposited in arid climates, such as the Norphlet Formation (Table 8.2), are exposed for other processes resulting in other precursors than for marine and fluvial environments. The Skagerrak Formation in the Central Graben is deposited in a fluvial-marine regime with smectite as the suggested precursor. A correlation between the depositional environment and the presence of chlorite seem to exist, however, exceptions may appear. Consequently, the distribution pattern of coated sand is a function of coat origin.

Table 8.2 Summary of the general depositional environment of formations with chlorite coating on the Norwegian Continental Shelf and worldwide.

Location	Age	Formation	Depositional environment	Suggested precursor	Reference
Knarr	Lower Jurassic	Cook Fm.	Marine sandstone units deposited in a tidally influenced deltaic setting with a variety of sub environments.	Berthierine	This thesis
South Texas	Paleogene	Lower Vicksburg Fm.	Reservoir consists of six progradational deltaic sandstones.	Odinite	Grigsby (2001)
Sawan gas field, Pakistan	Cretaceous	Goru Fm.	Deposited in a shallow marine setting, proximal wave-dominated delta system and barrier-bar complex.	Unknown	Berger et al. (2009)
Louisiana	Upper Cretaceous	Woodbine/ Tuscaloosa Fm.	Lower sand was interpreted to be a multi-storied composite meander belt point bar and channel deposit, upper sand was interpreted to be a single point bar and channel deposit of a distributary channel.	Berthierine	Thomson (1979) Ryan and Reynolds (1997)
Alabama and Mississippi	Upper Jurassic	Norphlet Fm.	Deposited in an arid climate on a broad desert plain.	Clay/iron oxide rims	Klicman et al. (1988) Dixon et al. (1989)
Central Graben	Late Trirassic	Skagerrak Fm.	Deposited in a fluvial regime, with marginal marine facies toward the top of the succession.	Smectite	Humphreys et al. (1989)
Haltenbanken, Norwegian Sea	Lower Jurassic	Tilje Fm.	Tidally dominated shoreline and delta lobe progradation.	Berthierine	Ehrenberg (1993) Ehrenberg et al. (1998)
Haltenbanken, Norwegian Sea	Lower Jurassic	Tofte Fm.	Local, tectonically sourced outpouring of very coarse sand into a deep marine basin.	Berthierine	Jahren et al. (1998) Ehrenberg (1993)
Veslefrikk Field	Lower Jurassic	Intra-Dunlin Sandstone	45-60 m thick upward coarsening unit reflecting progradation of near shore shallow marine sandstone over offshore silt and mud.	Berthierine	Ehrenberg et al. (1998) Ehrenberg (1993)
Haltenbanken, Norwegian Sea	Middle Jurassic	Garn Fm.	Regionally extensive braid delta with 40-120 m of nearly 100% clean sand deposited during a major sea level fall.	Berthierine	Bjørlykke (1998) Ehrenberg (1993)
Veslefrikk Field, North Sea	Upper-Lower Jurassic	Statfjord Fm.	3-7 m of transgressive marine sandstone capping a thick alluvial plain sequence.	Berthierine	Jahren et al. (1998) Ehrenberg (1993)

8.5 Reservoir quality of the Cook Formation

The reservoir quality of sandstone reservoirs, such as the Cook Formation, is influenced by, among others, the depositional environment, mechanical compaction, detrital composition, burial and diagenetic history, as well as fluid content. Reservoirs generally are a result of the complex combination of all these different factors.

8.5.1 Depositional environment and facies

The effect of facies on reservoir quality in clastic reservoirs is most pronounced in relatively shallow reservoirs, but is not restricted to these shallow depths. The Cook Formation is deeply buried (>3500m bsf) and has been partly diagenetic overprinted, however, the relative quality of each facies does not seem to have changed significantly. Facies variations reflect a fundamental control on the reservoir quality. Massive clean sandstone (Facies S1) and sandstone with mud beds (Facies S2, Table 5.2) has least bioturbation and is frequently encountered within the Cook Formation. Facies with least bioturbation seem to provide the highest porosities, resulting in good reservoir quality. Unfortunately, the clean sandstone is susceptible to carbonate cementation (Figure 5.5). Sandstones with mixing of clay and sand from bioturbation commonly have lower reservoir quality. For comparable depths, the analysed sandstone facies seem to be overall equally porous.

8.5.2 Mechanical compaction

Quartz-rich sandstones are commonly controlled by two diagenetic processes; mechanical compaction and quartz cementation (Lander and Walderhaug, 1999). Mechanical compaction starts immediately after deposition and is therefore considered the main porosity destroying mechanism in most reservoirs. However, mechanical compaction of the Cook Formation most likely diminished after only a small reduction in porosity. This is due to the fact that the Cook Formation consists of well to medium sorted sandstones with sub angular shape and minor amounts of clay matrix. Angular grains have a resistance to reorientation and more ductile grains are needed for more severe porosity loss. Grain dissolution at stylolites is disregarded in this study because it is suggested to have a small effect on rock properties.

The intergranular volume (IGV) is the porosity loss by mechanical compaction prior to quartz cementation. IGV ranges from 23-39% in the Cook Formation (Figure 6.10A). High values

indicate carbonate-cemented intervals. IGV is a function of grain size, which is reflected in Figure 6.10B where a decrease in IGV corresponds to an increase in grain size.

8.5.3 Diagenetic processes

Different diagenetic histories may cause different porosities in compositionally and texturally similar sandstones. Information about the burial history of the study area was not obtained in this thesis. However, the digenetic history was interpreted with the presented results and is considered to be complex (Table 8.3). Besides mechanical compaction, cements are regarded as the most porosity destroying elements. From point counting, illite, kaolinite, quartz, carbonate and chlorite are the cements detected within the Cook Formation (Table 6.1). However, petrographic observations indicate that the reservoir quality is mainly controlled by the appearance of chlorite coating, carbonate and quartz cement (Table 8.3).

Secondary porosity from dissolved feldspar has not been accounted for in this study, as it is believed to have a limited impact on the reservoir quality (Figure 6.5B). Where secondary porosity occur it has little effect on the accuracy of porosity predictions because it is counterbalanced by the local reprecipitation of the dissolved material (Giles and De Boer, 1990).

The presence of illite is regarded to have a negative effect on reservoir quality because of its fibrous behaviour that reduces the permeability (Table 8.3). The amount of illite in the Cook Formation is negligible and is not considered to have an impact on the reservoir quality (Table 6.1 and Figure 6.4 and 6.8C). Kaolinite is pore-filling (Figure 6.8A) and may result in lower reservoir quality. Since the amount is rather local and scattered, kaolinite is regarded to have an insignificant effect on reservoir quality.

Chlorite occurs as both pore-filling and coating. Chlorite may have a variable effect on the reservoir quality, whereas facies and thermal histories may impact the permeability of a sandstone reservoir. Due to a lack of permeability data, the effect of chlorite on this parameter has not been analysed. Pore-filling chlorite in the Cook Formation have a negative effect on porosity, whereas the chlorite coating is extensive and continuous, contributing to a good reservoir quality. Extensive and continuous chlorite coating has therefore inhibited quartz cementation and preserved anomalously high porosities. A porosity versus chlorite

coating plot confirms that chlorite coating is the major control on porosity (Figure 6.15A), where increasing chlorite coating corresponds with increasing porosity.

Quartz and carbonate cement

Petrographic and petrophysical results indicate that extensive chlorite coating has prevented the growth of quartz cement to a large degree. The effect of quartz cement on the reservoir quality is therefore considered less important in the Cook Formation.

Calcite cement were only detected in sample 3915.60 in well 34/3-1 S, but appeared as very extensive throughout the whole sample (Figure 5.15C). From petrophysical analysis and core description there is evidence for multiple calcite cemented intervals and carbonate cement is therefore considered a significant porosity destroying mechanism (Figure 7.8 and Table 8.3). Data points trending towards 0,05 neutron porosity often represents calcite-cemented sandstones, illustrated in well 34/3-1 S (Figure 7.1, 7.3 and 7.4).

Table 8.3 Summary of the proposed diagenetic history of the Cook Formation. How the processes influence the reservoir quality is also presented (bad-neutral-good-very good).

Temperature interval	Burial depth	Process	Influence on reservoir quality
Deposition		Mechanical infiltration of precursor clay.	Good
<70-80C^o	Shallow burial	Precipitation of grain coating berthierine.	Good
<70-80C^o	Shallow burial	Mechanical compaction and grain reorientation.	Bad
<70-80C^o	Shallow burial	Early development of calcite concretions.	Bad
<70-80C^o	Shallow burial	Dissolution of feldspar from meteoric water flushing. Generates secondary porosity.	Good
N/A	Intermediate burial	Precipitation of authigenic kaolinite.	Neutral-bad
65-105 C^o	Intermediate burial	Albitisation of detrital plagioclase.	Neutral
>70-80C^o	Intermediate burial	Precipitation of quartz overgrowths. Probably an ongoing process.	Bad
80-100C^o	Intermediate burial	Berthierine develop as chlorite.	Very good
>130C^o	Deep burial	Precipitation of authigenic illite.	Bad

8.5.4 Fluid content

Resistivity is sensitive to the fluids within the Cook Formation (Figure 7.5). Well 34/3-2 S is mainly water bearing, while well 34/3-1 S contains mainly hydrocarbons (oil). Well 34/3-3 S is both water and hydrocarbon bearing. This is confirmed from the NPD FactPage. The fluid content of the sandstone reservoirs may be important regarding the diagenetic history (Table 8.3). The oil in well 34/3-1 S may have ceased the diagentic processes as oil has emplaced the pores, if assuming oil-wet sandstone. Oil-wet sandstones may result in a slower development of the present chlorite. Water-wet sandstone may allow for more time for the chlorite to develop, resulting in a well-developed chlorite coating. However, to define which wettability state a rock has is very difficult, and almost impossible to define from logging of wells. Observations of the chlorite coating are interpreted to be very well developed in well 34/3-2 S, and less developed in well 34/3-1 S and 34/3-3 S (Table 6.1). These observations may indicate the state of wettability. However, further research is needed to confirm this. As a possible result, the wettability may have influenced the diagenetic history of the Cook Formation.

8.6 Porosity estimations

Porosity for the Cook Formation was calculated using the density log. Porosity equation 4.8 assumes that the empirical V_{sh} and $(\rho_{sh} - \rho_{qz})$ -estimates are correct, if not, this may result in negative values (Figure 7.7A). It is especially the empirical volume of shale (Eq. 4.6) and the chosen density values (Table 4.1) that will result in inaccuracies and cause negative values in the porosity plot (Figure 7.7A). Equation 4.5 assumes that the density of shale and sandstone is the same, resulting in a porosity plot with less negative values than for Equation 4.8 (Figure 7.7). The few negative values encountered using Eq. 4.5 corresponds with Figure 7.2 and 7.4, and is indicated to represent carbonate cemented intervals. Comparing calculated porosity with point counted porosity, similar trends can be seen (Figure 7.9). As a result, the porosity calculations do involve uncertainties, however, the calculations are assumed to give a relatively correct estimate of the porosity in the Cook Formation.

Sandstone units C5 and C4 have somewhat lower porosity readings than the remaining units in well 34/3-1 S and 34/3-2 S, indicating cemented or shaly sandstone (Figure 7.8).

Sandstone unit C2 is the thickest unit with the generally highest porosities. However, cemented intervals are detected within the sandstone (Figure 7.8), apparently causing lower reservoir quality. Apart from the cemented intervals, sandstone unit C2 is considered to have the overall best reservoir quality and future exploration should be focused on this unit.

9 Conclusion and recommendations

9.1 Conclusion

- Tidal sand bars close to a deltaic setting are the main depositional characteristic of the Cook Formation. A setting that is satisfactory because of the good correlation with facies analysis and the proposed precursors of the chlorite. Due to the large lateral extent of the Cook Formation a variety of depositional environment and sub-environments is reported in recent literature. Consequently, it is difficult for comparison to be drawn between the current study and other published studies. The Cook Formation was deposited as an offshore sand ridge in the Oseberg field (Livbjerg and Mjøs, 1989), which is similar to the depositional environment proposed in this study.

- The chlorite present in the Cook Formation is of a Fe-rich chamosite composition and is believed to develop from a mixed clay precursor fixed to the detrital grain during deposition. The mixed clay precursor has further partly developed into berthierine during early diagenesis. Furthermore, chlorite coating seems to favour shallow marine environments, such as estuaries and deltas, where the depositional precursor clay can mechanically infiltrate the sand.

- Quartz cementation is believed to be precipitation controlled, and occurs in only minor amounts throughout the studied samples. Quartz overgrowths are a function of the occurrence and behaviour of the chlorite coatings.

- The present study demonstrates that grain coating chlorite is an effective porosity preserving mechanism in the intermediate to deeply buried Cook Formation in the Knarr area. Extensive and continuous coating has prevented quartz cementation in large parts of the Cook Formation, resulting in anomalously high porosities within the formation. Mechanical compaction, carbonate and quartz cementation are factors causing porosity reduction within the study area.

- Based on the petrographic, sedimentological and petrophysical results obtained in this thesis the reservoir quality of the study area is regarded as good. However, further research regarding permeability should be performed.

9.2 Recommendations

This thesis has discussed the origin of the chlorite coating and compared it with other fields worldwide in order to establish common trends. Such trends can be useful for future exploration in deeply buried reservoir sandstones. However, it is difficult to quantify the effect of the chlorite coating prior to drilling. Presented are a few recommendations of further work to improve the present study:

- TEM analysis of chlorite in order to be more confident on the classification of the precursor clay.
- Cathode luminescence (CL) analysis in order to map the quartz overgrowths and obtain a more precise distribution pattern. A study of the burial history in the study area would also be relevant for the distribution and origin of the quartz cement.
- Integrate the diagenetic history with a sequence stratigraphic analysis.
- Detailed study on the rock physics in order to link the geologic reservoir parameters with seismic properties.
- Map modern tidal settings for construction of realistic reservoir models of tidal systems. This will improve our ability to estimate the probability of exploration success.

10 REFERENCES

BEARD, D. C. & WEYL, P. K. 1973. Influence of texture on porosity and permeability of unconsolidated sand. *AAPG bulletin,* 57**,** 349-369.

BERGER, A., GIER, S. & KROIS, P. 2009. Porosity-preserving chlorite cements in shallow-marine volcaniclastic sandstones: Evidence from Cretaceous sandstones of the Sawan gas field, Pakistan. *AAPG bulletin,* 93**,** 595-615.

BERNER, R. A. 1980. *Early diagenesis: A theoretical approach*, Princeton University Press.

BJØRLYKKE, K. 1994. Fluid-flow processes and diagenesis in sedimentary basins. *Geological Society, London, Special Publications,* 78(1)**,** pp.127-140.

BJØRLYKKE, K. 1998. Clay mineral diagenesis in sedimentary basins-a key to the prediction of rock properties. Examples from the North Sea Basin. *Clay minerals,* 33**,** 15-34.

BJØRLYKKE, K. 1999. Principal aspects of compaction and fluid flow in mudstones. *Geological Society, London, Special Publications,* 158**,** 73-78.

BJØRLYKKE, K. & EGEBERG, P. K. 1993. Quartz cementation in sedimentary basins. *AAPG bulletin,* 77**,** 1538-1548.

BJØRLYKKE, K. & JAHREN, J. 2010. Sandstones and Sandstone Reservoirs *In:* BJØRLYKKE, K. (ed.) *Petroleum geoscience: From sedimentary environments to rock physics.* Berlin: Springer.

BJØRLYKKE, K. & JAHREN, J. 2012. Open or closed geochemical systems during diagenesis in sedimentary basins: Constraints on mass transfer during diagenesis and the prediction of porosity in sandstone and carbonate reservoirs. *AAPG bulletin,* 96**,** 2193-2214.

BJØRLYKKE, K., RAMM, M. & SAIGAL, G. C. 1989. Sandstone diagenesis and porosity modification during basin evolution. *Geologische Rundschau,* 78**,** 243-268.

BJØRLYKKE, K. & AAGAARD, P. 1992. Clay minerals in North Sea sandstones. *Origin, Diagenesis, and Petrophysics of Clay Minerals in Sandstones,* 47.

BJØRLYKKE, K., AAGAARD, P., EGEBERG, P. K. & SIMMONS, S. P. 1995. Geochemical constraints from formation water analyses from the North Sea and the Gulf Coast Basins on quartz, feldspar and illite precipitation in reservoir rocks. *Geological Society, London, Special Publications,* 86**,** 33-50.

BLOCH, S., LANDER, R. H. & BONNELL, L. 2002. Anomalously high porosity and permeability in deeply buried sandstone reservoirs: Origin and predictability. *AAPG bulletin,* 86**,** 301-328.

BLOTT, S. 2000. GRADISTAT v 4.0. 4 ed. Department of Geology, University of London, UK.

BOLES, J. R. 1982. Active albitization of plagioclase, gulf coast Tertiary. *American Journal of Science,* 282**,** 165-180.

BUURMAN, P., JONGMANS, A. G. & PIPUJOL, M. D. 1998. Clay illuviation and mechanical clay infiltration—Is there a difference? *Quaternary International,* 51**,** 66-69.

CANT, D. J. 1992. Subsurface facies analysis. *Facies Models: Response to Sea level Change (Walker, RG; James, NP***,** 195-218.

CHANG, H. K., MACKENZIE, F. T. & SCHOONMAKER, J. 1986. Comparisons between the diagenesis of dioctahedral and trioctahedral smectite, Brazilian offshore basins. *Clays and Clay Minerals,* 34**,** 407-423.

CHARNOCK, M. A., KRISTIANSEN, I. L., RYSETH, A. & FENTON, J. P. G. 2001. Sequence stratigraphy of the lower jurassic dunlin group, northern North Sea. *Norwegian Petroleum Society Special Publications,* 10**,** 145-174.

CHRISTIANSSON, P., FALEIDE, J. I. & BERGE, A. M. 2000. Crustal structure in the northern North Sea: an integrated geophysical study. *Special publication-geological society of london,* 167**,** 15-40.

DALRYMPLE, M. 2001. Fluvial reservoir architecture in the Statfjord Formation (northern North Sea) augmented by outcrop analogue statistics. *Petroleum Geoscience,* 7**,** 115-122.

DESBRANDES, R. 1985. *Encyclopedia of well logging*, Editions OPHRYS.

DIXON, S. A., SUMMERS, D. M. & SURDAM, R. C. 1989. Diagenesis and preservation of porosity in Norphlet Formation (Upper Jurassic), southern Alabama. *AAPG Bulletin,* 73**,** 707-728.

DREYER, T. & WIIG, M. 1995. Reservoir architecture of the Cook Formation on the Gullfaks field based on sequence stratigraphic concepts. *Norwegian Petroleum Society Special Publications,* 5**,** 109-142.

EHRENBERG, S. N. 1990. Relationship Between Diagenesis and Reservoir Quality in Sandstones of the Garn Formation, Haltenbanken, Mid-Norwegian Continental Shelf (1). *AAPG bulletin,* 74**,** 1538-1558.

EHRENBERG, S. N. 1993. Preservation of anomalously high porosity in deeply buried sandstones by grain-coating chlorite: examples from the Norwegian continental shelf. *AAPG Bulletin,* 77**,** 1260-1286.

EHRENBERG, S. N., DALLAND, A., NADEAU, P. H., MEARNS, E. W. & AMUNDSEN, E. F. 1998. Origin of chlorite enrichment and neodymium isotopic anomalies in Haltenbanken sandstones. *Marine and Petroleum Geology,* 15**,** 403-425.

EL-GHALI, M. A. K., EL KHORIBY, E., MANSURBEG, H., MORAD, S. & OGLE, N. 2013. Distribution of carbonate cements within depositional facies and sequence stratigraphic framework of shoreface and deltaic arenites, Lower Miocene, the Gulf of Suez rift, Egypt. *Marine and Petroleum Geology,* 45**,** 267-280.

EVANS, D. 2003. *The Millennium atlas: petroleum geology of the central and northern North Sea,* London, Geological Society of London.

FALEIDE, J. I. & BERGE, A. M. 2000. The geometries and deep structure of the northern North Sea rift system. *Dynamics of the Norwegian Margin,* 167**,** 41.

FJELDSKAAR, W., TER VOORDE, M., JOHANSEN, H., CHRISTIANSSON, P., FALEIDE, J. I. & CLOETINGH, S. 2004. Numerical simulation of rifting in the northern Viking Graben: the mutual effect of modelling parameters. *Tectonophysics,* 382**,** 189-212.

FOLK, R. L. 1980. *Petrology of sedimentary rocks*, Hemphill Publishing Company.

FOLKESTAD, A., VESELOYSKY, Z. & ROBERTS, P. 2012. Utilising borehole image logs to interpret delta to estuarine system: A case study of the subsurface Lower Jurassic Cook Formation in the Norwegian northern North Sea. *Marine and Petroleum Geology,* 29**,** 255-275.

GABRIELSEN, R. H., FÆRSETH, R. B., STEEL, R. J., IDIL, S. & KLØVJAN, O. S. 1990. Architectural styles of basin fill in the northern Viking Graben. *Tectonic Evolution of the North Sea Rifts. Clarendon Press, Oxford***,** 158-179.

GIBBONS, K. A., JOURDAN, C. A. & HESTHAMMER, J. 2003. The Statfjord Field, Blocks 33/9, 33/12 Norwegian sector, Blocks 211/24, 211/25 UK sector, Northern North Sea. *Geological Society, London, Memoirs,* 20**,** 335-353.

GILES, M. R. & DE BOER, R. B. 1990. Origin and significance of redistributional secondary porosity. *Marine and Petroleum Geology,* 7**,** 378-397.
GLENNIE, K. W. 1998. *Petroleum geology of the North Sea: basic concepts and recent advances,* Oxford, Blackwell Science.
GRIGSBY, J. D. 2001. Origin and growth mechanism of authigenic chlorite in sandstones of the lower Vicksburg Formation, south Texas. *Journal of Sedimentary Research,* 71**,** 27-36.
HAQ, B. U., HARDENBOL, J. & VAIL, P. R. 1987. Chronology of fluctuating sea levels since the Triassic. *Science,* 235**,** 1156-1167.
HESLOP, K. & HESLOP, A. 2003. Interpretation of shaly-sands. *LPS DiaLog***,** 15.
HUMPHREYS, B., SMITH, S. A. & STRONG, G. E. 1989. Authigenic chlorite in Late Triassic sandstones from the central graben, North Sea. *Clay mineral,* 24**,** 427-444.
JAHREN, J. S. & AAGAARD, P. 1992. Diagenetic illite-chlorite assemblages in arenites. I. Chemical evolution. *Clays and Clay Minerals,* 40**,** 540-540.
JAHREN, S., OLSEN, E. & BJØRLYKKE, K. 1998. Chlorite coatings in deeply buried sandstones - Examples from the NOrwegian continental shelf. Balkema, Rotterdam.
JIAN, F. X., CHORK, C. Y., TAGGART, I. J., MCKAY, D. M. & BARTLETT, R. M. 1994. A genetic approach to the prediction of petrophysical properties. *Journal of Petroleum Geology,* 17**,** 71-88.
KJØLSTAD, C. 2014. *Reservoir quality, diagenesis and depositional environment of Early Jurassic sandstone reservoirs located in the northern North Sea, Knarr area. .* Master, University of Oslo.
KLICMAN, D. P., CAMERON, C. P. & MEYLAN, M. A. 1988. Petrology and depositional environments of lower Tuscaloosa Formation (upper Cretaceous) sandstones in the North Hustler and Thompson field areas, southwest Mississippi.
LANDER, R. H. & WALDERHAUG, O. 1999. Predicting porosity through simulating sandstone compaction and quartz cementation. *AAPG bulletin,* 83**,** 433-449.
LARIONOV, V. V. 1969. *Radiometry of Boreholes,* Moscow (in Russian), NEDRA.
LERVIK, K. 2006. Triassic lithostratigraphy of the northern North Sea Basin. *Norsk geologisk tidsskrift,* 86**,** 93.
LIVBJERG, F. & MJØS, R. 1989. The Cook Formation, an offshore sand ridge in the Oseberg area, northern North Sea. *Correlation in Hydrocarbon Exploration.* Springer.
MARCUSSEN, Ø., FALEIDE, J. I., JAHREN, J. & BJØRLYKKE, K. 2010. Mudstone compaction curves in basin modelling: a study of Mesozoic and Cenozoic Sediments in the northern North Sea. *Basin Research,* 22**,** 324-340.
MARJANAC, T. 1995. Architecture and sequence stratigraphic perspectives of the Dunlin Group formations and proposal for new type-and reference-wells. *Norwegian Petroleum Society Special Publications,* 5**,** 143-165.
MARJANAC, T. & STEEL, R. J. 1997. Dunlin group sequence stratigraphy in the northern North Sea: A model for Cook sandstone deposition. *Aapg Bulletin-American Association of Petroleum Geologists,* 81**,** 276-292.
MATLACK, K. S., HOUSEKNECHT, D. W. & APPLIN, K. R. 1989. Emplacement of clay into sand by infiltration. *Journal of Sedimentary Research,* 59.
MCBRIDE, E. F. 1989. Quartz cement in sandstones: a review. *Earth-Science Reviews,* 26**,** 69-112.
MIALL, A. D. 1985. Architectural-element analysis: a new method of facies analysis applied to fluvial deposits. *Earth-Science Reviews,* 22**,** 261-308.

MONDOL, N. H., BJØRLYKKE, K., JAHREN, J. & HØEG, K. 2007. Experimental mechanical compaction of clay mineral aggregates—Changes in physical properties of mudstones during burial. *Marine and Petroleum Geology,* 24**,** 289-311.

MORAD, S. 1998. *Carbonate Cementation in Sandstones: Distribution Patterns and Geochemical Evolution (Special Publication 26 of the IAS)*, John Wiley & Sons.

MORAD, S. 2009. *Carbonate Cementation in Sandstones: Distribution Patterns and Geochemical Evolution (Special Publication 26 of the IAS)*, John Wiley & Sons.

MORAD, S., AL-RAMADAN, K., KETZER, J. M. & DE ROS, L. F. 2010. The impact of diagenesis on the heterogeneity of sandstone reservoirs: A review of the role of depositional facies and sequence stratigraphy. *AAPG bulletin,* 94**,** 1267-1309.

MAAST, T. E. 2013. *Reservoir quality of deeply buried sandstones : a study of burial diagenesis from the North Sea. .* ph.d. PhD, University of Oslo.

NEEDHAM, S. J., WORDEN, R. H. & CUADROS, J. 2006. Sediment ingestion by worms and the production of bio‐clays: a study of macrobiologically enhanced weathering and early diagenetic processes. *Sedimentology,* 53**,** 567-579.

NICHOLS, G. 2009. *Sedimentology and stratigraphy*, John Wiley & Sons.

NORLEX. 2014. *NORLEX - Norwegian Interactive Offshore Stratigraphic Lexicon* [Online]. University of Oslo. Available: http://www.nhm2.uio.no/norlexlite/N_Viking_Graben.html 09.04.2014].

NPD. 2013. *Knarr* [Online]. Available: http://www.npd.no/publikasjoner/faktahefter/fakta-2013/kap-11/knarr/ [Accessed 27.10.2013.

NYSTUEN, J. P. & FÄLT, L.-M. 1995. Upper Triassic-Lower Jurassic reservoir rocks in the Tampen Spur area, Norwegian North Sea. *Norwegian Petroleum Society Special Publications,* 4**,** 135-179.

OFFSHORE-TECHNOLOGY. 2014. *Knarr Field, North Sea, Norway* [Online]. Available: http://www.offshore-technology.com/projects/knarr-field-north-sea/ [Accessed 15/1 2014].

PALMER, S. N. & BARTON, M. E. 1987. Porosity reduction, microfabric and resultant lithification in UK uncemented sands. *Geological Society, London, Special Publications,* 36**,** 29-40.

PARKINSON, D. N. & HINES, F. M. 1995. The lower jurassic of the north viking graben in the context of western european lower jurassic stratigraphy. *Norwegian Petroleum Society Special Publications,* 5**,** 97-107.

RAMM, M. 1992. Porosity-depth trends in reservoir sandstones: theoretical models related to Jurassic sandstones offshore Norway. *Marine and Petroleum Geology,* 9**,** 553-567.

RIDER, M. H. & KENNEDY, M. 2011. *The geological interpretation of well logs,* Aberdeen, Rider-French.

RITTENHOUSE, G. 1971. Mechanical compaction of sands containing different percentages of ductile grains: a theoretical approach. *AAPG Bulletin,* 55**,** 92-96.

RYAN, P. C. & REYNOLDS, R. C. 1997. The chemical composition of serpentine/chlorite in the Tuscaloosa Formation, United States Gulf Coast: EDX vs. XRD determinations, implications for mineralogic reactions and the origin of anatase. *Clays and clay minerals,* 45**,** 339-352.

RÜPKE, L. H., SCHMALHOLZ, S. M., SCHMID, D. W. & PODLADCHIKOV, Y. Y. 2008. Automated thermotectonostratigraphic basin reconstruction: Viking Graben case study. *Aapg Bulletin,* 92**,** 309-326.

RØE, S. L. & STEEL, R. 1985. SEDIMENTATION, SEA‐LEVEL RISE AND TECTONICS AT THE TRIASSIC‐JURASSIC BOUNDARY (STATFJORD FORMATION), TAMPEN SPUR, NORTHERN NORTH SEA. *Journal of Petroleum Geology,* 8**,** 163-186.

SAIGAL, G. C., MORAD, S., BJORLYKKE, K., EGEBERG, P. K. & AAGAARD, P. 1988. Diagenetic albitization of detrital K-feldspar in Jurassic, Lower Cretaceous, and Tertiary clastic reservoir rocks from offshore Norway, I. Textures and origin. *Journal of Sedimentary Research,* 58.

SCOTT, E. S. 1992. The palaeoenvironments and dynamics of the Rannoch—Etive nearshore and coastal succession, Brent Group, northern North Sea. *Geological Society, London, Special Publications,* 61**,** 129-147.

SCRUTON, P. C. 1960. Delta building and the deltaic sequence.

SCULL, B. J. & DEEGAN, C. E. 1977. *A Standard lithostratigraphic nomenclature for the central and northern North Sea,* London, H.M.S.O.

STEEL, R. J. Triassic–Jurassic megasequence stratigraphy in the Northern North Sea: rift to post-rift evolution. Geological Society, London, Petroleum Geology Conference series, 1993. Geological Society of London, 299-315.

THOMSON, A. 1979. Preservation of porosity in the deep Woodbine/Tuscaloosa trend, Louisiana.

UNDERHILL, J. R. 1998. Jurassic. *In:* GLENNIE, K. W. (ed.) *Petroleum geology of the North Sea: basic concepts and recent advances.* Oxford: Blackwell Science.

VELDE, B. 1985. *Clay minerals: a physico-chemical explanation of their occurrence*, Elsevier.

VOLLSET, J. & DORÉ, A. G. 1984. *A revised Triassic and Jurassic lithostratigraphic nomenclature for the Norwegian North Sea*, Oljedirektoratet.

WALDERHAUG, O. 1996. Kinetic modeling of quartz cementation and porosity loss in deeply buried sandstone reservoirs. *AAPG bulletin,* 80**,** 731-745.

WALDERHAUG, O. & BJØRKUM, P. A. 2003. The effect of stylolite spacing on quartz cementation in the Lower Jurassic Stø Formation, southern Barents Sea. *Journal of Sedimentary Research,* 73**,** 146-156.

WALDERHAUG, O., LANDER, R. H., BJØRKUM, P. A., OELKERS, E. H., BJØRLYKKE, K. & NADEAU, P. H. 2000. Modelling quartz cementation and porosity in reservoir sandstones: examples from the Norwegian continental shelf. *Quartz cementation in sandstones***,** 39-49.

WELTON, J. E. 2003. *SEM petrology atlas*.

WENTWORTH, C. K. 1922. A scale of grade and class terms for clastic sediments. *The Journal of Geology***,** 377-392.

WILSON, M. D. 1992. Inherited grain-rimming clays in sandstones from eolian and shelf environments: their origin and control on reservoir properties.

WOOD, L. J. 2004. Predicting tidal sand reservoir architecture using data from modern and ancient depositional systems.

WORDEN, R. H. & MORAD, S. 2003. *Clay minerals in sandstones: controls on formation, distribution and evolution*, Wiley Online Library.

ZIEGLER, P. A. & MIJ, P. 1982. Geological atlas of western and central Europe.

AAGAARD, P., JAHREN, J. S., HARSTAD, A. O., NILSEN, O. & RAMM, M. 2000. Formation of grain-coating chlorite in sandstones. Laboratory synthesized vs. natural occurrences. *Clay Minerals,* 35**,** 261-269.

11 APPENDIX

Appendix A: Sedimentological core logs

In the following a legend and the resulting sedimentological core logs from the three wells studied are presented. These are made from the provided core photos (BG Norge), whereas grain size analysis is based on (Kjølstad, 2014).

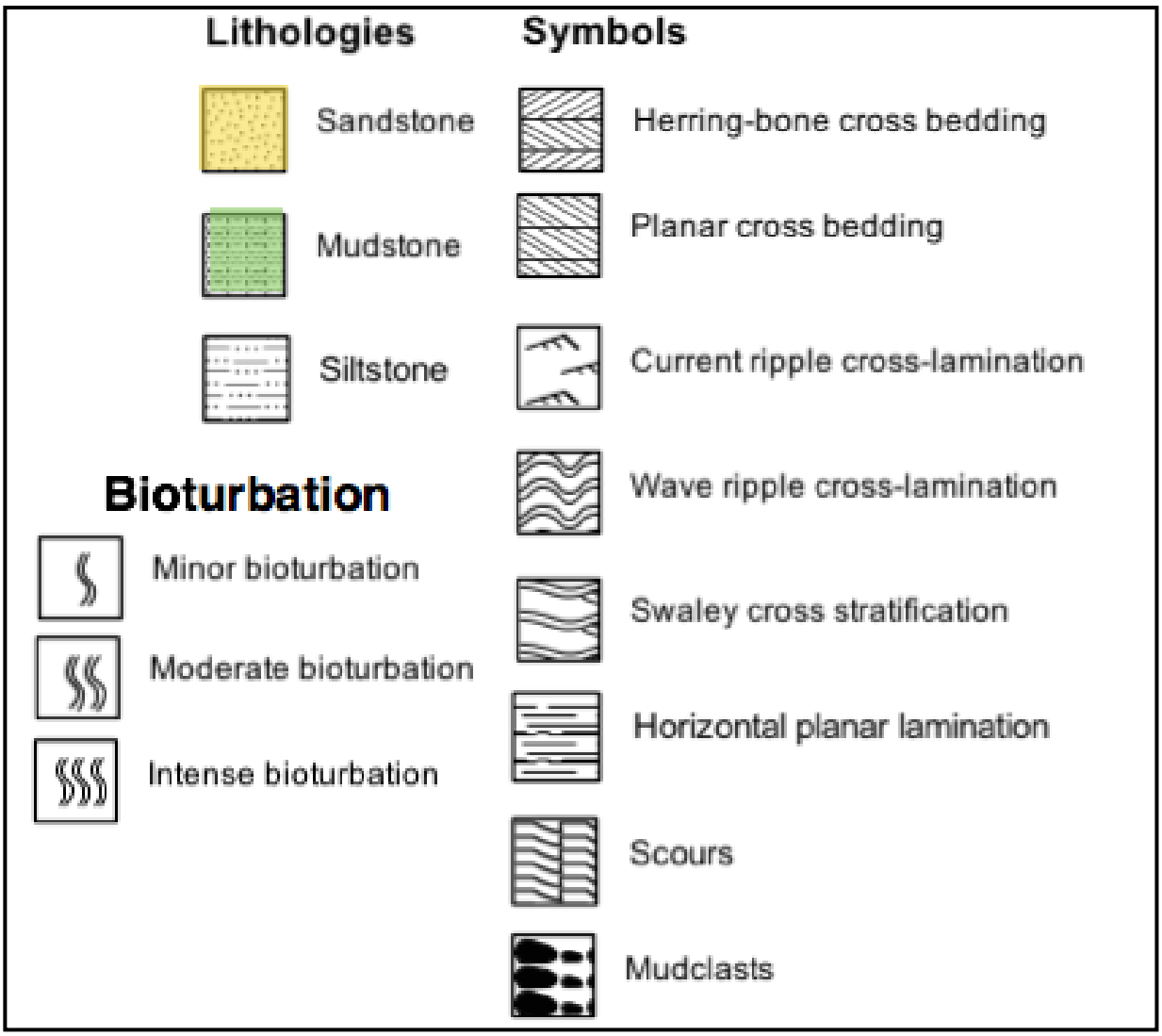

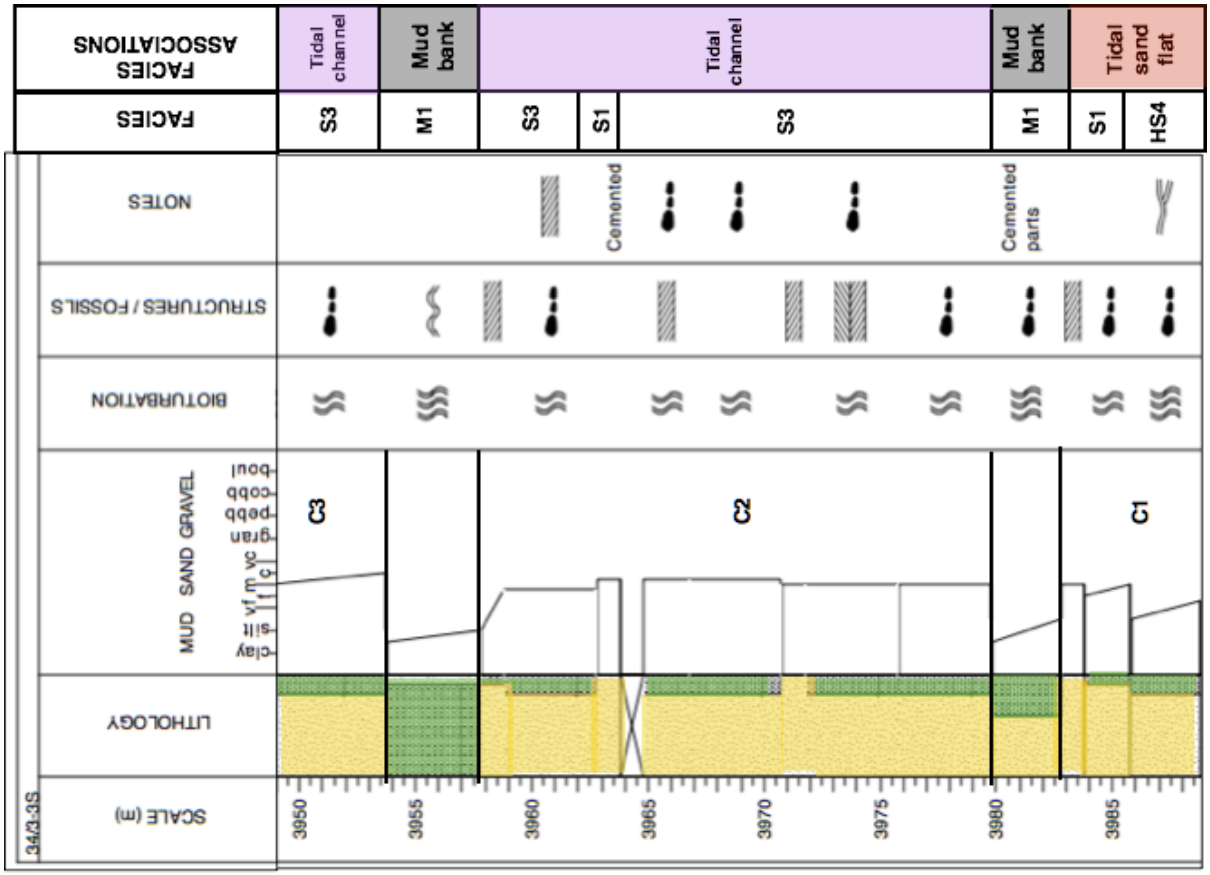
FACIES ASSOCIATIONS
Tidal channel
Mud bank
Tidal channel
Mud bank
Tidal sand flat
FACIES
S3
M1
S3
S1
S3
M1
S1
HS4
NOTES
Cemented
Cemented parts
STRUCTURES / FOSSILS
BIOTURBATION
MUD SAND GRAVEL
clay silt vf f m c vc gran pebb cobb boul
C3
C2
C1
LITHOLOGY
SCALE (m)
3950
3955
3960
3965
3970
3975
3980
3985
34/3-3S

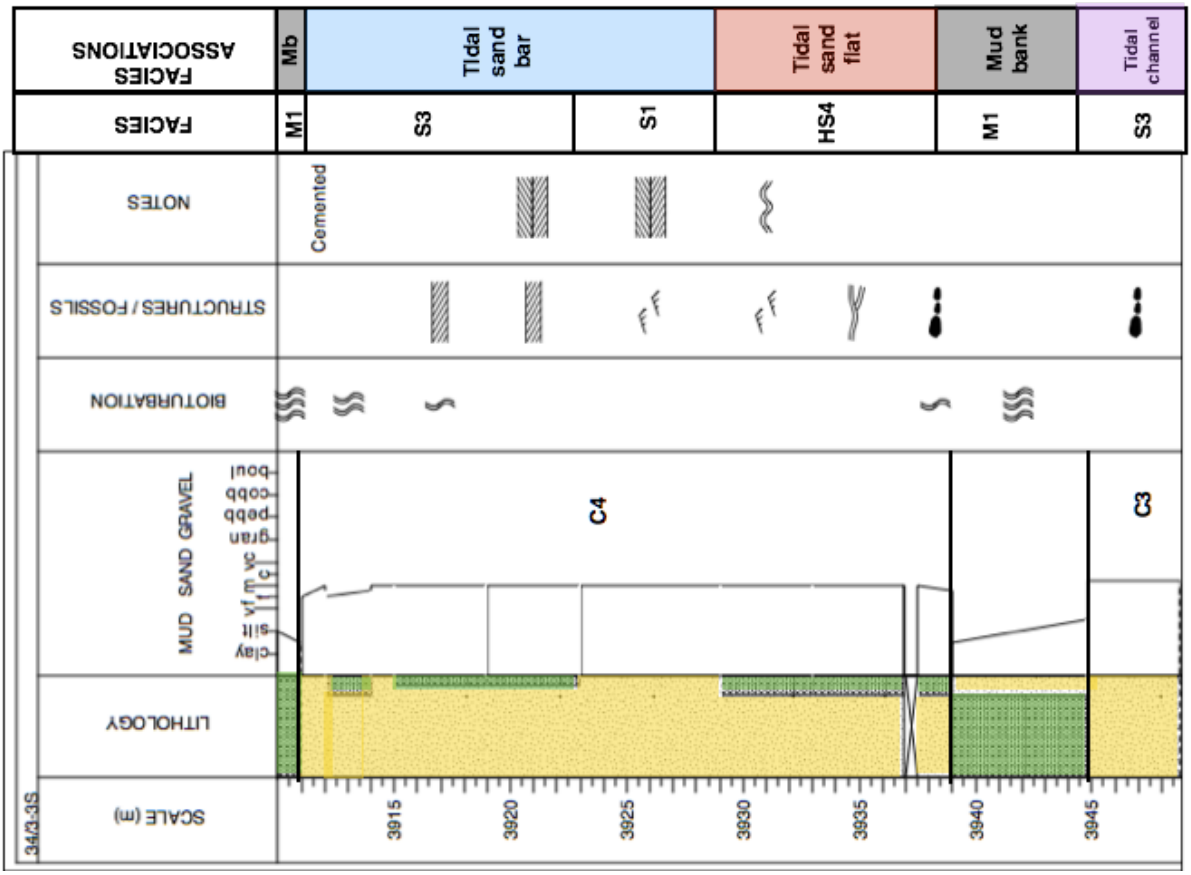
FACIES ASSOCIATIONS
Mb
Tidal sand bar
Tidal sand flat
Mud bank
Tidal channel
FACIES
M1
S3
S1
HS4
M1
S3
NOTES
Cemented
STRUCTURES / FOSSILS
BIOTURBATION
MUD SAND GRAVEL
clay silt vf f m c vc gran pebb cobb boul
C4
C3
LITHOLOGY
SCALE (m)
3915
3920
3925
3930
3935
3940
3945
34/3-3S

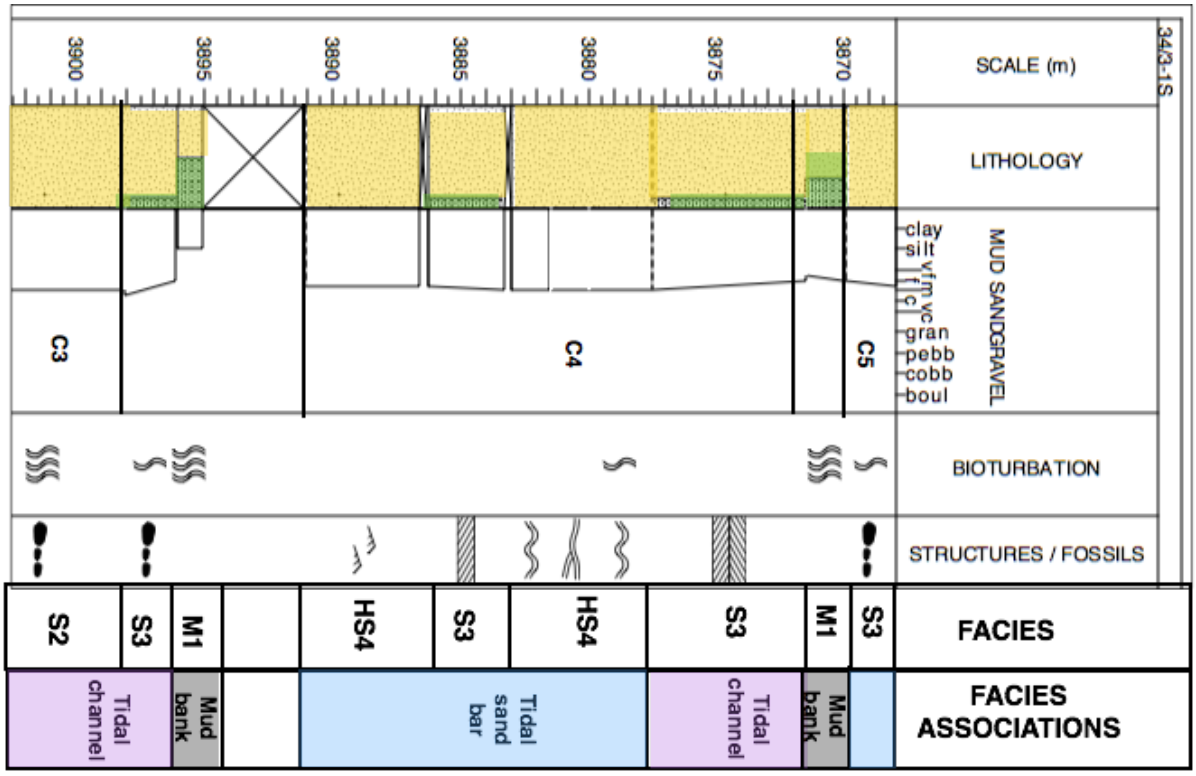
34/3-1S
SCALE (m)
3900
3895
3890
3885
3880
3875
3870
LITHOLOGY
clay
silt
vf
f
m
c
vc
gran
pebb
cobb
boul
MUD SANDGRAVEL
C3
C4
C5
BIOTURBATION
STRUCTURES / FOSSILS
FACIES
S2
S3
M1
HS4
S3
HS4
S3
M1
S3
FACIES ASSOCIATIONS
Tidal channel
Mud bank
Tidal sand bar
Tidal channel
Mud bank

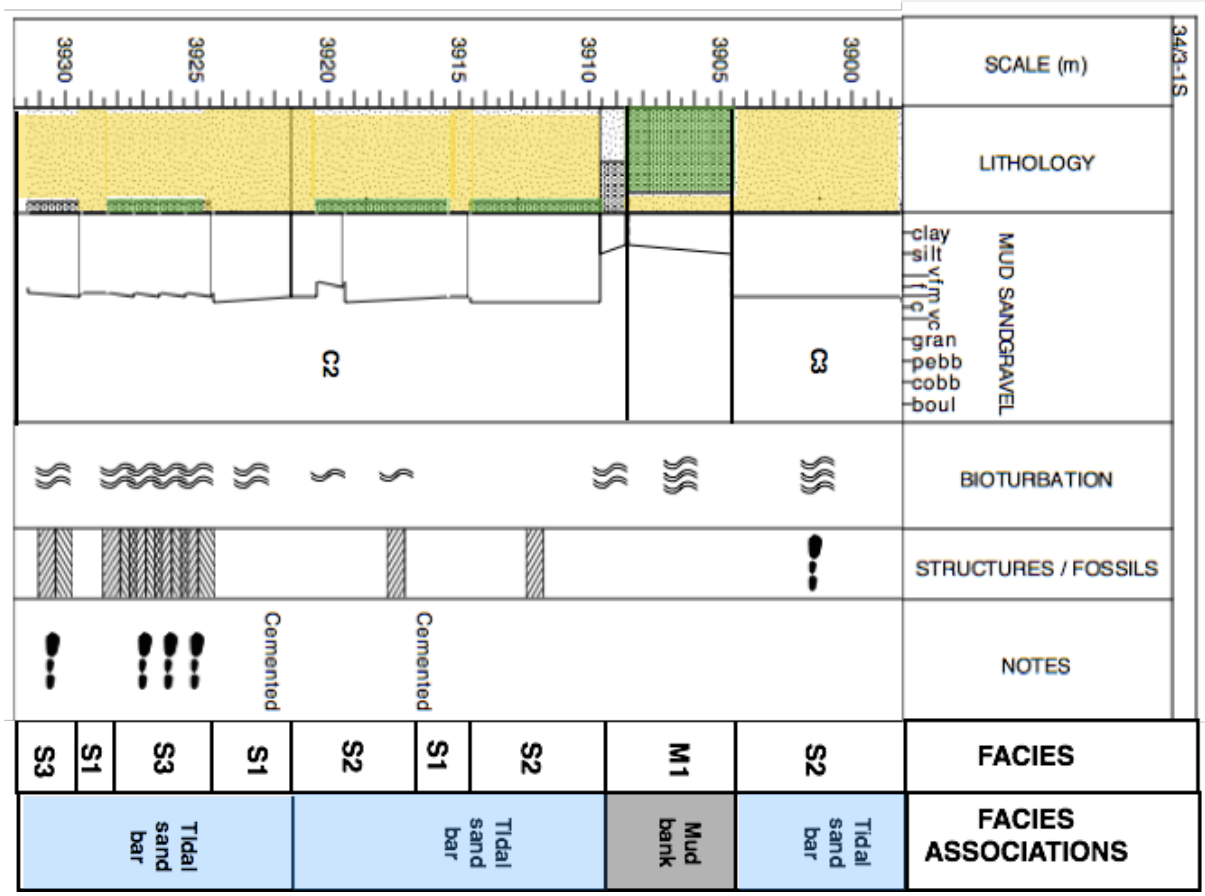
34/3-1S
SCALE (m)
3930
3925
3920
3915
3910
3905
3900
LITHOLOGY
clay
silt
vf
f
m
c
vc
gran
pebb
cobb
boul
MUD SANDGRAVEL
C2
C3
BIOTURBATION
STRUCTURES / FOSSILS
NOTES
Cemented
Cemented
FACIES
S3
S1
S3
S1
S2
S1
S2
M1
S2
FACIES ASSOCIATIONS
Tidal sand bar
Tidal sand bar
Mud bank
Tidal sand bar

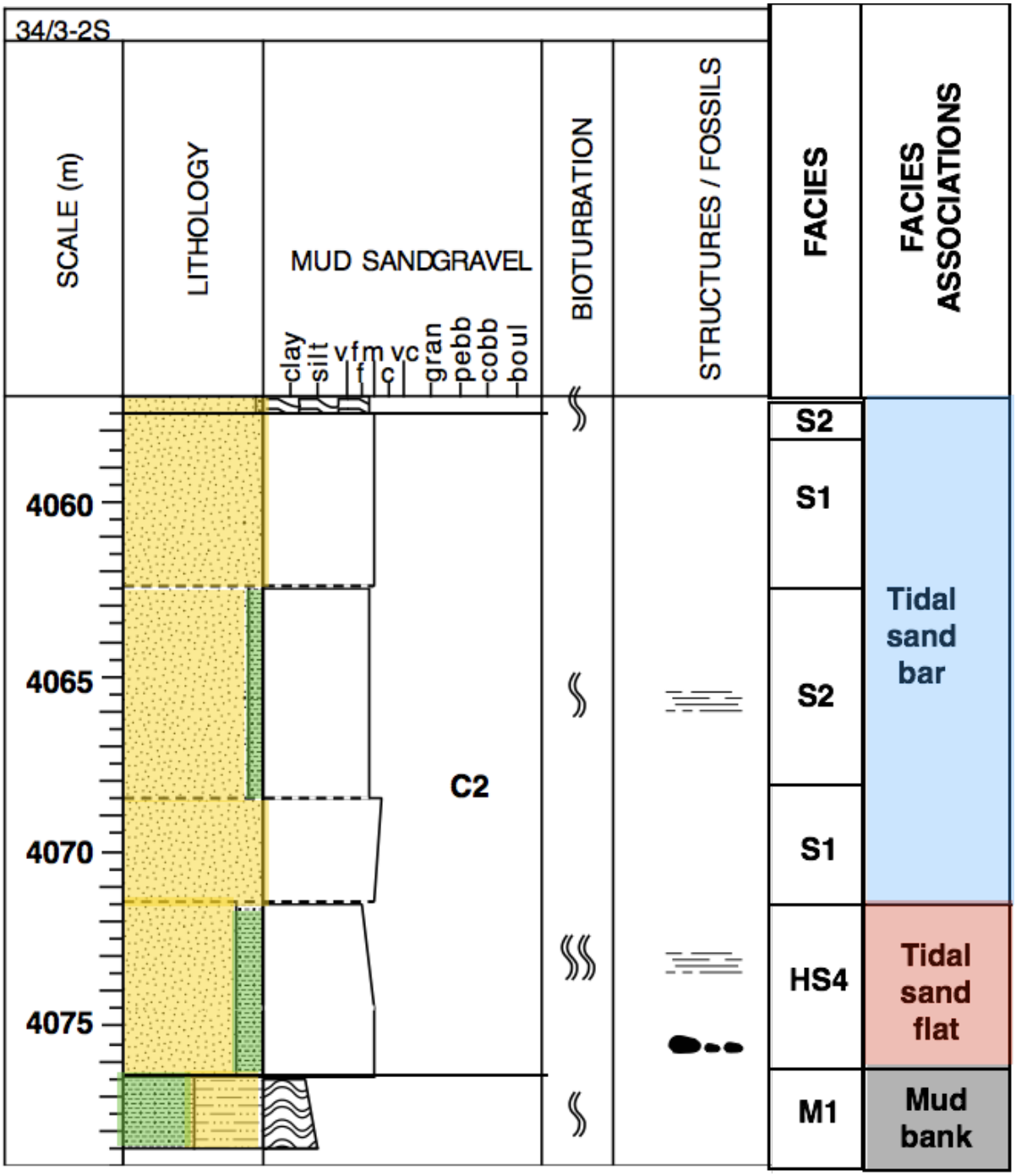
34/3-2S
SCALE (m)
LITHOLOGY
MUD SANDGRAVEL
clay
silt
vf
f
m
c
vc
gran
pebb
cobb
boul
BIOTURBATION
STRUCTURES / FOSSILS
FACIES
FACIES ASSOCIATIONS
4060
4065
4070
4075
C2
S2
S1
S2
S1
HS4
M1
Tidal sand bar
Tidal sand flat
Mud bank

Appendix B: Composition of chlorite

Sample 4061.75			Well 34/3-2 S		
Mg	**Al**	**Si**	**Fe**	**Al_tet**	**Al_okt**
0,910608415	2,844643988	2,535198296	3,752029011	1,464801704	1,379842284
0,915544967	2,548183443	2,866706373	3,528767123	1,133293627	1,414889815
0,719343025	2,314948396	2,95194762	3,904339141	1,04805238	1,266896016
0,961589757	2,830621499	2,925846893	2,940784209	1,074153107	1,756468392
0,811427228	2,748648013	3,038325888	2,988948977	0,961674112	1,786973901
0,847941296	2,486750917	2,838972687	3,743986955	1,161027313	1,325723604
0,733280143	2,524428592	2,880555686	3,718965598	1,119444314	1,404984277
0,926666667	2,253333333	2,99	3,713333333	1,01	1,243333333
0,837650493	2,829624225	2,802383558	3,313146054	1,197616442	1,632007783
0,891525424	2,403389831	2,969491525	3,56440678	1,030508475	1,372881356
0,881889764	2,856043758	2,925046583	2,983951434	1,074953417	1,781090341
0,859788184	2,82928129	3,137014587	2,622260707	0,862985413	1,966295877
0,556636368	2,448307022	2,57630362	4,618295859	1,42369638	1,024610642
Sample 3927.81			**Well 34/3-1S**		
Mg	**Al**	**Si**	**Fe**	**Al_tet**	**Al_okt**
0,831967213	2,750512295	2,974641393	3,092981557	1,025358607	1,725153689
0,900366255	2,640263207	3,078279223	2,982680489	0,921720777	1,71854243
0,809481056	2,874244329	2,963069372	2,953013707	1,036930628	1,837313701
0,582922298	2,92178592	3,719941067	1,594516687	0,280058933	2,641726987
0,694295466	2,786933203	3,483178937	2,158946855	0,516821063	2,27011214
0,682622533	2,573647358	3,944239338	1,568427753	0,055760662	2,517886696
0,785935132	2,541133677	3,420430433	2,561503486	0,579569567	1,96156411
0,680212014	2,724381625	3,890459364	1,45229682	0,109540636	2,614840989
0,84575256	2,858246925	3,363173826	2,1405294	0,636826174	2,221420751
1,206816524	2,597440488	3,06160069	2,773821365	0,93839931	1,659041178
0,688183078	2,340397147	2,718251321	4,364718559	1,281748679	1,058648468
0,935141163	2,453718378	3,240946176	2,902388918	0,759053824	1,694664554
Sample 3975.06			**Well 34/3-3S**		
Mg	**Al**	**Si**	**Fe**	**Al_tet**	**Al_okt**
0,833051838	2,699233468	3,630505392	1,857087177	0,369494608	2,329738859
0,749236864	2,769630447	3,367928817	2,36045983	0,632071183	2,137559265
0,796369138	2,421301059	3,441331316	2,689016641	0,558668684	1,862632375
0,813757524	2,637087991	3,245399828	2,739810834	0,754600172	1,882487819
0,636103152	2,651384909	3,82234957	1,742120344	0,17765043	2,473734479
0,392657237	2,842973217	3,400782426	2,541318086	0,599217574	2,243755642
0,755784062	2,476092545	3,703341902	2,123393316	0,296658098	2,179434447
0,448183556	2,442829828	4,33499044	1,217590822	-0,33499044	2,777820268
0,315641146	2,554720526	4,040864256	1,770549554	-0,040864256	2,595584782
0,972790441	2,598350542	3,062017014	3,005649718	0,937982986	1,660367556
1,070378357	2,453636542	3,465464288	2,318238254	0,534535712	1,91910083
0,58609426	2,99580028	3,139524032	2,641157256	0,860475968	2,135324312
0,647048499	2,452231908	3,851167144	1,97226935	0,148832856	2,303399052